DTU Mechanical Engineering
Department of Mechanical Engineering

Limits of lubrication in severe stamping operations

Marcel Moghadam

PhD Thesis

Limits of lubrication in severe stamping operations

PhD Thesis

Marcel Moghadam

Department of Mechanical Engineering
Technical University of Denmark

April 2019

Preface

The present thesis is submitted in partial fulfillment of the requirements for the PhD degree from the Technical University of Denmark. The work presented in this thesis was carried out from February 2016 to April 2019, at the Department of Mechanical Engineering, under the supervision of Associate Professor Chris Valentin Nielsen and Professor Emeritus Niels Bay. The presented work is part of the SHETRIB (*New environmentally benign sheet metal forming tribology systems)* framework programme, financially supported by the Danish Research Council for Independent Research in Production and Technology under grant no. DFF – 4005-00130.

Kongens Lyngby, April 2019
Marcel Moghadam

Abstract

Increasingly restrictive legislative initiatives have in recent years brought increased attention to the establishment of safe and environmentally benign manufacturing conditions, without the use of hazardous forming lubricants. The elimination of hazardous forming lubricants necessitates an adaption of new, environmentally friendly tribosystems for severe sheet metal forming processes. Production tests of new tribosystems are however connected to high costs and uncertainties regarding tool life and maintenance. This project presents an analysis of offline evaluation of tribosystem applicability for an industrial production platform from the company AAO Steel, where usage of chlorinated paraffin oils was currently deemed to be necessary. The specified production platform was based on a stamping operation for the production of an exhaust gas recirculation (EGR) component, where a drawbead geometry was implemented in the forming tools. Numerical analysis was carried out for evaluation of the wear conditions introduced by the different die features and for extraction of central testing parameters. A drawbead test was afterwards designed for the Universal Sheet Tribotester at DTU-MEK for offline replication of industrial forming conditions. Based on the offline simulative tests, the study highlighted several suitable tribosystems for replacement of the hazardous, chlorinated paraffin oil currently used in production.

An analysis of the performance and the tribological function of commercial forming lubricants for punching and blanking operations is furthermore presented in the thesis. Based on a process test, which emulates the forming conditions of a fine blanking operation, the efficiency of different lubricants were evaluated, and a clear correlation between the developed pick-up on the punch and the measured backstroke force was confirmed in accordance with previous studies. Analysis of the physiochemical properties of the forming lubricants highlighted certain intrinsic lubricant properties necessary for facilitation of stable production conditions in punching and blanking processes.

Online process monitoring of sheet metal forming operations can form the basis for condition-based tool maintenance for minimization of the production of scrap and maintenance costs. The project furthermore presents a methodology for evaluation of process conditions using measurements of acoustic emissions. Based on a series of simulative forming tests, the methodology was established for assessment of wear related process deviations commonly seen in different sheet metal forming operations.

Acknowledgments

Associate Professor Chris Valentin Nielsen and Emeritus Professor Niels Bay are gratefully acknowledged for their guidance and support over the course of the PhD programme. I am greatly thankful to Dr. Peter Christiansen for his valuable input regarding numerical simulation and experimental work. I would like to thank Kurt Pedersen from AAO Steel and Henrik Horup Reitz from the Danish Technological Institute for providing their facilities for the experiments conducted for the present work. Professor Peter Groche and MSc Yutian Wu are gratefully acknowledged for hosting my research stay at Technische Universität Darmstadt. Associate Professor André Dubois from The Polytechnic University of Hauts-de-France is gratefully acknowledged for the collaboratory work done regarding acoustic emission monitoring and analysis of lubricant function.

Lastly, I would like to thank my colleagues, friends and family for their support and encouragement.

Table of contents

Abbreviations

AE	Acoustic emission
AW	Anti-wear
BHF	Binder hold-down force
BUT	Bending under tension
COF	Coefficient of friction (Coulomb's friction law)
CPS	Counts per second
CVD	Chemical vapor deposition
DLC	Diamond-like carbon
DTA	Differential thermal analysis
EGR	Exhaust gas recirculation
EP	Extreme pressure
FEM	Finite element method
FFT	Fast Fourier transform
FM	Friction modifier
PLB	Pencil lead breaking
PLC	Programmable logic controller
PVD	Physical vapor deposition
RMS	Root mean square
SEM	Scanning electron microscopy
SRT	Strip reduction test
STFT	Short-time Fourier transform
UST	Universal sheet tribo-tester
WC/C	Tungsten carbide/carbon
XPS	X-ray photoelectron spectroscopy
XRF	X-ray fluorescence

Nomenclature

$DBRF$	Drawbead restraining force (kN)
F_d	Drawing force (kN)
F_h	Blank holder force (kN)
F_N	Normal force (kN)
F_T	Tangential force (kN)
g	Bead gap (mm)
h	Film thickness (μm)
H	Hardness (HRC)
H_b	Bead penetration (mm)
HC	Heat capacity (J/Kg·K)
HTC	heat transfer coefficient (kW/m^2K)
K	Wear coefficient
L	Sliding length (mm)
P	Normal pressure (MPa)
p	Penetration (mm)
R	Drawbead radius (mm)
Ra	Arithmetical mean roughness value (μm)
R_0	Indentor radius (mm)
RPM	Revolutions per minute (min^{-1})
t	Sheet thickness (mm)
TC	Thermal conductivity (W/m·K)
Λ	Film parameter
Nri	Number of valleys less than 0.5 μm
v_t	Sliding velocity (mm/s)
w	wear volume (mm^3)
w_t	Tool width (mm)
Z	Wear work (MPa·mm)
Z_b	Burr zone
Z_f	Fracture zone
Z_r	Roll over zone
Z_s	Shear zone
ε_{eq}	Equivalent strain
Θ_1	Maximum angle of contact (°)
σ_f	Flow stress (MPa)

Chapter 1 Introduction

Since 2000 increasingly restrictive legislation has been passed in Europe and Japan regarding the usage of hazardous lubricants for industrial applications [1]–[4]. In 2006-2007 the EU introduced the REACH (Registration, Evaluation Authorisation, and Restriction of Chemicals) legislation with the purpose of improving the protection of human and environmental health by regulation of the production and usage of industrial chemicals. The legislative initiatives have brought increased attention to manufacturing with safe working conditions while minimizing the strain on the environment. For industrial metal forming, these initiatives necessitate an elimination of hazardous chemicals such as chlorinated lubricant additives, which are suspected of being carcinogenic and bio-accumulative. The initiatives furthermore imply a reduction of waste with prolonged tool and lubricant life along with recovery and reuse of lubricants [5]–[7]. While the legislation becomes increasingly restrictive and the use of tribologically difficult materials such as advanced high strength steel (AHSS), stainless steels, aluminum, and titanium alloys becomes more prevalent, the demand for effective tribosystems increases. Since the specific tribological process characteristics dictate the type and efficiency of the required tribosystem, a significant amount of research has been conducted on the improvement of the tribological performance in different metal forming operations with new lubricants, anti-seizure tool materials and tool coatings [8]–[10]. Certain lubricant compounds like chlorinated paraffins, however, have unique lubricating properties such as broad operating temperatures and applicability to a wide range of manufacturing processes [11], which makes them difficult to replace. While several studies [12] have been successful in finding alternative lubricants to chlorinated paraffin oils for specific manufacturing processes, finding alternative tribosystems with similar versatility and efficiency has proven difficult. Further research is therefore still required for the development of environmentally benign tribosystems for tribologically severe metal forming operations where the usage of hazardous lubricants additives is currently necessary.

1.1 Scope of the project

The present project is part of a larger framework programme, *SHETRIB - New environmentally benign sheet metal forming tribology systems,* which has the aim of finding alternative tribosystems to replace environmentally hazardous lubricants for sheet metal forming processes. The overall project objectives are defined as:

- Development of a sensor system for determining the onset of lubricant film breakdown
- Evaluation of the performance of new, environmentally benign tribosystems in severe stamping operations, e.g. stamping with drawbeads, punching and blanking.
- Analysis of the performance and lubricating ability of new lubricants with film-forming additives.

The objectives of the project are to develop a sensor system based on acoustic emission (AE) for identification of the onset of lubricant film breakdown. An online process monitoring system allows for well defined and easy to determine the limit of lubrication in the simulative laboratory test. Such a surveillance system for online determination of lubricant film breakdown in production can aid with minimization of scrap production and tool maintenance costs.

Offline testing procedures start with numerical analysis of the production process in order to determine the main parameters governing lubrication, i.e., normal pressure, surface expansion, sliding length, sliding velocity and tool/workpiece interface temperature. The results of these calculations are used as input to design of the laboratory test. Numerical analyses of the tests are done to obtain similar pressure conditions and temperature development as in production using a recently developed universal sheet-tribotester (UST) at DTU-MEK. The tribotester allows repetitive tests at high speed from a coil with adjustable sliding length, sliding speed, idle time, cycle time and a total number of strokes in order to emulate the production conditions in long term testing. The methodology is under development and has been applied to a production platform in Danish industry [13] including a five-step progressive deep drawing tool for the production of a stainless steel component, where chlorinated paraffin oil has previously been necessary to apply. It is clear, however, that a considerable amount of research and development is still to be done before a complete methodology is established and it has yet to be applied to severe sheet stamping operations, e.g. stamping with drawbeads.

As regards testing of new, tailored tribosystems, development of lubricant systems for severe metal forming operations have so far been focused on properties of boundary lubrication by chemical bonding to the workpiece surface [14], [15].

Studies at DTU-MEK [16] have clarified that the reason for the excellent lubrication properties of chlorinated paraffin oil in severe punching operations is that it has the ability to react with the tool surface forming a very thin boundary layer that prevents metal-to-metal contact between tool and workpiece. However, only preliminary studies have been conducted within this research area. The project, therefore, aims at testing the most promising, environmentally benign, boundary lubricants to analyze the chemical reactions between the lubricants and tool surfaces, as these lubricants have been proven to be necessary for tribologically severe metal forming operations.

1.2 Thesis outline

The following chapter presents a brief overview of the basic principles of sheet metal forming tribology along with a review of the state of the art in environmentally benign sheet metal forming tribosystems. Chapter 3 introduces the topic of online process monitoring of sheet metal forming processes using acoustic emission. In this chapter, a series of laboratory tests are presented for the establishment of a methodology for evaluation of tribological process deviations using measurements of acoustic emissions. Chapter 4 introduces an industrial case study on wear and lubrication in stamping dies with drawbeads. Chapter 5 presents a supplementary study on wear in semi-circular drawbeads. Chapter 6 presents the topic of wear and lubrication in punching and blanking processes. Chapter 7 presents the main conclusions of the project and an outlook for future work based on the research findings from the present project.

Chapter 2 State of the art of sheet metal forming tribology

An overview of the basics of sheet metal forming tribology is presented in this chapter as an introduction to the background of the present work. A summary of the main challenges and advances within the field of environmentally benign sheet metal forming tribosystems is subsequently presented, with a special focus on the developed laboratory tests at DTU-MEK.

2.1 Sheet metal forming

Forming processes are defined in the DIN 8580 [17] as a group of manufacturing processes where dimensional modification of a workpiece geometry is obtained while retaining mass and material cohesion. The forming techniques are further classified in the DIN 8582 [18] by the main direction of the applied stress during forming. These subcategories are:

- Forming under compressive conditions
- Forming under combined tensile and compressive conditions
- Forming under tensile conditions
- Forming by bending
- Forming under shearing conditions

Within the classification based on the main stress states during forming, the DIN standard differentiates between 17 different forming processes based on the relative motion and the geometry of the forming tools and workpieces. Deep drawing is a sheet metal forming process, where a sheet metal blank is radially drawn into a die cavity, introducing combined tensile and compressive conditions, for forming of a component. Deep drawing is one of the most important sheet metal forming operations for forming of complex three-dimensional geometries and is extensively used in especially automotive and aircraft industry, as deep drawing supports the production of components with strict dimensional tolerances and high production rates. Sheet metal forming processes often present highly demanding tribological conditions, as sheet metal forming operations often include severe process loads due to elevated temperatures, high contact pressures and moderate levels of surface expansion combined with strict demands for surface finish and tool life.

2.2 Wear in sheet metal forming

Wear is defined as a progressive deterioration of the surface of a solid body due to mechanical or chemical action. The wear behavior is characterized as a system response and is dictated by the different process variables of the tribosystem, see Figure 1.

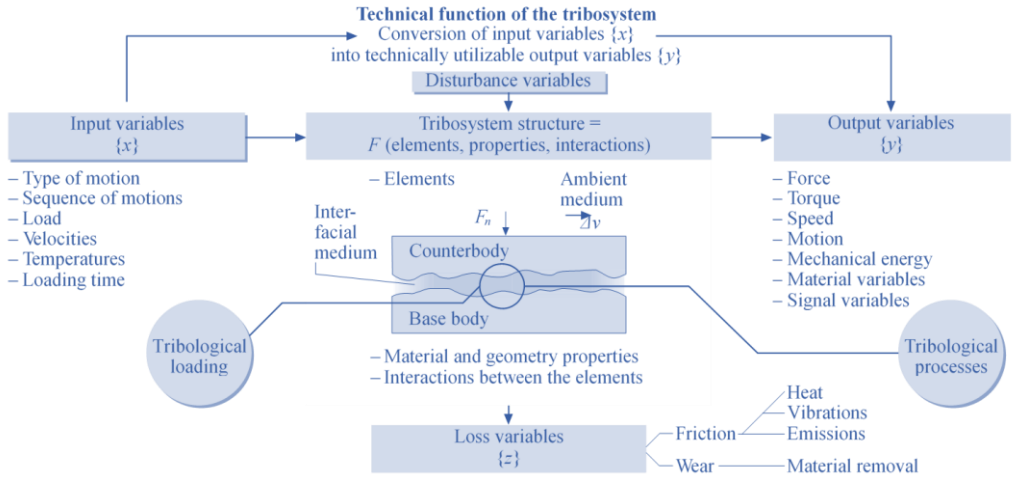

Figure 1: Overview of the main components of a tribosystem [19].

A tribosystem consists of four main elements: the material pair of the base body and the counter body, the interfacial medium, and the environment. The exact combination of the input variables and the tribosystem structure characterizes the tribological load exerted on the specific tribosystem.

The German standard DIN 50320 [20] defines four main mechanisms of wear: adhesive wear, abrasive wear, surface fatigue, and tribochemical wear. A brief description of the main characteristics of these wear mechanisms is given in the following section. The four main wear mechanisms are illustrated in Figure 2.

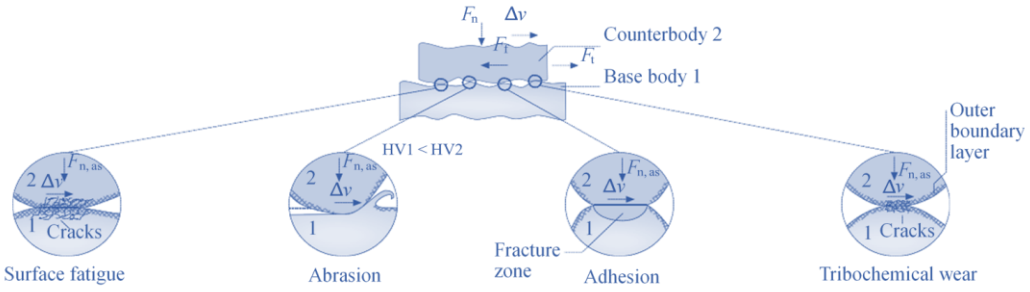

Figure 2: Illustration of the main wear mechanisms defined in DIN 50320 [19].

Adhesive wear

Adhesive wear is characterized by a transfer of material particles between contacting surfaces due to adhesive bonding of asperities. Adhesive wear initiates as a microscopic transfer of wear particles but progresses macroscopically. The severity of the wear mechanism is highly dependent on the material pair, as different material combinations have different affinities for adhesive bonding.

Abrasive wear

Abrasive wear occurs when relative sliding takes place between solid bodies in contact, where the asperities of the hardest surface abrade the surface of the softer body with localized plastic deformation (two-body abrasion). Three-body abrasion occurs when solid particles are entrapped as the interfacial medium between the base body and the counter body.

The combined wear mechanism of local adhesion and abrasion in contacting surfaces is in the field of metal forming called galling. The galling mechanism is characterized by macroscopic adhesion of metallic particles, due to insufficient lubrication or tribosystem breakdown, which create localized friction junctions above the original surface [21]. The creation and the subsequent growth of the local friction junctions result in the scoring of the surface of the formed sheet material [22]. The occurrence of galling is often the limiting factor of sheet metal forming tribosystems [23].

Surface fatigue

Damage due to surface fatigue is characterized by a deterioration of the surface structure due to the formation and propagation of cracks caused by cyclic loading.

Tribochemical wear

The tribochemical wear mechanism is a mechanism of surface damage that is based on rubbing contact between solid bodies in a corrosive media. The process is often characterized by progressive creation and removal of corrosion products with very high wear rates.

2.3 Lubrication mechanisms

The main tribological function of a sheet metal forming lubricant is the separation of the contacting surfaces of the tribosystem, in order to minimize friction and tool wear. A common secondary function of the forming lubricants is cooling of the forming tools in order to avoid softening and oxidative wear. Apart from the main tribological requirements for the forming lubricants, several other requirements may include corrosion protection, vanishing properties, easy application and cleaning and storage stability, depending on the specific conditions of the manufacturing process. The lubrication regimes for liquid lubricants are summarized in the Stribeck curve in Figure 3.

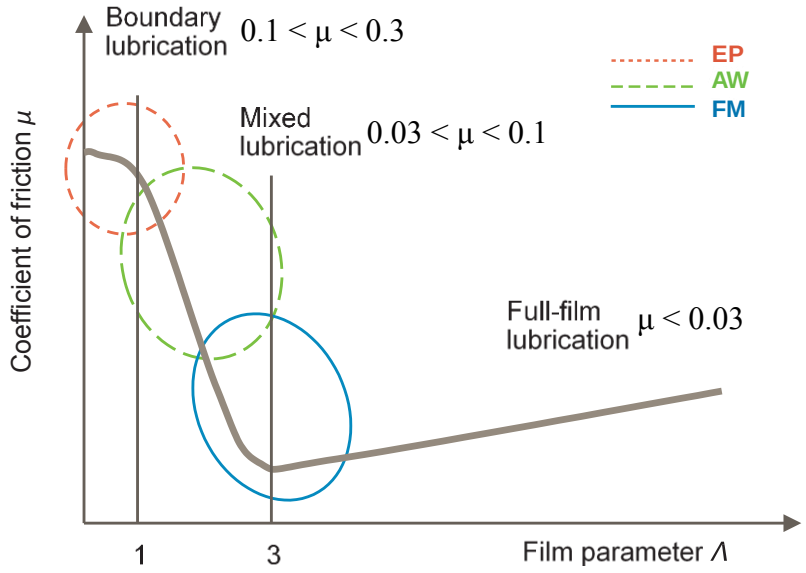

Figure 3: Stribeck curve [24] with identification of the main lubricant regimes where the different types of film-forming additives (Extreme pressure (EP), Anti-wear (AW), Friction modifier (FM)) are utilized.

The Stribeck curve shows the coefficient of friction (COF) as a function of the film parameter Λ *(h/Ra)* for the three different lubricant regimes, where *h* is lubricant film thickness and *Ra* is the average roughness of the two surfaces in contact. Fig. 3 furthermore shows the three main groups of film-forming lubricant additives and the lubrication regimes where they function. The primary mechanisms of lubrication are illustrated in Figure 4.

Full-film lubrication (also called hydrodynamic lubrication) occurs when a complete separation of mating surfaces is achieved through an intermediate, pressurized lubricant film. A film parameter value of more than 3 indicates that there is no asperity contact between the base body and the counter body of the tribosystem.

The full-film lubrication mechanism is therefore characterized by a very low COF.

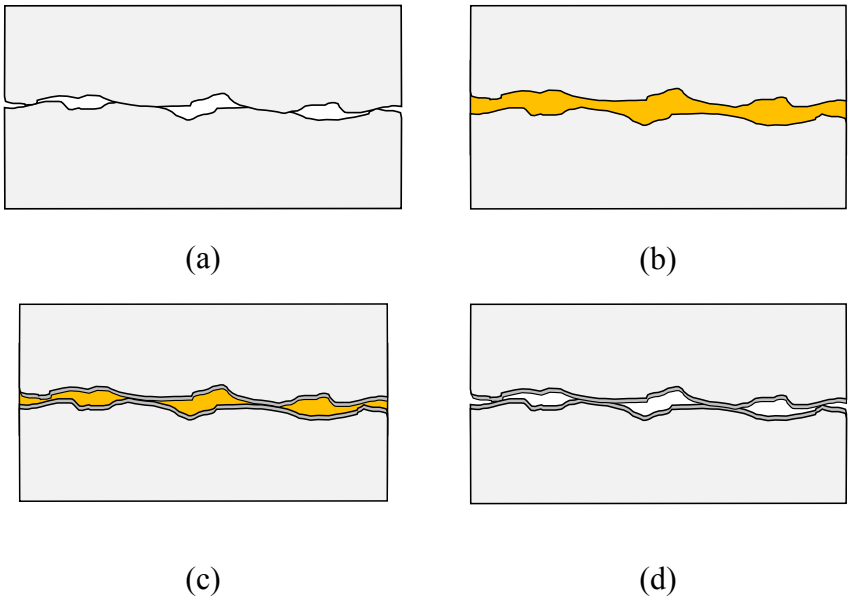

Figure 4: Illustration of the lubricant regimes: (a) dry friction, (b) full-film lubrication, (c) mixed lubrication and (d) boundary lubrication.

Pure hydrodynamic lubrication is experienced in a few sheet metal forming processes e.g., high speed sheet rolling where the high velocities of the process introduce hydrodynamic conditions. The elastohydrodynamic lubrication mechanism is part of the full-film lubrication regime and occurs when the pressurized fluid film induces elastic deformation of the contacting surfaces of the tribosystem. The boundary lubrication regime [25]–[27] is characterized by heavy contact between the mating surfaces of the tribosystem, with a film parameter value of less than 1. The boundary lubrication mechanism is furthermore characterized by the formation of an intermediate surface layer generated through tribochemical reaction, which lowers the COF. The characteristics of the generated surface layer are dictated entirely by the specific additive composition of the lubricant. The mixed lubrication regime combines the lubrication mechanism of boundary lubrication and full-film lubrication, where the exerted load is distributed partly between a pressurized lubricant film and asperities in contact.

2.4 Sheet metal forming lubricants

The physical and chemical properties of forming lubricants are dictated by the chemical composition of the base oil and the specific formulation of the additive package. Base oils are derived from either crude oil, natural resources or chemical synthesis and normally account for 70-99% of the volume of the formulated lubricant. Since the base oil makes up the majority of the formulated lubricant, the intrinsic properties of the base oil e.g. viscosity, viscosity index and volatility, greatly influence the properties of the lubricant. Additives are furthermore added to the base oil in order to enhance different lubricant properties [28]. Figure 5 shows an overview of the most common lubricant additives.

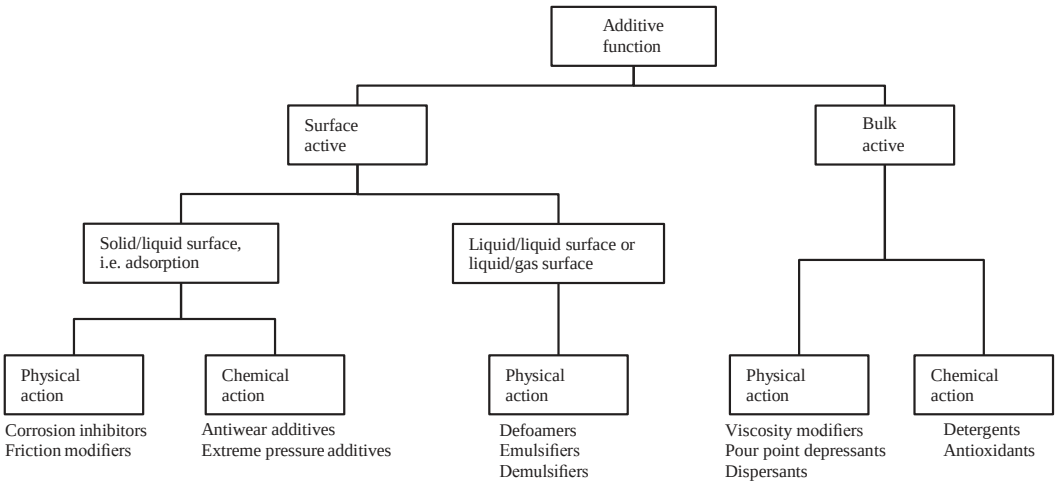

Figure 5: Overview of the main groups of lubricant additives [24].

The different classes of lubricant additives are added to the base oil in order to tailor the properties of the lubricant for different uses. Friction modifiers (FM), Antiwear additives (AW) and Extreme pressure additives (EP) belong to the additive group commonly called film-forming agents, due to their film-forming action in the solid/liquid interface during forming. FM reduce the friction in the mixed lubrication regime, by the formation of physisorbed surface films. Physiosorption is characterized by the formation of mono- or multilayers through the creation of Van der Waals bonds with metal surfaces at low temperatures. FM, therefore, form a weakly bonded film that desorbs at increased temperatures or contact with aggressive solvents. AW and EP additives modify the surface of a metal by the creation of films through chemisorption and chemical reaction, often induced by thermal activation of the lubricant additives. AW and EP additives, therefore, create a film that is strongly adhered to metallic surfaces for applications with higher tribological severity. AW and EP additives form sacrificial surface films, which inhibit metal-to-metal contact and thereby reduces friction and material adhesion.

The primary tribological function of a forming lubricant is therefore dictated by lubricant properties such as the load-bearing capacity, applicable temperature range and the chemical reactivity of the lubricant additives [29], [30]. Excessive reactivity is however reported to introduce increased rates of corrosion, while additives with low reactivity are conversely unable to preserve a protective surface film. The specific additive composition of the film-forming agents therefore heavily influence the tribological performance of the formulated lubricant. Cl-, P- and S-based additives are extensively used AW/EP additives in sheet metal forming lubricants. Corrosion inhibitors similarly belong to the additive group of film forming agents. While corrosion inhibitors do not exhibit any tribological function, they are often used in metal forming lubricants for enhancement of corrosion properties by acid neutralization or creation of a passivation film that reduces the electrochemical reactivity of the metal surfaces. The tribochemical action of film-forming agents has been subject for extensive research. Comprehensive reviews of the tribochemistry of AW and EP additives and the developed surface films is given by Xue and Weimin [31], Papay [32] and Matsumoto [33].

Detergents and antioxidants are bulk active lubricant additives that chemically react with species in the lubricant, respectively used for control of contaminants and delaying the aging mechanism of the lubricant. Bulk active additives with physical action like viscosity modifiers and pour point depressants are used for enhancement of the viscosity index and refinement of the applicable temperature range for the handling of the lubricant.

2.5 Simulative testing in sheet metal forming

With a comprehensive review of the tribological tests used within the field of sheet and bulk metal forming, Bay et al. [34][8] proposed a classification of the laboratory tests as either process or simulative tests. Bay et al. suggested that process tests are characterized as tests, where the characteristics of a conventional forming operation are emulated without changing the process kinematics, while simulative tests are used for studying the tribological conditions of a forming process in a controlled manner. Simple simulative tests such as the pin-on-disc test or block-on-ring test are well established and often used for different tribological investigations. These tests do, however, not account for the complexity of an actual metal forming operation in terms of simulation of comparable process characteristics. Various simulative tests have therefore been developed in order to emulate the forming conditions in a deep drawing operation. Figure 6 shows an overview of the most commonly used simulative tests for analysis of sheet metal forming operations.

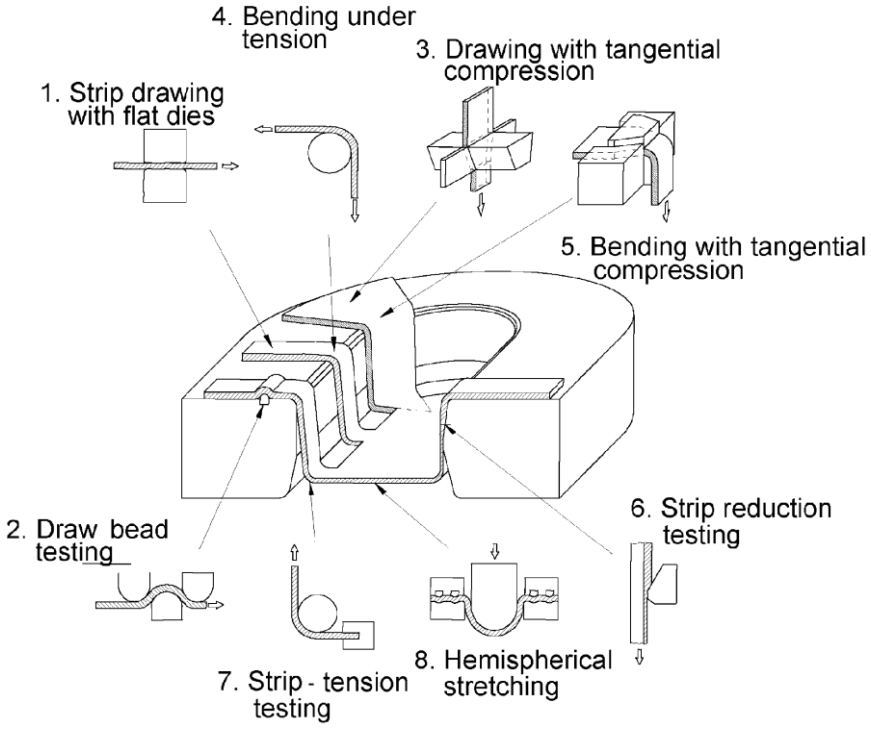

Figure 6: Schematic illustration of simulative tests used for sheet metal forming [8].

Tests 1-3, shown in Figure 6, represent the forming conditions in the flange region. Tests 4-5 represent the forming conditions of a bending action over the die shoulder. Test 6 simulates an ironing process with a conical die. Tests 7-8 represent the forming conditions when stretching sheet material over a die shoulder and a punch nose. These simulative tests allow for an offline replication of industrial forming

conditions in terms of normal pressure, sliding length, surface expansion and interface temperature [35][36]. Simulative tests are therefore highly valuable for offline screening of the efficiency of alternative tribosystems as actual production trials are often connected to high costs due to production downtime and uncertainties regarding tool life and maintenance.

As representatives of the varied process conditions experienced in sheet metal forming, the research conducted at DTU MEK has been focused on three different simulative tests: the drawbead test, the bending under tension test (BUT) and the strip reduction test (SRT). A short summary of these tests is given in the following sections.

2.5.1 Drawbead test

The drawbead simulator, Figure 6, was initially developed in 1978 by Nine [37], and the test has since become widely used for studying friction and lubrication in sheet metal forming. With the drawbead simulator, Nine showed that friction measurements could be made by conducting a series of tests respectively with fixed and roller drawbeads. Nine furthermore showed that the measured drawing forces agreed with calculations based on Coulomb's law. Nine later presented a series of studies [38], [39] where lubricant performance was evaluated with a drawbead test with varying bead penetrations. Based on Nine's studies, Olsson et al. [40] proposed a tool design where the friction coefficient could be measured directly without differential testing. This was possible with a tool design, where the drawing force and the torque exerted on the tool pin is measured directly during testing. Wang and Shah [41] investigated different drawbead configurations in terms of the drawbead restraining force, the flow of sheet material through the drawbeads and the sensitivity towards different lubricants. Based on the study, Wang and Shah proposed some preliminary design guidelines for shop floor practices. Dalton and Schey [42], [43] found that the COF and the rate of metal transfer in the contacting interface are heavily influenced by the topography of the drawbeads, the surface treatment of the sheet material and the type of lubricants used for the test. Vermeulen and Hobleke [44] conducted a series of tests using a drawbead simulator with a multi-strip procedure for evaluation of the wear characteristics. The multi-strip galling test revealed that the specific surface treatment of the strip materials highly influences the wear development. The development of the galling mechanism was, however, found to be less influenced by the surface texture of the strip material. Zonker et al. [45] conducted an extensive study on the wear behavior during the drawbead deformation of aluminium. In the study, Zonker et al. examined the friction and galling behavior of different tool materials, aluminium alloys, surface treatments and dilution levels of the applied lubricants. The study

showed that the Wearalloy^{TM} and CrN tool coatings consistently exhibited high wear resistance, despite having a high COF compared to other tool coatings. Hunz et al. [46] presented a study where the performance of forming lubricants with different formulations and concentrations of EP additives were evaluated with a drawbead test. The study showed that Cl-based lubricant additives exhibited excellent tribological performance compared to straight oils and lubricants with conventional EP additives. The performance of the forming lubricants was furthermore found to be highly influenced by the concentration of the EP additives. Several studies have since been conducted for evaluation of parameters influencing friction and lubrication in drawbeads [47]–[52].

2.5.2 Bending under tension test

The bending under tension (BUT) test, see Figure 6, is a simulative test, where plane strip material is drawn over a stationary tool pin with superimposed back tension to simulate the forming conditions experienced around the die shoulder. The BUT test has been studied for a wide range of tribological investigations by several different authors [53]–[64]. Schey and McLean [65] performed several different simulative sheet metal forming tests, including the BUT test, for evaluation of lubricant performance. The tribological characteristics of uncoated and electrogalvanized steels have been studied by Saha and Wilson [66] by use of the BUT test with a range of different forming and process variables.

Similar to the drawbead test, the BUT test conventionally required differential testing, respectively with a stationary and a rotating tool pin in order to characterize the friction in the contacting interface. Andreasen et al. [67] developed a test setup with a torque transducer that enables direct measurement of the friction force. Direct measurement of the friction force was found to be valuable for monitoring lubricant film breakdown. Based on an industrial case study, Ceron et al. [68]–[70] presented a series of investigations, where the BUT test was tailored to emulate an industrial production platform for analysis of forming conditions for offline screening of the efficiency of different environmentally friendly lubricants. The BUT test was similarly used by Üstünyagiz et al. [71] for evaluation of the tribological performance of a DLC/Hyperlox® tool coating under dry and lubricated conditions.

2.5.3 Strip reduction test

The strip reduction test (SRT), see Figure 6, emulates the forming condition of an ironing operation, by reducing the thickness of a sheet metal strip in a drawing operation. The SRT is therefore characterized as a severe tribological test due to the high contact pressures, substantial surface expansion and a high amount of heat generated during testing. Fukui et al. [72] presented a preliminary study where the effect of several different tribological factors such as the lubricant type, strip material, drawing speed and surface finish were characterized by measurement of the friction force in a SRT. Le and Sutcliffe [73] studied the frictional behavior in sheet metal forming under thin film lubrication conditions with a SRT. The study found that the COF increases significantly when the lubricant film thickness ranges from 1-40 nm, due to the increased contact area between the contacting surfaces and an increase in local friction. Aleksandrović [74] later presented a methodology for determination of the COF when ironing sheet material in a SRT. Dohda and Kawai [75] investigated the compatibility of different material combinations by examination of frictional characteristics and inspection of the surface structure, after reducing the thickness of a strip through a wedged die. Dohda et al. [76] later presented a study where a similar test setup was used for evaluation of the tribological performance of DLC-Si coatings for ironing of high strength steel and brass. Takaki et al. [77] studied the anti-galling properties of sulfurized olefin and overbased calcium with a cup internal ironing test. Based on surface analysis of the ironed cups, Takaki et al. were able to find the optimal blending ratio of the lubricant additives and evaluate their synergistic, lubricating effect. Andreasen et al. [78]–[83] presented a series of studies where the SRT was conducted with a cylindrical tool for evaluation of the performance of different commercially available forming lubricants. Andreasen et al. found that the tool rest temperature heavily influences the threshold sliding length for lubricant film breakdown for the different lubricants. Andreasen et al. proposed that analysis of the surface roughness of the tested sheet material could be used to quantify the surface damage occurring during testing. The SRT was similarly used by Wadman et al. [84] for assessment of the wear characteristics of textured workpiece surfaces of lean duplex and austenitic stainless steels. Üstünyagiz et al. [85] presented the design and implementation of a SRT tool for offline evaluation of different environmentally friendly tribosystems for a specific industrial production platform.

2.6 Drawbeads

Drawbeads are local die features placed on the surface of the draw ring and blank holder, for control of the material flow into the die cavity [86], [87]. Drawbeads introduce a restriction of the material flow by subjecting the sheet material to sequential bending and unbending, as the sheet material slides over the groove shoulder and the drawbead, see Figure 7. The restriction of the material flow is controlled by the deformation induced by the bending and unbending action as well as the experienced sliding friction. Drawbeads are commonly used in complex forming dies for ensuring proper flow of the sheet material and for avoiding forming defects.

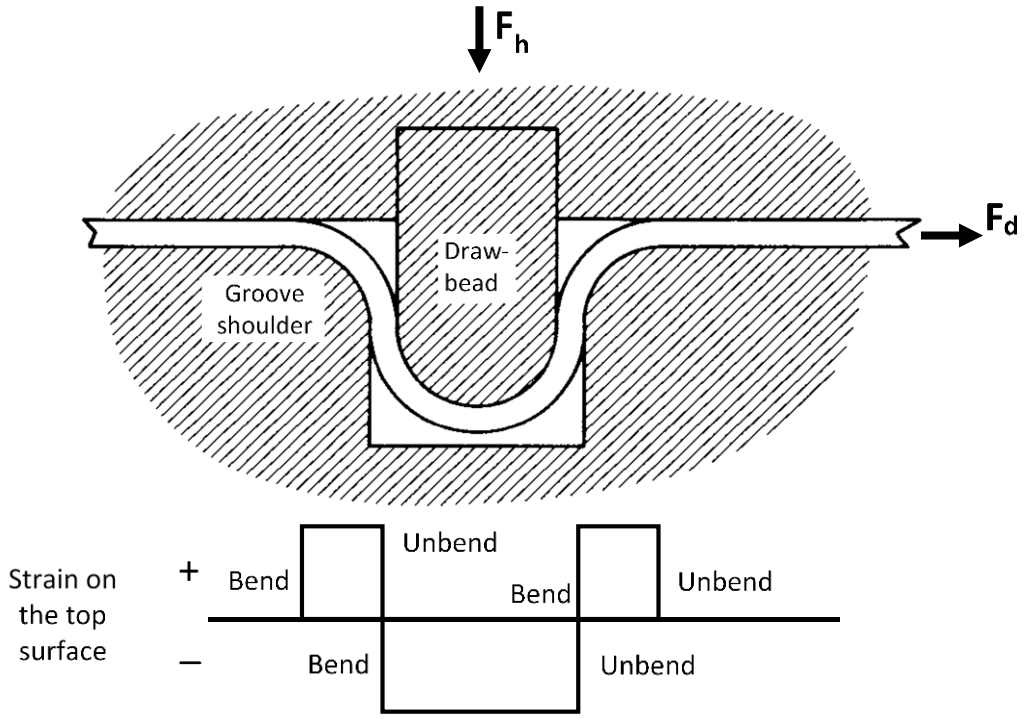

Figure 7: Principal illustration of the bending action of a semi-circular drawbead [88].

Three main drawbead types are illustrated in Figure 8. These drawbead geometries are characterized by respectively imposing four, six and eight bending deformations to the sheet material during forming. The main geometrical parameters controlling the bending action of the drawbeads are the rounding radii R, the bead penetration H_b, and the bead gap g.

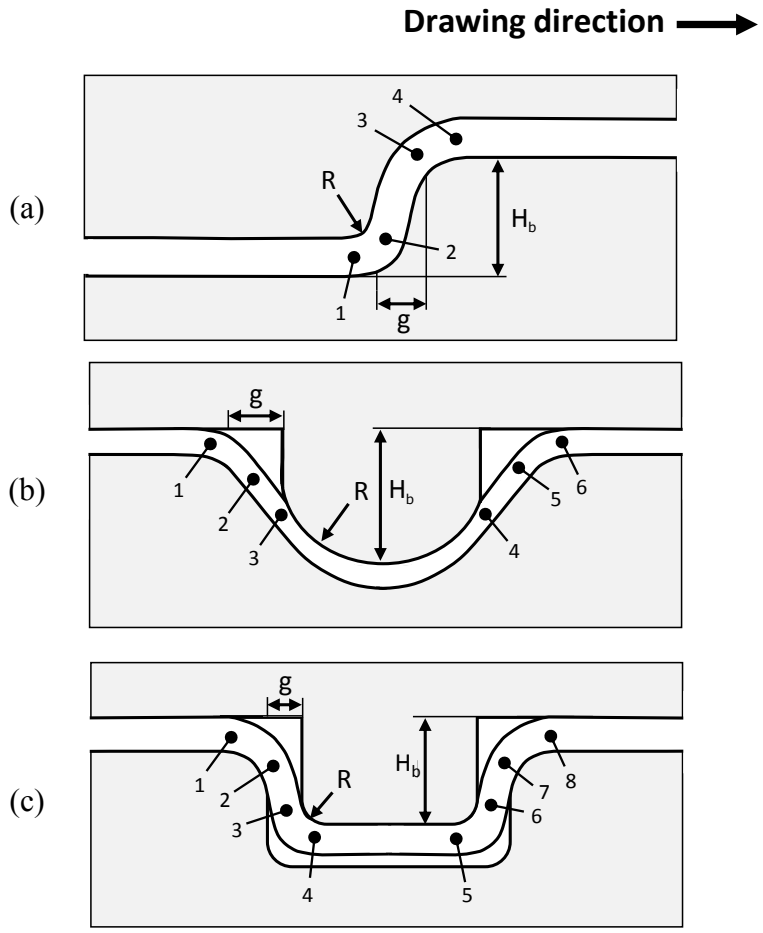

Figure 8: Overview of the most common drawbead geometries: (a) stepped drawbead (edge drawbead), (b) Semi-circular drawbead (c) rectangular drawbead [89].

While several simplified guidelines exist for the design of drawbeads [90]–[94], the actual drawbead design implemented in industrial forming dies is highly dependent on the component geometry, the sheet thickness and the experience of the die manufacturer. In the die tryout stage, the die manufacturer modifies the drawbead geometry by manual grinding in order to adjust the flow of the sheet material while trying to avoid a drawbead geometry that introduces excessive thinning of the sheet material and forming defects such as cracks, wrinkles, and orange peeling. The die tryout stage is furthermore influenced by several economical considerations such as minimization of the blank size and optimization of tool life. This trial and error approach results in a wide range of different drawbead geometries used in industrial forming dies. These die geometries are often prone to introduce severe wear conditions, as certain die features like the die shoulder and drawbeads are often subjected to high wear rates, due to high localized normal pressures [95].

Several analytical models are described in literature for estimation of the drawbead restraining force (DBRF) and the binder hold-down force (BHF). In 1978, Weidemann [96] proposed a model for calculation of the DBRF, based on a calculation of the bending action imposed by the drawbeads. Weidemann's model has a very simple form and is convenient to use for initial assessment of the DBRF, but the model has several substantial shortcomings. The shortcomings stem from a simplification of the drawbead action, where several central characteristics are neglected, such as the strain hardening and thinning behavior of the sheet material, elastic deformation and the applicability of the formula for partial penetrations. Tukefci et al. [90] showed that Weidemann's model underestimated the DBRF with 40-59% for steels and 35% for 2036-T4 aluminium. Kluge [97] proposed an analytical model where strain hardening behavior is introduced by calculation of the average flow stress after each bending action. Based on the principle of virtual work Stoughton [98] proposed an analytical model, where the shortcomings of the previous models were addressed. Comparison with experimentally obtained drawing values showed that the model proposed by Stoughton gives an accurate description of the restraining force, with an accuracy of approximately 5% for the DBRF and 13% for the BHF. Other analytical models for the description of the DBRF and the BHF include the work done by Wang [99], Heindrich [100], Sanchez and Weinmann [101], Levy [102] and Yellep [103]. Several studies have furthermore been conducted for numerical simulation of the drawbead action [104][105]. Chabrand et al. [106] described the first numerical model for simulation of the DBRF using a finite strain elasto-plastic analysis. Several authors have since investigated the possibility of adapting equivalent models for numerical simulation of the drawbead action for forming complex three-dimensional geometries [107]–[109].

2.7 Universal sheet tribotester

The Universal Sheet Tribo-tester (UST) was developed at the DTU-MEK in 2012, for conducting simulative sheet metal forming tests. An overview of the main components of the UTS [110], [111] is shown in Figure 9.

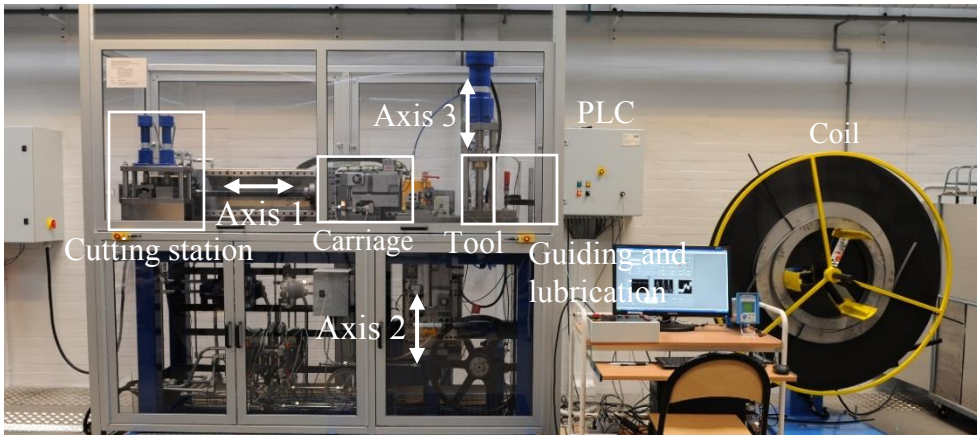

Figure 9: Overview of the UST

The UTS has three main hydraulically driven axes, controlled by electromechanical valves for adjustment of speed and load. Axis 1 is used for drawing the strip material through the forming tool while measuring the drawing force with a 50 kN load cell. Axis 1 can draw the strip 500 mm before returning to the starting position to restart the drawing sequence. Axis 2 is used for application of back tension for BUT testing, while axis 3 is used for application of the test load for SRT and drawbead testing. The three axes are controlled through a PLC, via a Labview program. The sheet material is drawn from a 500-1000 m coil, enabling simulative testing of thousands of strokes. Upon drawing of the strip material, automatic cutting, for shortening of the scrap material, can be enabled with the cutting station. The UST can thereby accurately simulate the tribological conditions of a manufacturing platform with specific process parameters, i.e. sliding length, sliding speed, idle time for offline evaluation of different tribosystems. An overview of the operational parameters of the UST is given in Table 1 [112].

Table 1: Overview of the operational parameters of the UST

Sliding length	0 - 500 mm
Sliding speed (mm/s)	0 - 150 mm/s
Cycle time (spm)	0 - 95 spm
Load, Axis 1 (kN)	0 - 50 kN
Load, Axis 2 (kN)	0 - 50 kN
Load, Axis 3 (kN)	0 - 100 kN

2.8 Environmentally benign tribosystems

The environmental issues related to the field of metal forming tribology can be divided into the following categories [113]:

1. Health and safety of people
2. Influence on equipment and buildings
3. Destruction and disposal of waste and remaining products

Along with increasingly restrictive legislative initiatives, continuous efforts have been made for the elimination of hazardous chemicals, reduction of waste and development of alternative, environmentally benign tribosystems. With a comprehensive overview of the recent developments and trends within the field of metal forming tribology Bay et al. [5], [6], [114] reviewed the conducted research for the development of alternative, environmentally benign tribosystems for cold, warm and hot forging and sheet metal forming. Bay et al. highlighted the recent development of new lubricant types, tool coatings, textured tool surfaces and anti-seizure tool materials used as environmentally benign tribosystems for sheet metal forming processes.

In 2005, the Danish Ministry of Environment presented a comprehensive report on mapping and development of alternatives to chlorinated lubricants used in metal forming industry [12]. The report presented a list of demands and specifications for the non-chlorinated lubricants and an extensive health and environmental assessment of alternative lubricant additives. Based on different simulative tests, four lubricant systems were identified to have promising lubricating qualities. These lubricant systems where however not able to facilitate a full-scale production test with forming operations consisting of several production steps. Friis et al. [115] conducted a study for evaluation of alternative lubricants for the production of a stainless steel pump cover with a progressive forming tool. The study showed that a TiAlN tool coating combined with a mineral oil with a Ca-, P- and S-based additive package could replace the highly chlorinated paraffin oil that was previously used in production. Jewvattanarak et al. [116] similarly conducted a test series for analysis of the efficiency of chlorine-free lubricants. The study showed that chlorinated lubricants have excellent lubricating abilities due to synergy with different lubricant additives. The study furthermore found that only a fraction of the sulphur additives in the lubricants interact with the surface oxides and that a higher amount of interaction could be promoted with increased temperatures. Rao and Xie [117] conducted a benchmark study, where the performance of boric acid was compared to several different types of commonly used dry and liquid lubricants for forming of aluminium 6061 and pure copper. Based on a series of deep drawing and stretch forming tests, Rao and Xie found that the boric acid provided the best

lubrication in forming operations which involved long sliding lengths. The tribological performance of boric acid for forming of aluminium was later studied by Wei et al. [118] who found that boric acid dry films and combinations with mineral oil films provide a low COF with better lubricating properties than different commercial forming lubricants. Takaki et al. [119] presented a study on the development of chlorine free lubricants for cold forming of stainless steel. Based on multistep cup internal ironing test, the performance of commercially available chlorine free, S-based lubricants were evaluated by measurement of the surface roughness of the workpiece after testing. The performance of the most promising commercially available lubricant was enhanced with the addition of S-, Ca- and Zn-based EP-additives. Djordjevic [120] conducted a benchmark study with a SRT with a double wedge die, where the performance of an environmentally benign lubricant was compared to the performance of conventional forming lubricants. Rehbein [121] characterized the tribological behavior of different lubricant additives with different physical and chemical properties with a strip drawing test and an SRV test. The investigation showed that the lubricants containing sulfurized triglycerides exhibited the lowest COF. The size, polarity and concentration of the additive compounds were found to have the most significant influence in the tests, while the chemical reactivity of the sulphur bridges in the molecules was found to have less importance.

The application of dry film lubricants has gained increasing popularity due to its tribological properties, cleanliness and the small amount of lubricant required compared to liquid lubricants [122]. Altan et al. [123]–[126] presented a series of investigations on the applicability of new lubricants as substitutes for petroleum-based oils in automotive sheet metal forming. The lubricants were evaluated through a number of different simulative sheet metal forming tests, including deep drawing and ironing tests, where the performance was evaluated by the measured ironing load, the surface quality of the ironed cup and the apparent shear friction factor. Meiler and Pfestorf et al. [127] studied the use of dry film lubricant for deep drawing of complex body panels. The dry film lubricant enhanced the deep drawing performance while enabling a cleaner production process compared to conventional forming lubricants. Sgarabotto and Ghiotti [118] compared the tribological performance of environmentally friendly solid lubricants to conventional synthetic forming lubricants, by evaluation of surface topography and the measured COF in a flat die test. The study found that solid lubricants on average provide a lower COF compared to synthetic forming lubricants. The stability of the COF for solid lubricants is, however, heavily influenced by the adhesion to the substrate. Several studies [128], [129] have furthermore investigated the characteristics of minimum quantity lubrication, as a method for reducing the amount of lubricant needed for production.

Along with the advances of new environmentally benign lubrication systems, the development of advanced anti-seizure tool materials has proven valuable for enhancement of the tool life of forming tools [130]. Azushima and Jimbo [131], [132] studied the anti-seizure properties of high chromium steels and high-speed steels for cold rolling of low-carbon steels. With an investigation of seven different steel variants, the study showed that the tribological characteristics of the tool material are highly correlated to the morphology of the carbides on the roll surface. Comprehensive experimental investigations have been carried out by Tamaoki et al. [133]–[135] on the applicability of ceramics as tool materials for deep drawing of different types of sheet material. The studies showed that ceramic tooling for deep drawing allows a dry forming process. The ceramic tool materials, however, have different compatibilities with the different types of sheet material. Different electroconductive ceramics were found to possess promising characteristics, due to their tribological performance and their electric discharge machinability.

During the last 70 years, a number of processes have been developed for prolonging tool life with diffusion and deposition techniques [136]–[138]. PVD and CVD coatings have in the recent years gained significant popularity in metal forming industry due to their intrinsic high wear resistance and low friction properties. Podgornik et al. [113] studied the galling properties of tool steels with four different PVD coatings. The study showed that deposition of a DLC coating of the WC/C type provided excellent protection against material transfer in the contacting interface. A comparative study on the mechanical and tribological characteristics of DLC coatings was furthermore conducted by Vercammen et al. [139]. The study concluded that the mechanical and tribological properties of DLC coatings could vary greatly depending on the specific coating type. Murakawa et al. [140], [141] and Taube [142] investigated the applicability of DLC coated forming tools for deep drawing of aluminium under dry conditions. The studies showed that certain surface coatings possessed promising anti-galling properties with good adhesion to the substrate. Sgarabotto and Ghiotti [143] presented a study on the mechanical and tribological characteristics of TiAlN and CrN coatings with a S390 cold working tool steel. The coatings were evaluated with a flat drawing test, pin-on-disc test and a scratch test for evaluation of the COF, wear resistance and adhesion to the substrate. The TiAlN coating was found to have superior wear resistance and adhesion behavior, while the CrN coating was found to have the lowest COF in both dry and lubricated conditions. In 2011 Ghiotti and Bruschi [144] conducted a similar study for evaluation of the performance of DLC coatings compared to TiAlN and CrN coatings with a K340 cold working tool steel substrate, by reproducing the kinematic and mechanical conditions of a typical industrial forming process. The study showed that a CrN-DLC coating system exhibited a low COF, low wear rates and strong adhesion to the substrate. Sresomroeng et al.

[145] characterized the tribological performance of commonly used PVD coatings by nano-indentation, ball-on-disk testing, scratch testing, and U-bend testing. The study found that the most efficient anti-galling tool coatings for high strength steels are characterized by having high hardness and a high elastic modulus. The anti-galling properties of the tool coatings are furthermore highly influenced by the adhesion between the coating and the substrate. Several authors [146]–[152] have conducted similar studies, with simple tabletop test equipment, for characterization of the tribological properties of different tool coatings for forming operations. Sato and Besshi [153] evaluated the anti-galling performance of cemented carbide and TiC, TiN, CrN tool coatings on an SKD11 substrate with a U-bending test. The U-bending test was conducted with a sheet material of alumnium 5052 with a white spindle oil with respectively 0, 5, 10 and 20 wt% chlorinated paraffins added to the oil. The study found that all the tool coatings which provided increased anti-galling performance compared to the untreated substrate. The cemented carbide was, however, found to exhibit the best tribological performance. Tamaoki et al. [154] studied the performance of a polycrystalline diamond coating for dry deep drawing of aluminium, mild steel and stainless steel. The study found that the polycrystalline diamond coating could obtain a similar limiting drawing ratio as when forming sheet material under lubricated conditions with a conventional die steel. The tool coating furthermore exhibited promising tribological performance when polished to a surface roughness of R_z= 0.5 μm with a special ultrasonic polishing technique. Liljengren et al. [155] conducted a comprehensive study on a systematic approach for selection of die materials, hardening methods and surface treatments for forming of high, extra high and ultra-high strength steels. Based on a U-bend test combined with a visual inspection of the surface quality of the formed component, a preliminary guideline was created for the selection of material and surface treatment of different deep drawing tool components.

The influence of the topography of the contacting surfaces of a tribosystem on friction and lubrication is well established in literature [156]–[159]. Enhancement of tribological properties by altering the surface topography of the tool and workpiece surfaces has been subject for research since the early 1980s [54], [160], [161] and a number of different techniques have since been applied for texturing of hardened tool surfaces. These techniques include shot blasting, electro-discharge machining [162], laster texturing [163], [164], electron beam texturing [165], chemical etching [166], rolling ball indentation [167] and milling combined with grinding and manual polishing [168]. The mechanism of lubrication by lubricant entrapment in tailored surface structures was initially described by Mizuno and Okamoto [169], who named the lubrication mechanism microplasto hydrodynamic lubrication. The mechanism of microplasto hydrodynamic lubrication has since been studied extensively by Kudo [170] and Azushima et al. [171]. Bech et al.

[172] studied the mechanism of lubricant entrapment in sheet metal forming, with a strip drawing test with a transparent tool with a similar test setup as described by Azushima et al. [171]. Bech et al. tested the influence of varying lubricant viscosity, drawing speed, reduction, die angle, back tension, workpiece material and frictional conditions. Based on the experimental observations a theoretical model was established for the mechanism of lubricant escape. Models for the description of the lubricant entrapment mechanisms have since been developed by Lo and Wilson [173], Azushima [174] and Stephany et al. [175]. Mousavi et al. [176] showcased a preliminary study on the combined influence of blank preparation, tool coating and tool structuring for supporting a deep drawing operation under dry conditions. Several studies have furthermore investigated the enhanced wear and friction conditions introduced by the implementation of structured tool surfaces [177]–[181].

Chapter 3 Process monitoring in sheet metal forming

Galling is a wear phenomenon commonly encountered in various sheet metal forming processes, often occurring when working with tribologically difficult materials such as stainless steel, Al- or Ti-alloys. The galling mechanism is characterized as a localized macroscopic transfer of metallic material between contacting surfaces, where surface damage progressively increases in severity. The occurrence of galling is a major issue in sheet stamping industry since it causes tool damage, poor surface quality of the formed components and production stops. It is reported that galling accounts for up to 71% of the cost of die maintenance [182], [183] in stamping industry. Online process monitoring of sheet metal forming operations is therefore of significant interest in order to actively minimize the occurring wear in production to increase productivity, reduce maintenance costs and increase tool life. Online evaluation of the wear state of the forming tools can, therefore, form the basis for scheduling of condition-based tool maintenance and eliminate the unscheduled stoppages in production due to tool wear. Early detection of the onset of galling can thereby allow for the implementation of preventive measures such as repolishing and recoating of the forming tools. While online condition monitoring of machining process like turning, milling and drilling have been subject for extensive investigation during the last 40 years, condition monitoring of forming processes has received less attention [184]. Different types of strain, acceleration, force, proximity, optical, acoustic emission (AE) and audio sensors [185] have been applied in preliminary studies on condition monitoring of sheet metal forming processes. Since tool wear, in conventional sheet metal forming, occurs in the contacting interface between the sheet metal and the forming die, online process monitoring for sheet metal forming operations require an indirect measuring technique with sufficiently high sensitivity to detect any minute differences in the process, in order to evaluate the wear state of the process. Direct evaluation methods such as visual inspection and image processing techniques are therefore deemed to have limited applicability for this purpose. Conventional indirect measuring techniques, e.g. measurement of process loads, have however typically been found to have too limited sensitivity for assessment of tribological conditions in complex stamping operations [186]. Measurement of AE has, on the other hand, been successfully applied as an online monitoring technique for evaluation of different tribological characteristics in different metal forming operations [187]–[189]. Behrens et al. [190] found that acquisition and analysis of

AE signals allow for online assessment of production conditions and deviations in production processes. Skåre [191] similarly noted that energy analysis of the AE signals allows for an evaluation of the quality of lubrication and detection of process deviations in the sheet metal forming operations such as the stick-slip effect and cracking. Mostafavi and Pashmforoush [192] successfully applied the AE technique for detecting the onset of galling in a slider-on-sheet test, noting a direct relation between the wear mechanism and peak AE amplitudes. Several studies [187], [188], [193]–[206] have noted a similar correlation between wear severity and different time domain parameters. Common for these studies are, however, that they were conducted with simple simulative tests e.g. pin-on-discs tests with reciprocating or rotary motion, that do not encompass the complexity of simulative sheet metal forming tests or actual production tests. Most studies found in literature, are furthermore conducted in controlled laboratory environments, and less attention is paid to the applicability of the AE technique for industrial applications. The present study, therefore, aims at evaluating the applicability of the AE technique for detection of the onset of galling and description of the continuous wear progression, for development of a methodology for online process monitoring for sheet metal forming operations. Based on preliminary studies on process monitoring of simulative sheet metal forming tests, the present study aims at deriving a methodology for characterization of friction, wear and process deviations that can be applied for monitoring of a deep drawing process.

3.1 Basics of acoustic emission

AE is a non-destructive testing technique based on the measurement of dynamic surface motion induced by a transient release of elastic stress waves. Elastic waves are generated transiently in solids in the ultrasonic frequency range due to mechanical stimulus e.g. caused by cracking, rubbing, polishing, impact, cavitation and leakage [207]. The occurrence of AE events is experienced as dispersed energy propagating as elastic waves, which can be detected using piezoelectric AE sensors. AE signals generally occur in two distinguishable forms; namely as burst signals or continuous signals. Burst-type emissions are characterized by being individual emission events of very short duration and larger amplitudes. A continuous AE signal is on the other hand defined as having a sustained signal level, which is produced by rapidly occurring AE events. Common waveform parameters for analysis of AE are defined in the ISO 12716: 2001 standard, see Figure 10.

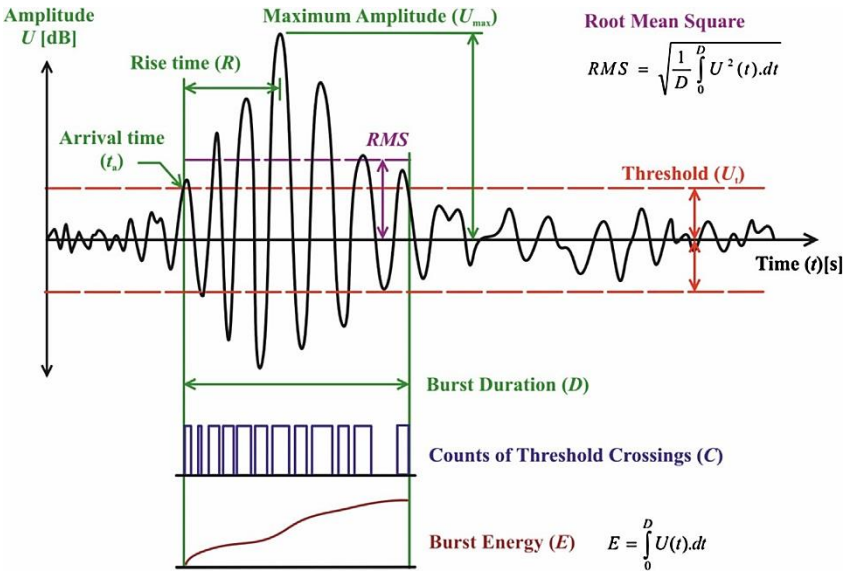

Figure 10: Illustration of common waveform parameters [208].

AE signals are composite signals [209] from different AE sources and different sources of background noise. The ability to detect abnormalities non-destructively has resulted in extensive use of AE for monitoring of different manufacturing processes [187], [210] and structural health monitoring [211], [212]. Signal processing of acquired AE signals, therefore, aims to evaluate the nature of the AE source by analysis and quantification of signal characteristics. Signal processing of AE signals often encompasses analysis of time-, frequency- and time-frequency domains. Selection of adequate signal processing methods is, however, highly dependent on the nature of the AE source and the objective of the analysis.

3.2 Determination of the coefficient of friction in a strip drawing test with acoustic emission

Preliminary study with AE monitoring was done with a strip drawing test for characterization of frictional conditions during the test with a common metal forming operation that emulates the forming condition in the flange region of a deep drawing die. The strip drawing test is furthermore a direct friction test that is commonly applied for evaluation of the COF in sheet metal forming. The study, therefore, aims at evaluating the COF with AE as an indirect measuring technique, compared to the COF normally evaluated by measurement of the normal force and the drawing force with conventional load cells.

3.2.1 Experimental setup

The strip drawing test was conducted with 500x50x1.5mm strips of aluminium NG5754. The strips were lubricated with a synthetic forming lubricant with a viscosity of 244.5 cSt with an applied coating weight of 1.5 g/m^2. For the test, 41.5x30mm tool inserts were used with an applied CrN coating on a base material of D2 tool steel. Two series of tool inserts were manufactured with surface finishes of respectively Ra=0.1 μm and Ra=1.7μm. A normal force of 10 kN was applied during testing. The strip drawing test consisted of four strokes drawn consecutively on the same tool surface with a total sliding length of 800mm.

The generated AE was measured with a National Instruments 9223 analog-to digital-converter with a sampling rate of 1MHz at a 16-bit resolution, connected through a National Instruments 9174 4-slot expansion chassis. Simultaneous data acquisition was carried out using a preprogrammed setup in LabView, with a data segmenting function in order to avoid buffer overflow. A R15α general purpose, narrowband AE sensor from Physical Acoustics was attached to the base of the tool holder, see Figure 11, with a thin layer of grease-paste to improve acoustic coupling. The AE sensor has an operational frequency range of 50 - 400 kHz and a resonant frequency of 75 kHz. The sensor was connected to a Physical Acoustics 2/4/6 analogue signal preamplifier with a 60 dB signal gain. The analogue signal preamplifier had a built-in bandpass filter of 20-1200 kHz. The Nyquist sampling theorem states that a continuous signal can be represented correctly if the captured waveform is sampled at a sampling rate of more than twice its highest frequency component. If this condition is not fulfilled the captured signal will experience an overlap of signal frequencies. This phenomenon is called signal aliasing. A sampling rate of 1 MHz was therefore selected in order to support the operational range of the AE sensor and suppress signal aliasing and loss of signal amplitude at

high frequencies. The same AE test setup is used for the following laboratory tests described in this chapter.

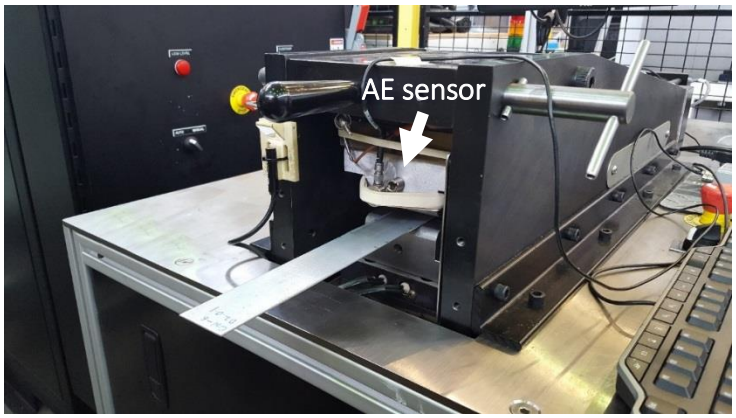

Figure 11: Strip drawing tester at the University of Warwick.

Due to a physical restriction in the test machine, the only possible location for placement of the AE sensor was at the base of the tool holder, as shown in Figure 11.

3.2.2 Experimental results

The measured COF and AE signal is shown in Figure 12.

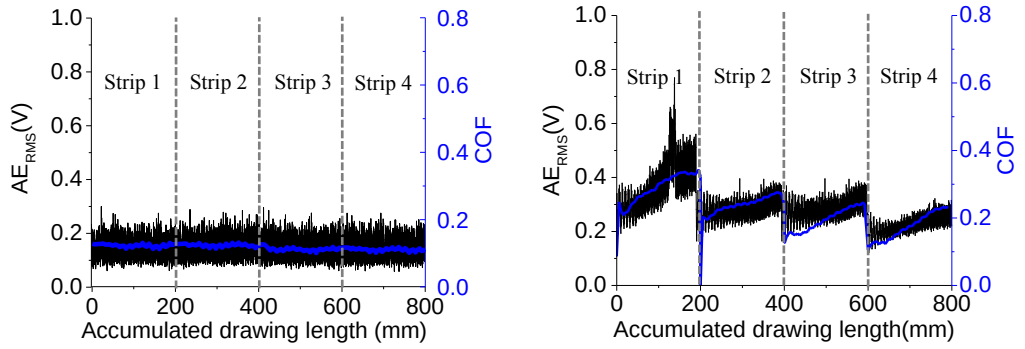

Figure 12: Development of the COF and the AE signal with a tool insert with a surface finish of (a) Ra=0.1 µm and (b) Ra= 1.7 µm.

Upon testing, the surface structure of the aluminium samples were evaluated with white light interferometry with the Alicona Infinite Focus G4. An overview of the surface structure of strips after testing is shown in Figure 13.

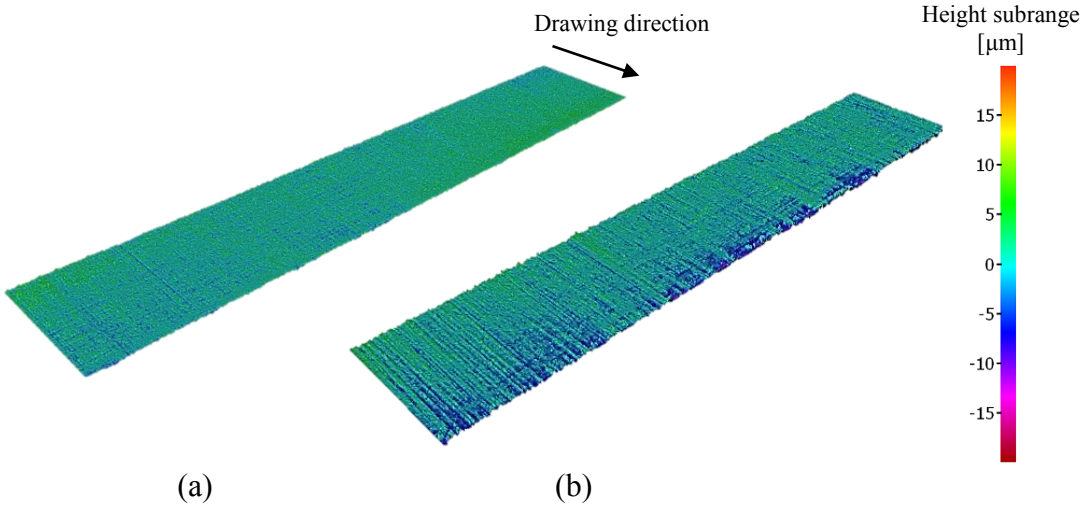

Figure 13: Surface structure of the aluminium strips after testing with a tool insert with a surface finish of (a) Ra=0.1 µm and (b) Ra= 1.7 µm.

Evaluation of the surface structure of the strip material after testing and the measured COF indicates that the highly polished tool surface introduces stable forming conditions that generates a smooth surface on the strip material and a low COF of approximately 0.1. The test series conducted with a tool insert with a surface roughness of Ra=1.7 µm is found to have cyclic increase and decrease in the measured COF between each strip that was drawn. This behavior is attributed to the increased surface roughness of the tool, which causes delamination of the CrN coating. The delaminated wear particles act as third body wear particles in the interface between the tool and the workpiece and thus introduce increased abrasion on the surface of the workpiece material, as seen in Figure 13b. The sudden decrease in the measured COF is caused by the removal of third body wear particles when a new strip is inserted into the strip drawing tester between each stroke. The measured RMS signal is found to be in good agreement with the COF that was determined by measurement of the drawing force and the normal force with piezoelectric load cells. The AE signal is furthermore found to have comparable sensitivity to the changes in the frictional conditions experienced during testing in the two different test series, as the measurements made with conventional load cells.

The preliminary test with AE as an indirect measuring technique for evaluation of the basic forming conditions in a strip drawing test was found to give promising results. Further testing is required for establishing a methodology for measurement of the generated AE, data treatment and quantification of tribological characteristics during testing.

3.3 Determination of the coefficient of friction in an upsetting ironing test

For further characterization of the frictional conditions in forming operations, the upsetting sliding test is used as a supplementary test for evaluation of the COF with AE. The upsetting sliding test developed at The Polytechnic University of Hauts-de-France is [213] used for evaluation of forming tribological conditions in bulk metal forming operations.

3.3.1 Experimental setup

The upsetting sliding test is conducted by inducing plastic deformation by upsetting a cylindrical workpiece with a semi-circular forming tool, followed by a vertical displacement of the workpiece, see Figure 14.

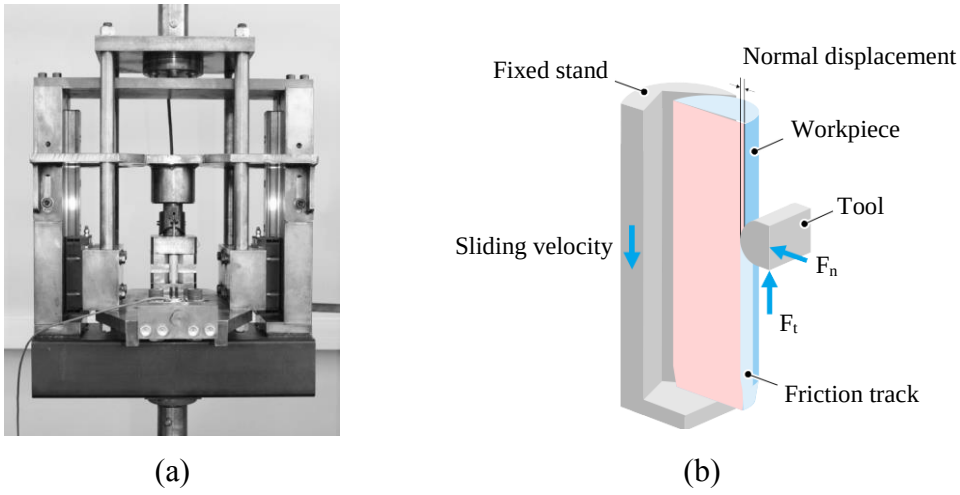

Figure 14: Upsetting sliding test shown by (a) the test stand and (b) a schematic illustration of the upsetting sliding process [214].

The upsetting sliding test was conducted with a 49 mm Ø15 6082-T6 aluminium alloy cylinder as the test workpiece and an R20 tool of X38CrMoV5-3 hot work tool steel lapped to a surface roughness of Ra=0.4 µm. A 5 mm beveled edge was machined into the base of the billet to ensure proper initial contact upon displacement of the workpiece. The test was conducted with a 0.1 mm penetration and a sliding speed of approximately 50 mm/sec. A pure, high viscosity mineral oil was applied to the surface of the billet prior to testing. The test stand, shown in Figure 14a, was equipped with two load cells for measurement of normal and tangential forces during testing. Eq. 2 shows how the COF can be determined using the measured forming forces [215].

$$\theta_1 = arcos\left(1 - \frac{p}{R_0}\right) \quad (1)$$

$$\mu = \frac{\sin\theta_1 \frac{F_T}{F_N} - (1 - \cos\theta_1)}{\sin\theta_1 + (1 - cos\,\theta_1)\frac{F_T}{F_N}} \quad (2)$$

where p is the penetration, R_0 is the indentor radius, θ_1 is the maximum angle of contact between the indentor and the workpiece, F_T is the tangential force and F_N is the normal force.

3.3.2 Experimental results

The measured forming forces and an overview of the tool and workpiece geometry are shown in Figure 15. The acquired AE signal during testing and a spectrogram made with a Short Time Fourier Transform (STFT) for analysis of the frequency components, is shown in Figure 16.

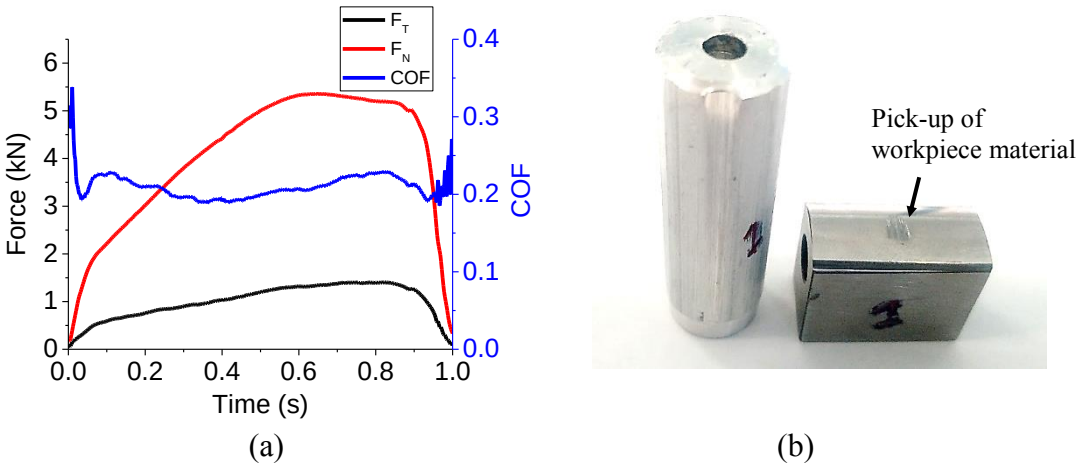

Figure 15: Experimental results from the upsetting sliding test with (a) the measured tangential, F_t, and normal force, F_b, during testing and (b) an overview of the workpiece and forming tool after testing.

Figure 15 shows that upon initial stabilization of the forming forces, the COF fluctuates between 0.19 and 0.22 during testing. Inspection of the tool surface reveals minor levels of adhesive wear accumulated on the tool surface. The minor increase in the COF initiating after approximately 0.4 s is therefore attributed the pick-up of workpiece material on the tool surface.

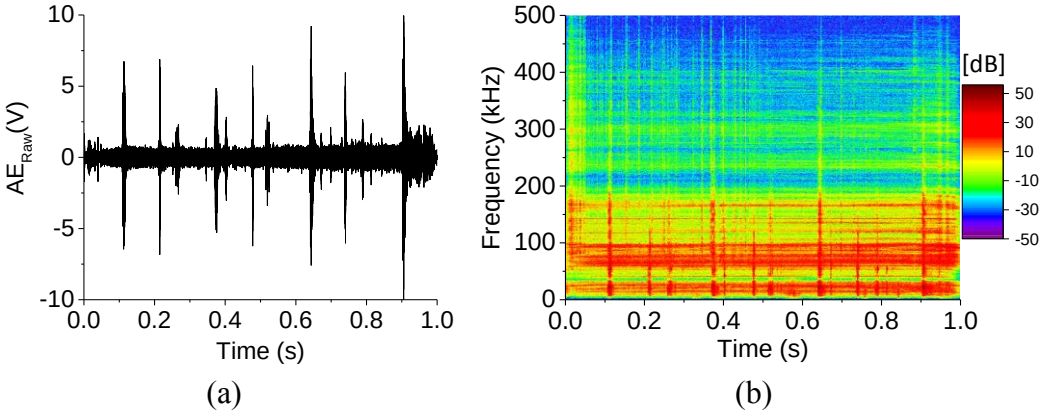

Figure 16: Signal analysis of the acquired AE during testing with (a) the raw AE signal and (b) STFT of the AE signal.

The captured AE signal is found to contain highly periodic burst type emissions with high amplitudes, as seen in Figure 16a. Spectral analysis of the AE signal shows that these burst emissions appear in a wide frequency range from 5-340 kHz, with the highest amplitude found in the 5-200 kHz frequency range. The frequency range central to the forming process is found to be 5-95 kHz, where continuous emissions are measured during testing. The periodic burst emissions are possibly attributed to the hydraulic drive system implemented in the test setup. In order to minimize the influence of the external noise sources a band-pass filter of 5-95 kHz is introduced, see Figure 17.

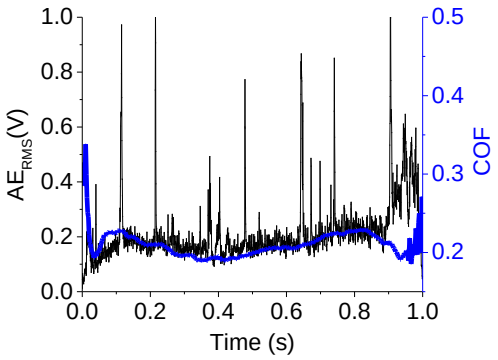

Figure 17: Development of the COF and the AE signal during the upsetting sliding test after introducing a 5-95 kHz band-pass filter.

As seen in Figure 17, the application of a highly restrictive band-pass filter aids the suppression of the influencing signal noise. Several high amplitude peaks are, however, still present after filtering. Good agreement is found between the RMS value and the COF, as also seen in the strip drawing test. Minor deviations between the AE signal and the measured COF is found in the first and last 0.1 seconds of the test due to the start and stoppage of the sliding sequence.

3.4 Detection of the onset of galling in a strip reduction test using acoustic emission

Based on the findings from the preliminary studies with the two friction tests, a SRT was studied for monitoring of wear conditions during testing and evaluation of the influence of different test setups and their implicated characteristics (e.g. noise sources and process kinematics) on the captured AE signal.

3.4.1 Experimental setup

The SRT, see Figure 18, is a testing method used to emulate the forming conditions in an ironing process. The SRT is conducted by placing a strip on a supporting plate, which is fixed in a tool jaw, while a cylindrical tool pin is loading the top of the strip to a defined reduction in thickness. The strip is subsequently drawn with constant speed.

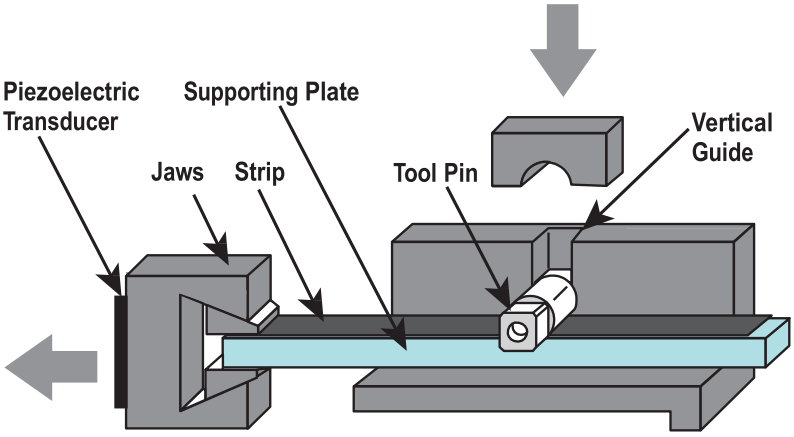

Figure 18: Schematic illustration of the experimental setup for the SRT [216].

The SRT was performed with a 20% reduction in thickness of a 1mm EN 1.4307 stainless steel strip using a Ø15 mm AISI M3:2 tool pin, polished to a surface roughness of Ra = 0.06 µm. The drawing length was 300 mm, and the drawing speed was approximately 70-100 mm/s. Three different lubricants were used for the test. A description of the lubricants is given in Table 2.

Table 2: Overview of the lubricants used for the SRT.

Code	Name	Description	Viscosity at 40°C (cSt)
CR5/Sun60	Houghton Plunger CR5, Sunoco Sun 60	Mixture of 50 wt.% Sunoco Sun 60 plain low viscosity naphthenic mineral oil and 50 wt.% Houghton Plunger CR5 high viscosity mineral oil.	60
Pn226	Castrol Iloform PN 226	Medium chlorinated paraffin oil with S-, P-, ester-additives, and ZDDP	66
D321R	MOLYKOTE D321-R	Air-curing dry lubricant with molybdenum disulfide and graphite	-

The lubricant was applied manually on the surface of the strip with two different configurations. In the first configuration, the lubricant covered the entire surface of the strip material, while in the second configuration the lubricant was only applied to the surface on the first half of the strip. This was done in order to have a well-defined limit where a transition from good to poor lubrication is experienced during testing.

After the SRT, the surface roughness of the strip was measured with a 30 mm measurement interval with a Surtronic 4+ roughness tester with a cut-off filter of 0.8 mm. The surface quality of the tested strips was furthermore inspected with scanning electron microscopy (SEM).

3.4.2 Pencil lead breaking test

The pencil lead breaking test is a commonly used method for determining system performance with analysis of a reproducible artificial AE source [217]. This source type is often called a Hsu-Nielsen source based on the work done by Hsu and Nielsen [218]. The pencil lead breaking test was conducted by pressing a mechanical pencil at an inclined angle against a surface, with a sufficient pressure to cause breakage of the lead. The breakage of the lead releases transient stress waves that can be used for evaluation of system characteristics like the sensor coupling and signal attenuation in the structure. For the current study, the pencil lead breaking test was applied for the evaluation of optimal sensor placement during testing. The sensor placement is, in the current study, limited to the tool housing due to a restriction of the physical space in the tool setup. The influence of placing the sensor on different positions on the tool housing is, however, to be studied with the pencil lead breaking test. The pencil lead breaking test was conducted with a Ø0.5mm 2H type pencil lead at an angle of 30° with a length of 3mm. The pencil lead breaking test was conducted with four repetitions, in accordance with the

ASTM-E-2374-10 standard, for each of the two different sensor placement locations, see Figure 19.

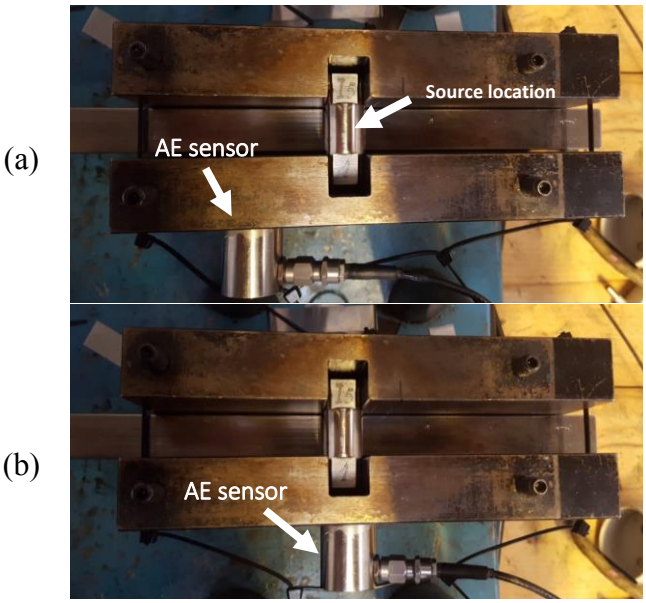

Figure 19: Sensor positioning for the pencil lead breaking test. (a) Position 1: 32mm from the center of the tool pin. (b) Position 2: At the center of the tool pin.

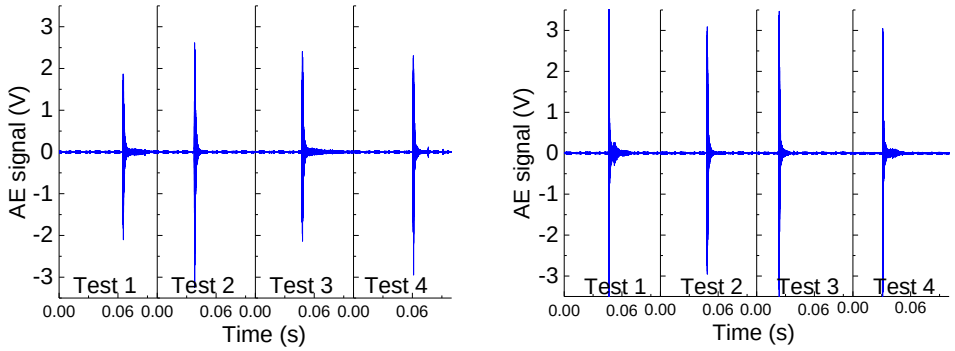

Figure 20: Measured signal amplitude during the pencil lead break testing at (a) Position 1 and (b) Position 2.

By evaluation of the measured signal amplitudes in the two test series, it is found that across the four test repetitions an average reduction of 1,23 V is measured in the peak amplitude of the signal when the sensor is moved 32mm from the center of the tool pin. The optimum sensor placement, for the present study, is therefore at the center of the tool pin, closest to the interface between the tool and the surface of the workpiece, where the signal experiences the smallest amount of signal attenuation.

3.4.3 Experimental results

An overview of the surface structure of the strips after testing is shown in Figure 21 and Figure 22. The corresponding measurements of surface roughness and the raw AE signal are shown in Figure 23 and Figure 24.

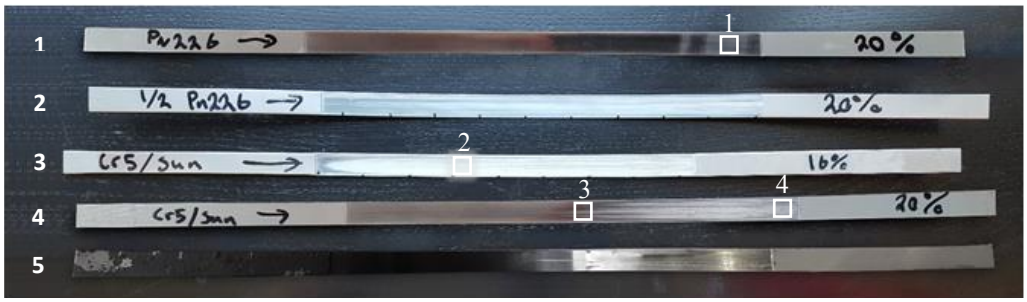

Figure 21: Overview of the surface structure of the strips upon reduction of the thickness.

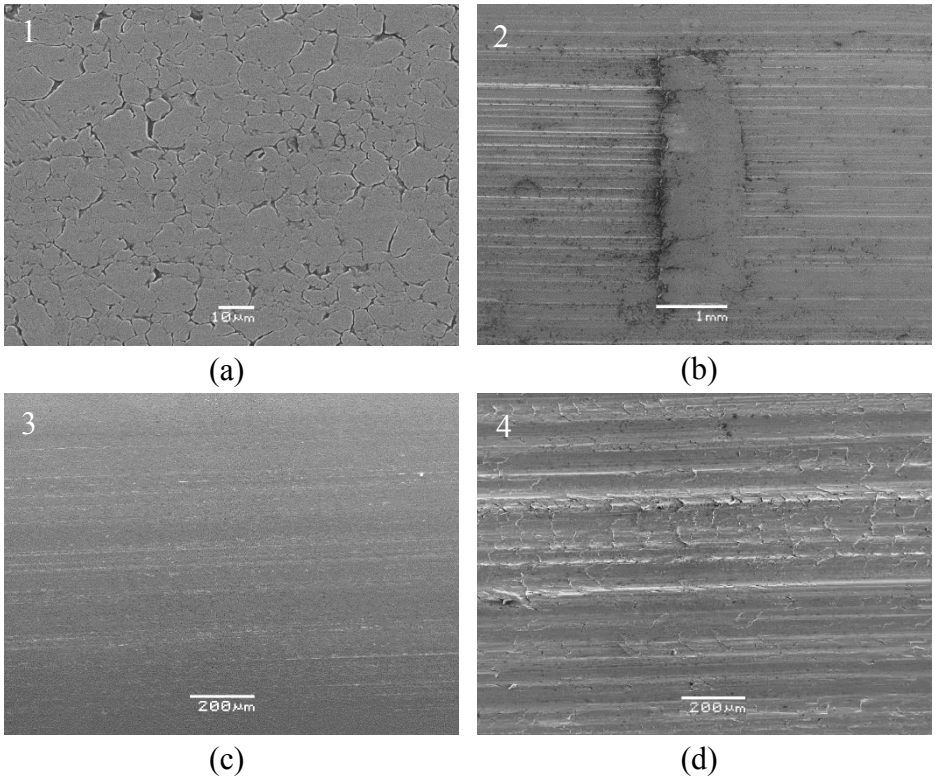

Figure 22: SEM micrographs of different regions of the strips after testing. The listed numbers refer to the locations shown in Figure 21. (a) Smooth surface finish obtained with the Pn226 lubricant. (b) Fracture of a friction junction using the Cr5/Sun60 lubricant. (c) Minor scratches on the sheet surface using the CR5/Sun60 lubricant. (d) Severe scoring of the sheet material using the CR5/Sun60 lubricant.

By evaluation of the surfaces structure of the strips after testing, it is found that the Pn226 lubricant with the chlorinated additive package exhibits a very good lubricant performance that inhibits the occurrence of galling. The SEM image, shown in Figure 22a, shows that the strip has a smooth surface structure, where the surface asperities have been flattened during testing. The Cr5/Sun60 lubricant conversely shows very poor performance, with substantial scoring of the workpiece surface during testing. Figure 22c shows the initial stage of galling with Cr5/Sun60 lubricant, with the development of minor scratches on the workpiece surface. At an increased sliding length, seen in Figure 22d, the developed wear increases in severity due to the breakdown of the lubricant film and pick-up of wear particles on the tool surface.

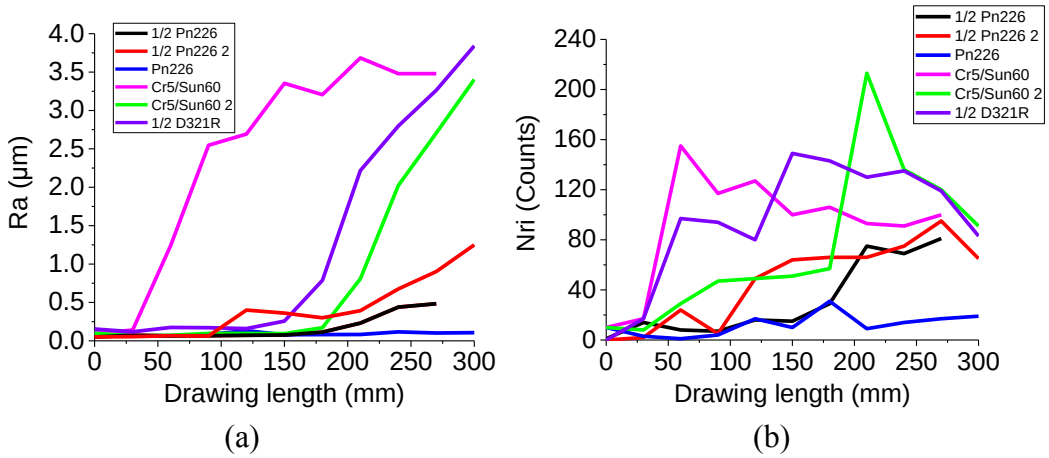

Figure 23: Measured surface roughness after testing: (a) Arithmetic mean roughness value and (b) Number of valleys deeper than 0.5 µm.

For characterization of the surface structure of the strips after testing two roughness parameters were evaluated, see Figure 23. Evaluation of the Ra-parameter is from previous studies [79] found to give a good indication of the overall wear state during testing. The Nri-parameter was defined by Andreasen et al. for quantification of wear in a SRT. The Nri-parameter is defined as the number of valleys deeper than 0.5 µm in the captured surface profile. The Nri-parameter can thereby give supplementary information about the surface structure, e.g. the occurrence of minor scratches, which is lost when averaging the roughness value as done with the Ra-parameter. The sudden increase in the Ra-parameter indicates the threshold sliding length for lubricant breakdown and subsequent initiation of galling.

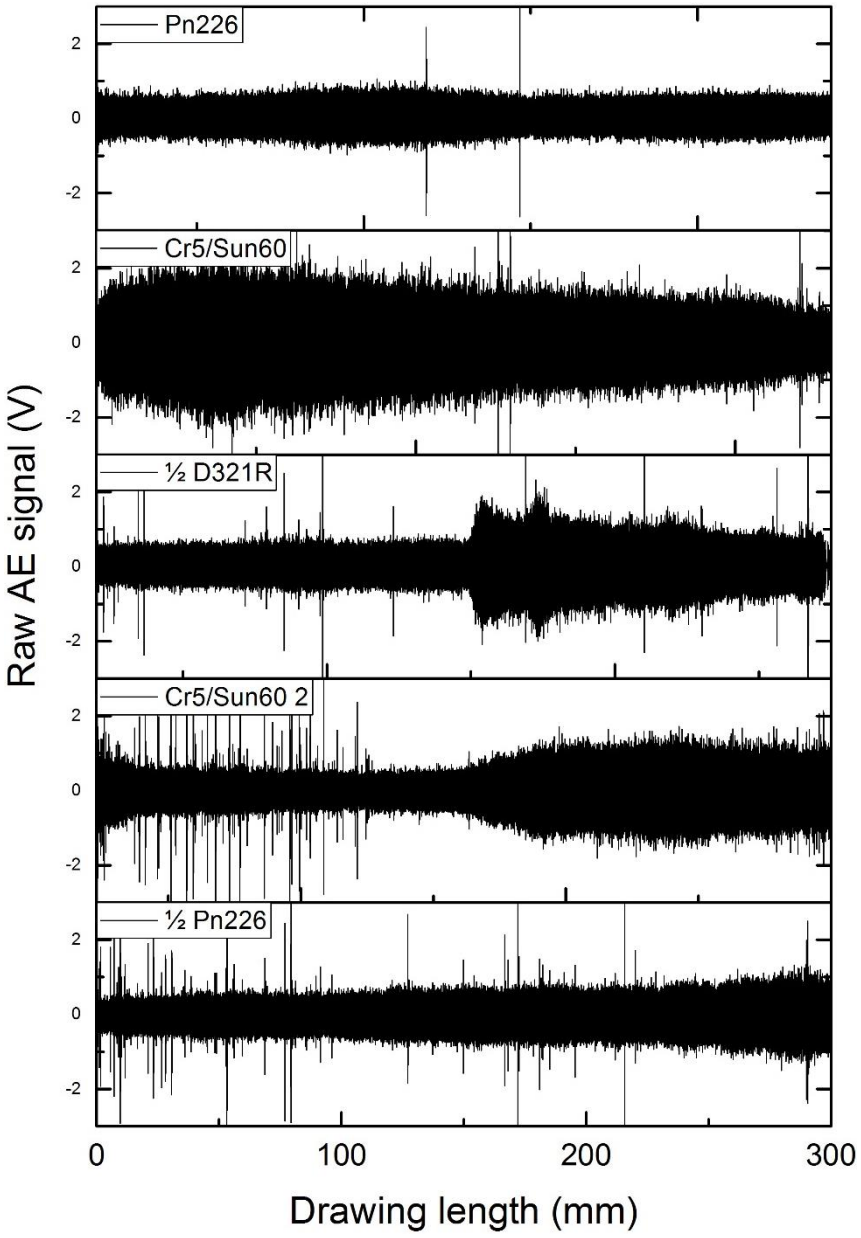

Figure 24: Raw AE signals from the different test series.

Initial comparison of the developed surface roughness of the workpiece during testing and the generated AE reveals a correlation between the wear severity and the signal activity of the captured AE signal. The occurrence of a sudden, rapid change in the frictional conditions e.g. seen in the ½ D321R and Cr5/Sun60 2 test series can be seen in the captured AE signal as a large, continuous increase in the signal amplitude. The ½ D321 R test series, which is partly lubricated, furthermore reveals a very sharp transition in the captured AE signal due to the sharp transition from lubricated to dry conditions at the center of the strip.

The occurrence of other process deviations such as fracturing of friction junctions, see in Figure 22b, can also be detected with AE, where it is seen as a local decrease in the signal amplitude. This corresponds to the local decrease in the average surface roughness in the Cr5/Sun60 test series at a sliding length of approximately 110mm.

A preliminary frequency analysis was made with a Fast Fourier Transform (FFT) for characterization of the frequency composition of the acquired AE signals, see Figure 25.

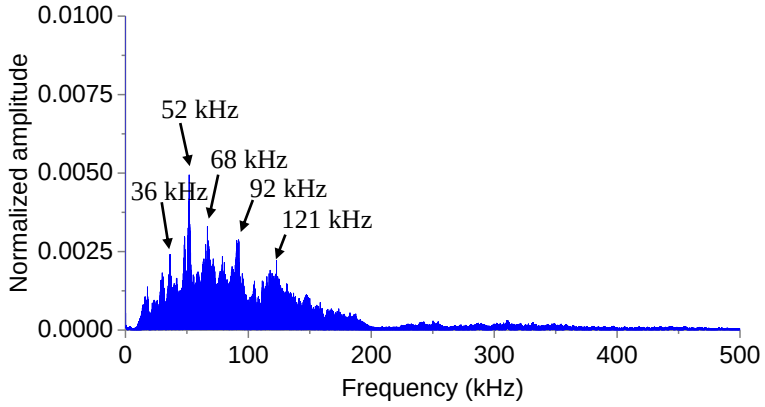

Figure 25: FFT of the AE signal from the ½ D321R test series.

From the spectral analysis of the acquired AE signal, it is found that five major frequency peaks at 36, 52, 68, 92 and 121 kHz can be distinguished. Based on these central frequency peaks, the influence of signal filtering is evaluated in Figure 26.

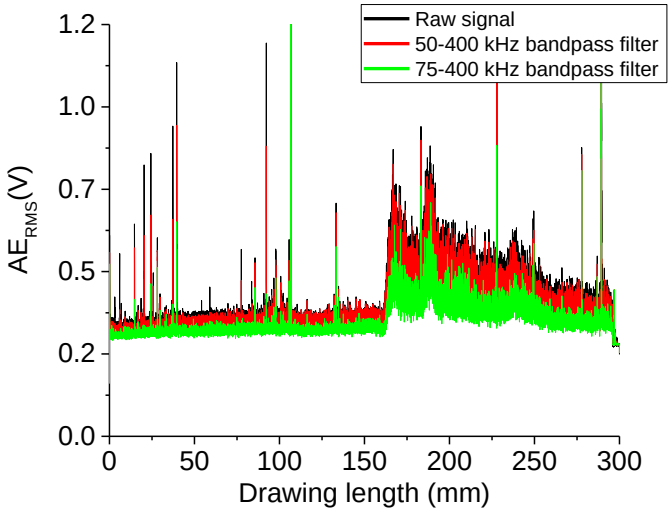

Figure 26: RMS of raw and filtered AE signals.

Figure 26 shows the RMS value of the raw AE signal compared to the RMS of the signals subjected to a band-pass filter of respectively 50-400 kHz and 75-400 kHz. The 50-400 kHz band-pass filter corresponds to the operational range of the sensor,

as specified by the manufacturer. The comparison of the signals shows that adapting progressively restrictive band-pass filters reduces the amplitude of the AE signal, while still maintaining the same development of the signal. This indicates that the acquired AE is not noticeably influenced by external mechanical or electrical noise sources. Analysis of the frequency content of the acquired AE signal furthermore shows that the signal generated during the SRT contains major peaks at lower frequencies in the range of 10-50 kHz. These peaks were detected with the R15α sensor, indicating that the sensor has a level of sensitivity outside the specified operational range defined by the manufacturer. In order to assess the frequency content of the signal and how it changes over the duration of the SRT a spectrogram was made with the STFT, see Figure 27.

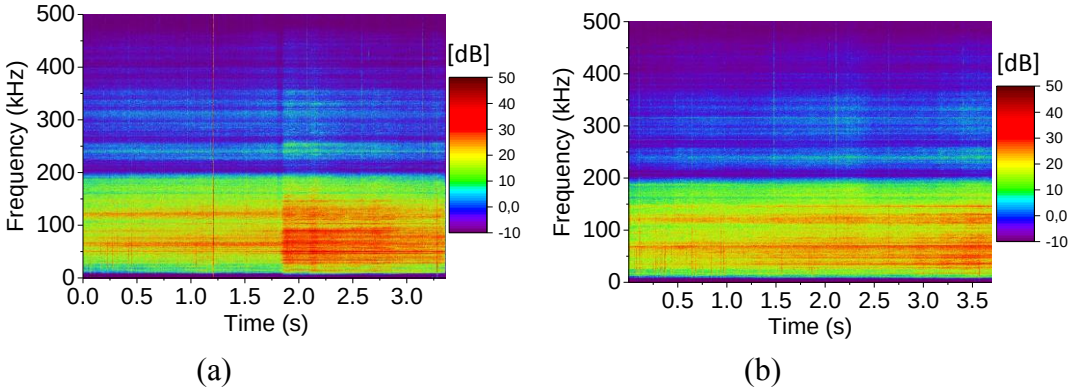

Figure 27: STFT analysis of the AE signal from the (a) ½ D321R test series and the (b) ½ Pn226 test series.

The spectrogram, shown in Figure 27, shows the central frequencies of the two test series, ½ D321R and ½ Pn226, over the duration of the test. Both test series were partially lubricated, where the onset of galling initiated at approximately a 150 mm sliding length with different severity of the subsequent wear development for the respective lubricants. For both test series the first half of the test, prior to lubricant film break down, is characterized by signal activity in the frequency range from 10-200 kHz, with the largest frequency peaks at 68 kHz and 121 kHz. At the onset of galling the ½ D321R test series experienced a sharp transition from lubricated to dry conditions, where the AE signal gains a large increase in signal amplitude for the frequency range 10-150 kHz. An increase in amplitude in the same frequency range is seen in the ½ Pn226 test series, however, with a gradual increase in signal activity due to the mild transition from lubricated to dry conditions for the oil-based lubricant. Across the different test series, the STFT shows that the occurrence of galling is in the AE signal reflected by an increase in signal amplitude in the frequency range of 10-150 kHz. The wear mechanism can, therefore, be quantified using a time domain based analysis. In order to methodically compare the different

test series, a threshold limit is established as a reference value for the signal activity under stable conditions without the occurrence of galling, see Figure 28.

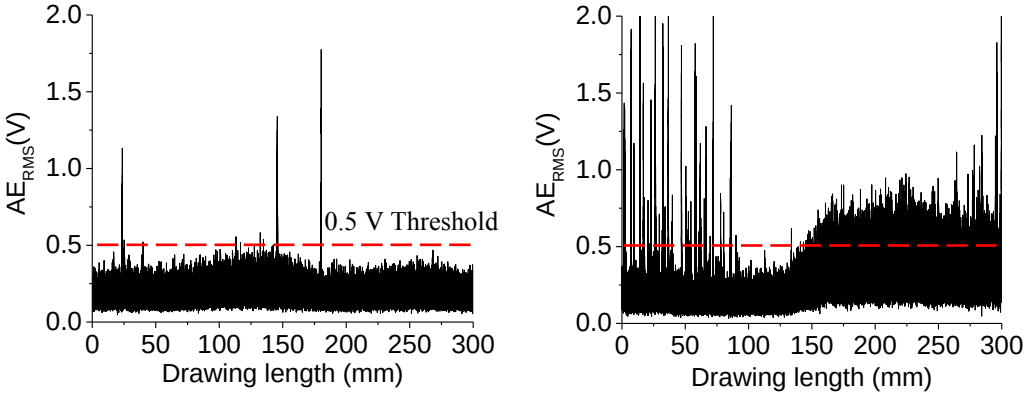

Figure 28: RMS of the AE signal from (a) the Pn226 test series and (b) Cr5/Sun60 2 test series.

The threshold value is established by taking the AE signal from the Pn226 test series, which resulted in a smooth surface structure, as a reference value. This threshold value encompasses the AE generated from the sliding friction, deformation of the workpiece material and possible influencing noise sources during testing. Comparing the Cr5/Sun60 2 test series to this threshold value shows a steady amount of threshold crossings within the first 150mm drawing length. Mild scratching was observed on the surface of the workpiece material in the first 150mm drawing length, corresponding to the increase in the number of valleys deeper than 0.5 µm, seen in Figure 23b. An increase in the count rate is found at a sliding length of approximately 150mm when the onset of galling is initiated, where a large increase in the Ra-value was measured. This indicates a correlation between the count of the threshold crossings and the wear severity experienced during testing.

In order to reduce the computationally expensive analysis of the captured signal, signal decimation was carried out by calculation of the RMS value of the signal with a 0.01 ms integration constant [219]. This eases the process of data analysis since the high sampling rate typically used for analysis of AE often results in the generation of very large data sets. Adaption of the RMS value therefore greatly decimates the size of the data set and rectifies the signal. The RMS value describes the AE energy over time, which is the main parameter of interest for evaluation of the frictional conditions, as seen in the strip drawing test and the upsetting sliding test. An overview of the number of threshold crossings and the corresponding development of the measured surface roughness is shown in Figure 29.

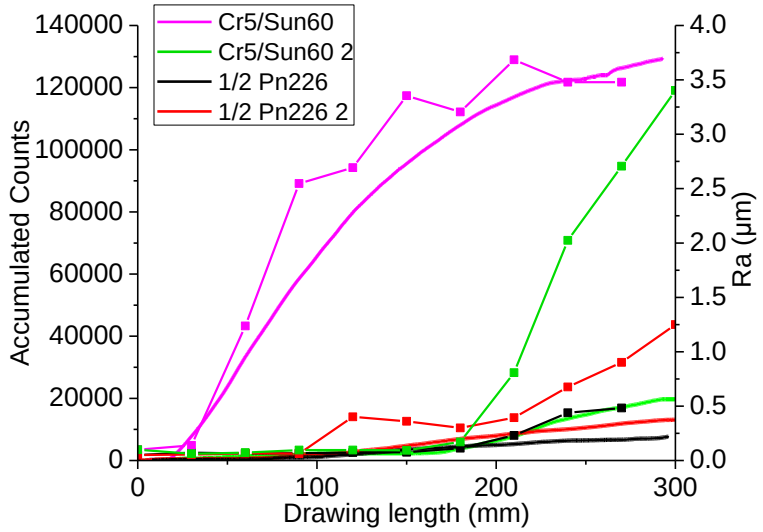

Figure 29: Accumulated threshold counts compared to the developed surface roughness (marked with dots).

It can be gathered from Figure 29, that the first test series with the CR5/Sun60 lubricant has a high level of AE activity, due to the immediate onset of galling. This is in good agreement with the developed surface roughness, which correspondingly indicates a rampant increase in the surface roughness. The second test series with the same lubricant indicates a lower wear rate with increased severity approximately at a 150mm drawing length. The strips, which were partly lubricated with the Pn226 lubricant, indicate a minor level of signal activity after a drawing length of 150 mm, in accordance with a small increase in the average roughness values. This indicates that the AE method has sufficient sensitivity to detect the occurrence of minor levels of galling. The presented methodology thus allows for an initial estimation of the onset of galling through assessment of the acquired AE. Accumulating the counts above the threshold value allows for an assessment of the point in which galling initiates, defined as the threshold drawing length where a continuous increase in signal activity is experienced. The severity of the occurring wear and the lubricant quality can therefore also be evaluated by comparing the total amount of counts above the threshold value. This furthermore indicates a direct correlation between signal activity and the roughness of the generated surface, which is indicative of the wear severity. This allows for a direct ranking of the lubricant efficiency during testing.

3.5 Continuous monitoring of a strip reduction test using acoustic emission

Since the preliminary tests were all limited to single stroke operations with sliding lengths of 50-500mm where accelerated wear rates are experienced, a final test campaign was conducted for evaluation of the gradual deterioration of a tribosystem with process conditions that emulate an industrial process layout. The usage of DLC tool coatings [220] has previously been found to prolong the tool life of forming tools while reducing the demands of the lubricants used for different metal forming operations. This allows for a more environmentally benign production without the use of hazardous lubricants. While facilitating production without the use of hazardous lubricants, the occurrence of coating deterioration can cause damage to the forming tools and produce components with diminished surface quality. The present study, therefore, aims at evaluating the progressive deterioration of a tool coating and the subsequent onset of galling during testing using AE.

3.5.1 Experimental setup

The SRT test was conducted with two cylindrical tool pins of AISI M3:2 with a diameter of Ø15mm, polished to a surface roughness of Ra = 0.02µm prior to deposition of a surface coating of 3µm DLC upon a 3 µm AlTiN-based base coating of Hyperlox®. An illustration of the SRT setup is shown in Figure 30. The workpiece material used for the SRT was EN 1.4307 stainless steel, with a width of 30mm and a thickness of 1mm, where a 20% reduction in the sheet thickness was performed during testing. For the test, a drawing sequence was performed with a 40mm stroke length and a sliding speed of 50mm/s with an idle time of 0.5s between each stroke. A schematic illustration of the tool setup is shown in Figure 30.

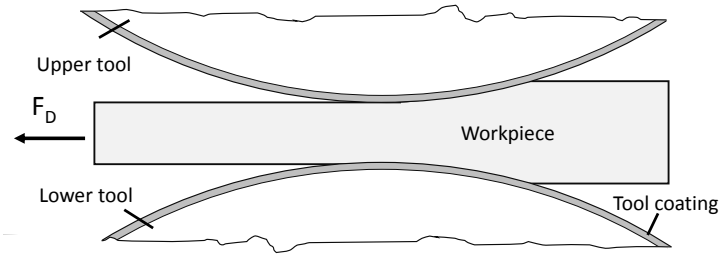

Figure 30: Illustration of the SRT tool setup developed for the UST.

3.5.2 Experimental results

The surface structure of the tool pins after testing is shown in Figure 31, where pick-up of workpiece material and delamination of the tool coating is observed. The generated surface structure of the workpiece material, which was in contact with the upper tool, is shown in Figure 32.

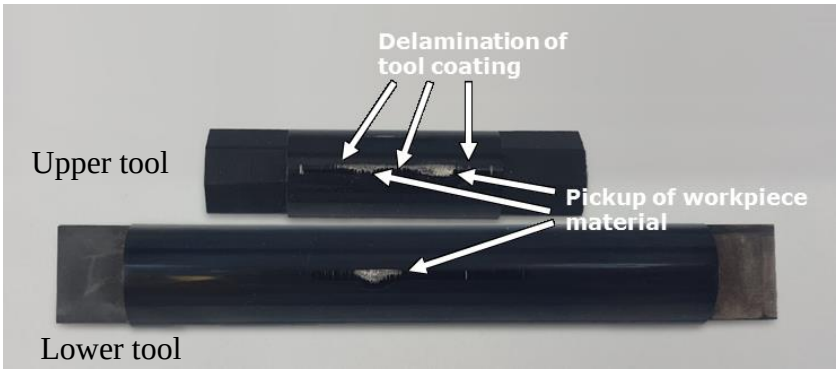

Figure 31: Tool pins after 726 strokes.

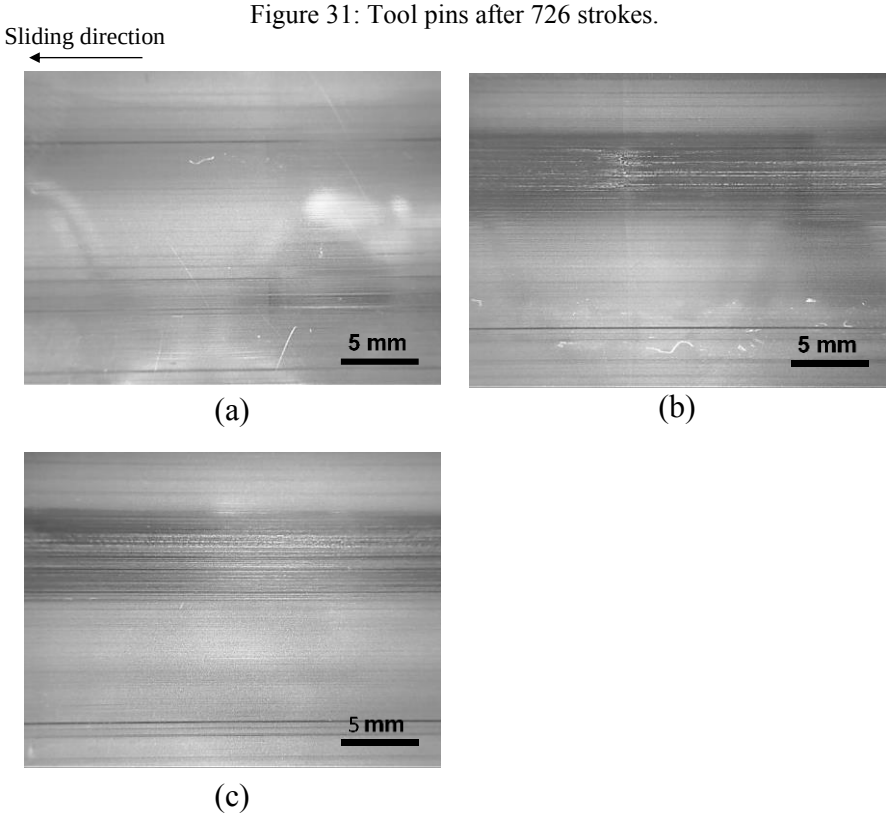

Figure 32: Surface structure of the ironed strip after (a) 38 strokes (b) 495 strokes (c) 722 strokes. The drawing direction is from right to left.

The drawing force and the generated AE during testing are shown in Figure 33.

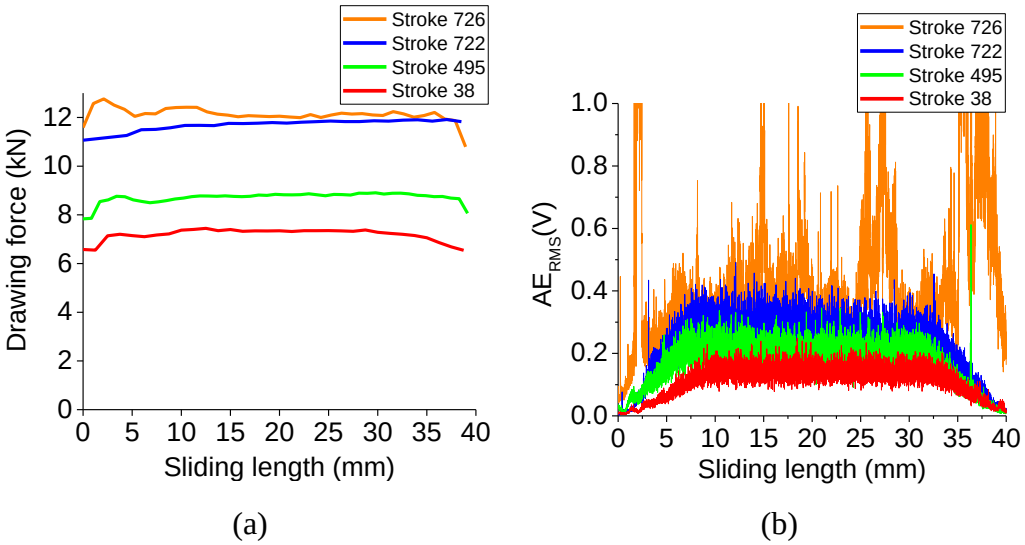

Figure 33: (a) Drawing force and (b) AE measured during testing.

From the force measurements, seen in Figure 33a, a stable drawing force is seen at stroke number 38, corresponding to the smooth surface structure in Figure 32a. At the onset of deterioration of the tool coating, at approximately stroke 495, an increase of the drawing force was measured. As the surface damage progressively increases in severity in the subsequent strokes, an increase in the drawing force was measured. Evaluation of the development of the drawing force is thus found to give a good basis for monitoring the occurring surface damage during testing. The generated AE during testing reveals a similar tendency, with a very low signal level at the initial strokes, while a significant increase in the signal level is noted after stroke 495, where surface damage is apparent on the workpiece material as shown in figure Figure 32b. Common for the AE measurements is furthermore that, an increase and decline in the signal amplitude is found in each stroke due to acceleration and deceleration of the carriage of the UST. From the surface structure of the tool pins after testing, seen in Figure 31, it is seen that the tool pins have experienced noticeable delamination of the top and base coating and subsequent accumulation of wear particles from the sheet material. AE activity measured in stroke 38, therefore, serves as a baseline that captures the AE generated during normal forming conditions, without a deteriorated tool coating. The gradual increase in the signal amplitude in the subsequent strokes indicate a deviation in the process due to accumulated damage of the tool coating. A drastic increase in signal amplitude is seen in stroke 726, where the strip fractures at the end of the stroke due to excessive pick-up on the tool pins. The generated AE during testing is therefore found to be highly correlated to the tribological conditions during testing. Assessment of simple time domain parameters such as the RMS level can, therefore, give detailed information about the process conditions during forming.

3.6 Monitoring of a deep drawing process

Several simulative forming tests have been examined, in this chapter, for derivation and refinement of a methodology for characterization of AE for online process monitoring of frictional conditions in sheet metal forming operations. Based on these findings an analysis on process monitoring of a deep drawing process is presented.

3.6.1 Experimental setup

Deep drawing of cylindrical cups was done with a Roell & Korthaus KG deep drawing machine. The test was conducted with Ø55mm 70/30 brass blanks with a 1mm thickness. For the test, a Ø35mm die with a rounding radius of 5mm on the die shoulder was used, with a blank holder force of 0,4 kN. Molykote DX paste was applied to the surface of the blanks prior to each test. Two die sets were used for the test. The first test series was conducted with a newly polished forming die, while the second test series was conducted with a worn die in order to evaluate the differences in the generated AE.

3.6.2 Experimental results

An overview of the surface quality of the cups drawn with the two die sets is shown in Figure 34. The cup formed with the worn die is found to have severe scoring on the cup wall, while the polished die results in a smooth surface structure.

(a) (b)

Figure 34: Deep drawn 70/30 brass cups formed with (a) a polished die and (b) a worn die.

An FFT analysis of the frequency components of the acquired AE signals during the drawing operation is shown in Figure 35.

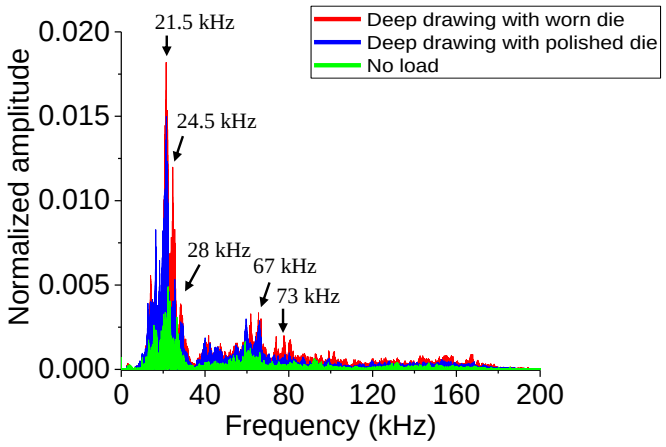

Figure 35: FFT of captured AE during deep drawing.

The FFT analysis reveals that the central frequencies of the deep drawing operation are primarily in the range of 10-180 kHz, as also seen in all the simulative process tests. The characteristic frequency peaks are highlighted in Figure 35. For evaluation of influencing noise from the hydraulic system, a test series was conducted where the blank holder force is applied without drawing of the sheet material. The frequency content of measured process noise is found to be centered around frequencies of 22 kHz and 61 kHz. In order to suppress the influence of the hydraulic noise, the AE signal is filtered with a high-pass FFT filter, as shown in Figure 36.

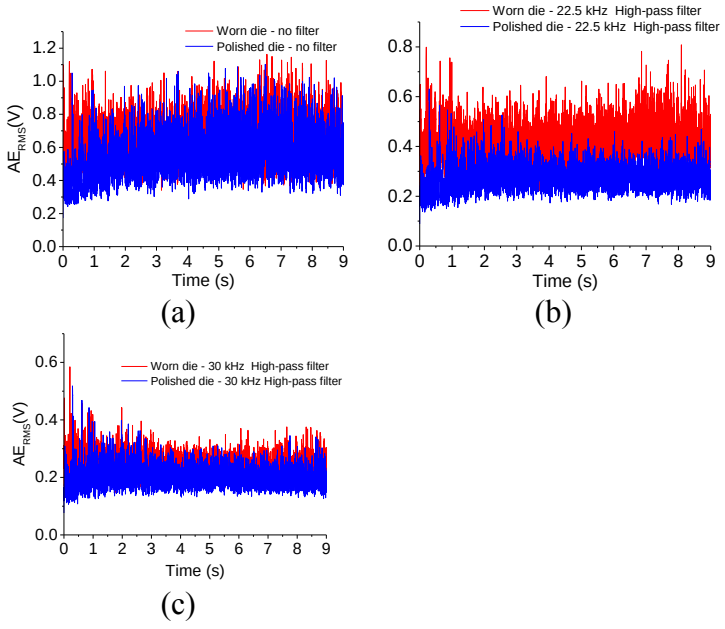

Figure 36: RMS of signals with (a) no filtering , (b) a 22.5 kHz high-pass filter and (c) a 30 kHz high-pass filter.

Adaption of a high-pass FFT filter is found to suppress the most dominant frequency components of the hydraulic noise. The central frequency range of the drawing operation is, however, found to overlap with the frequencies characteristic of the hydraulic system. Adapting an increasingly restrictive FFT filter can therefore also reduce the amplitude of the AE signal that contains information about the tribological characteristics of the drawing process. It is therefore difficult to evaluate the exact cut-off frequency necessary for optimal signal filtering. Adaption of a high-pass filter in the range of 22.5-30 kHz is however found to reduce the influence of the low-frequency process noise for initial characterization of the generated AE. Comparison of the two drawing sequences shows that deep drawing with the worn die generated an AE signal with a higher signal amplitude due to the scoring of the surface of the sheet material, as shown in Figure 36. A similar correlation between wear severity and signal amplitude has been found in all the previous simulative tests. Several concurrent studies [221]–[224] have similarly highlighted the possibility of characterizing wear behavior in stamping processes with time domain parameters.

3.7 Conclusion

The presented study examined the possibility of using measurements of AE as an online monitoring technique for characterization of forming conditions. Based on several different simulative forming tests, a correlation was found between the tribological conditions experienced during different sheet metal forming operations and the generated AE. Analysis of a strip drawing test and an upsetting sliding test showed that measurements of AE could be used for evaluation of the COF during testing with comparable sensitivity to measurements of process loads with conventional load cells. Measurement of the AE generated during the SRT allowed for assessment of different process parameters such as lubricant efficiency, quantification of surface damage and tool deterioration by comparing the developed AE signal to a reference value that indicates stable process conditions. Through analysis of these simplified laboratory tests, a methodology was derived for evaluation of process conditions with AE as an indirect measuring technique. Based on the derived methodology, measurement of AE was used for characterization of process deviations in a deep drawing operation. The study found that analysis of time domain parameters, with adequate signal filtering, could be applied for analysis of wear related process deviations.

Chapter 4 Wear and lubrication in stamping

Tool wear is a mechanism of surface damage commonly seen in sheet metal forming processes, caused by relative motion between tribologically stressed surfaces. Understanding the wear behavior and being able to evaluate the efficiency of different tribosystems is therefore valuable in order to facilitate a robust sheet metal stamping production. The nature of the wear mechanism is however highly dynamic and dependent on a range of different process and material parameters such as tool geometry, tool/workpiece material, surface conditions, process loads, speeds and temperatures. This makes a selection of a suitable tribosystem for a specific production platform difficult, in terms of evaluation of the necessary tool life and maintenance costs [225]. Several studies have highlighted the wear issues stemming from the adaption of new high strength steel grades in the automotive industry [226], further emphasizing the importance of selecting suitable tribosystems for sheet metal forming operations.

A number of studies have been conducted for characterization of tool wear in sheet metal stamping with numerical simulation. Hoffmann et al. [227] presented a methodology to simulate tool wear in sheet metal forming based on a wear coefficient that was determined by the deep drawing of a cup for quantification of the occurring wear. They furthermore presented a simulation scheme, where the changes in tool geometry caused by wear is implemented for simulation of the life cycle of stamping tools. Eriksen [228] presented a study where the optimization of a die geometry, in terms of minimization of the occurring tool wear, was achieved by FEM simulation of the Wear Index (which is identical to the wear work introduced later by Eq. (6)). It is similarly shown in several recent studies that an adaptation of the Archard wear equation gives an accurate description of the development of the tool wear. Pereira et al. [229] studied the influence of the contact sliding distance in a typical sheet metal stamping process. The analysis of contact conditions showed that a specific region in the tool interface is subjected to long sliding distances combined with high contact pressures, resulting in critical conditions in terms of the overall wear development. Wang et al. [230] investigated the influence of several process variables like binder pressure, lubrication coefficient and tool coatings on the tool wear distribution of a stamping die with numerical simulations. Based on the numerical simulations a selection of appropriate process parameters was tailored for optimization of the tool life. Wang and Masood [231] investigated the influence of various die profiles on the wear

properties of forming tools. Ersoy-Nürnberg et al. [232] presented a method of wear simulation with a modified Achard model, where a variable wear coefficient is implemented. Numerical simulation with the modified Archard model was shown to give an accurate description of the wear development at different stages of the tool life.

In the present chapter, an industrial case study on analysis of wear and lubrication in an industrial production platform is showcased. The case study is based upon the production of an exhaust gas recirculation (EGR) component made by the Danish company AAO Steel. A highly chlorinated forming oil has been used for stamping of the sheet material, to form the body of the EGR component. The company expresses the aim of substituting the chlorinated forming oil with an environmentally friendly lubricant in order to meet the legislative requirements. Based on the industrial case study, the presented work, therefore, aims at characterizing the tribological severity of the specified production platform for the selection of suitable tribosystems.

4.1 Industrial case study - Stamping of an emission gas recirculation component

EGR components are used in automotive applications for reduction of emissions in internal combustion engines and improvement of fuel economy. The manufacturing process for production of the EGR component is illustrated in Figure 37.

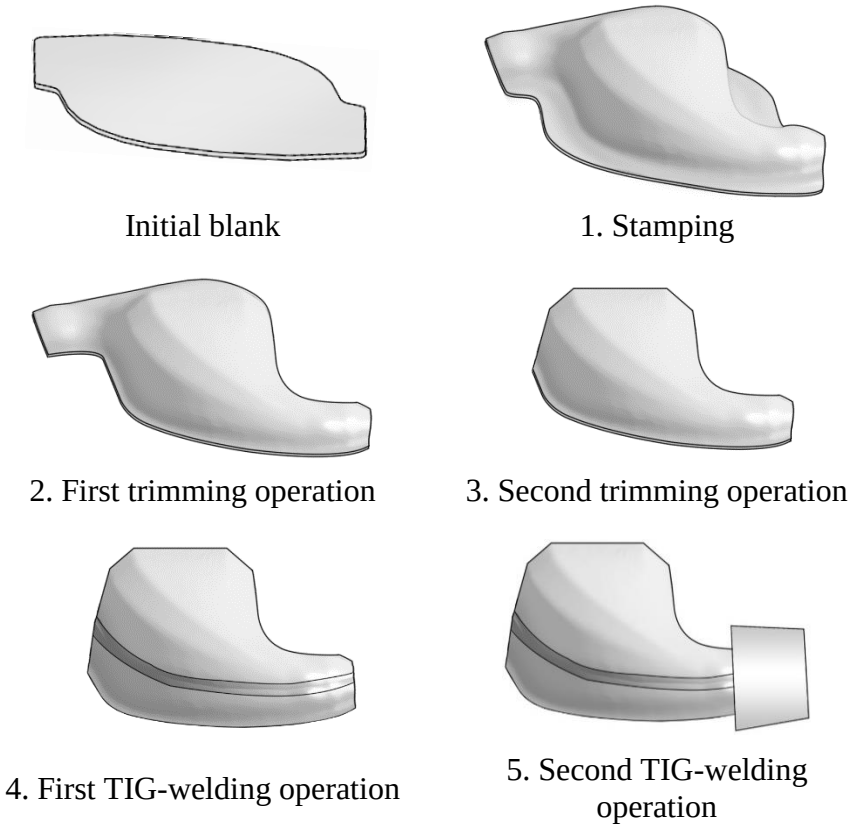

Figure 37: Schematic illustration of the production of the EGR component.

The initial manufacturing step consists of a one-step stamping operation of a 1.5mm thick blank of EN 1.4301 stainless steel. The formed component then undergoes a blanking operation for trimming of the remaining flange after the stamping operation. A second trimming operation is afterwards conducted, where the formed component is trimmed around the center line. The trimmed component is afterwards TIG-welded to a mirrored shell component, forming the body of the EGR component. In the final production step, the body of the EGR component is TIG-welded to a connector valve. The presented study is centered around the tribological problems related to the first production step, where the sheet metal is formed through a single stroke stamping operation. The stamping operation is carried out

with a manually operated hydraulic, single-action press with a draw cushion, where the forming die is lowered down upon a stationary draw punch. An overview of the forming tools is shown in Figure 38.

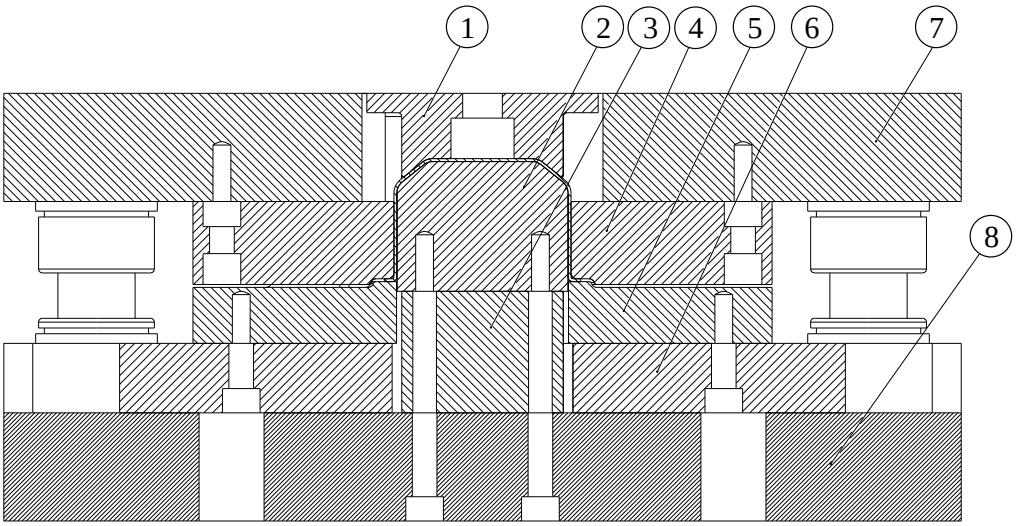

1. Counter-holder/ejector
2. Draw punch
3. Punch holder
4. Forming die
5. Blank holder
6. Draw cushion
7. Top plate
8. Press bed

Figure 38: Schematic overview of the forming tool components.

The forming tools were made from a Sleipner® tool steel, which is hardened to 60 HRC and polished to a surface finish of Ra = 0.05 μm. The first generation of the tool design was made without any further surface treatment of the tool steel. The manufacturer later made a second forming tool with a Tenifer® QPQ surface treatment for improved anti-galling performance. The lubricant used for the stamping process is Illoform BWN 205, which is a heavy duty deep drawing oil containing chlorinated paraffins. During production, the lubricant is manually applied to the surface of the sheet metal blank, with a paint roller by the press operator. This suggests that the lubricant dosage is loosely controlled and could vary significantly between the different press operators. The production rate of the component is approximately 150 parts per hour. The manufacturer specifies that a forming lubricant for this specific production platform should support a minimum of 200 strokes without deterioration of the surface quality of the formed component due to breakdown of the lubricant.

The manufacturer furthermore specifies that an alternative forming lubricant, besides a comparable tribological performance to the Iloform BWN 205, should be easily degreased and filtered by the lubricant recovery system in the press shop.

As shown in Figure 38, the forming die and the blank holder has a stepped drawbead geometry around the perimeter of the die opening in order to facilitate a correct flow of the sheet metal during the forming operation. The initial drawbead design proposed prior to die tryout is a fully penetrating drawbead with a rounding radius and bead gap approximately equal to the initial blank thickness. The final geometry of the drawbead was obtained through a trial and error procedure in the die tryout stage. In the die tryout stage, the die manufacturer alters the drawbead geometry by manual grinding, in order to tailor the restriction of the material flow. The final drawbead geometry, therefore, has a significant influence on the forming behavior of the component and the tribological conditions experienced in production. For automotive components made in stainless steel, like the EGR component, a guideline value for the maximum reduction in the thickness of the sheet material during forming is 20-30%, in order for the component to maintain sufficient mechanical integrity. This limits the maximal restriction of the material flow induced by the drawbead.

4.2 Methodology for offline testing of sheet metal forming tribosystems

As a systematic approach for analysis of tribosystem efficiency Ceron [13] proposed a methodology for offline testing of sheet metal forming tribosystems. The flowchart shown in Figure 39 summarizes the workflow of the methodology.

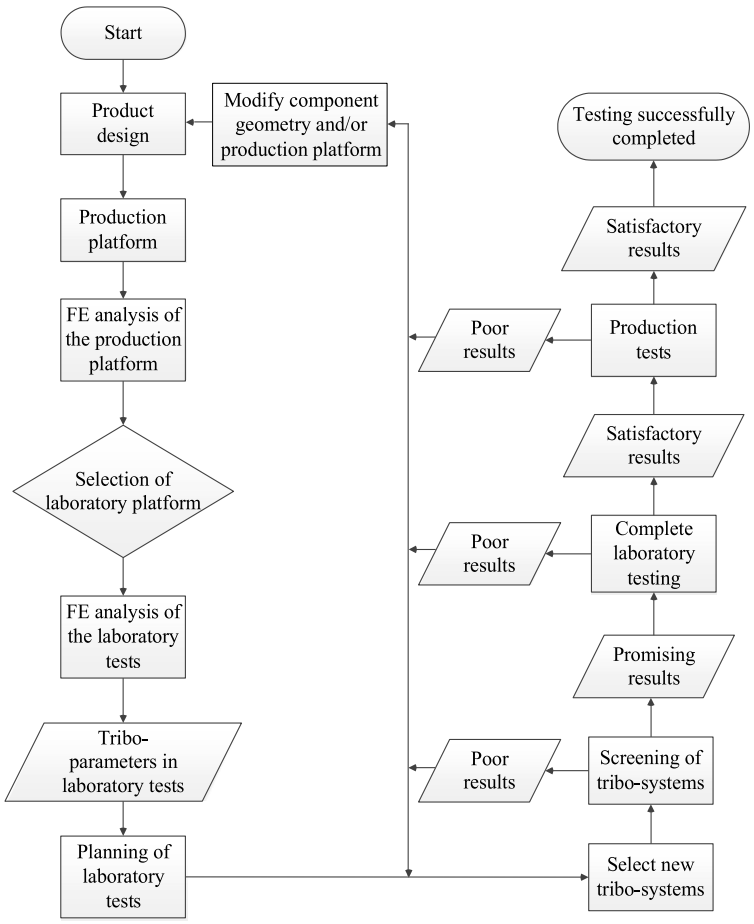

Figure 39: Methodology for offline testing of sheet metal forming tribosystems [13].

The methodology for offline simulative testing takes its starting point with reference to a specific product design, produced on an industrial production platform. The product design forms an initial outline of the main geometrical and mechanical properties that characterize the tribosystem e.g. blank size, shape and workpiece material. The production platform further specifies main process parameters like production rate, tool material and tool geometry. Finite element analysis can afterwards be used for investigation of the main tribological parameters that characterize the production process, for extraction of experimental parameters

that can be used for selection of an appropriate laboratory platform. Once a laboratory platform is selected, FE analysis can furthermore be used to ensure that the designed laboratory platform replicates comparable process characteristics compared to the reference production platform. Promising tribosystems can afterwards be evaluated by offline testing; whereafter full-scale production tests can be initiated with the most promising tribosystems.

4.3 Analysis of production conditions

4.3.1 Load and travel

Initial characterization of the forming conditions of the stamping operation was made by measurement of load and travel of the main press cylinders with built-in pressure and displacement transducers. The travel of the main cylinders of the press and the corresponding forming forces are shown in Figure 40.

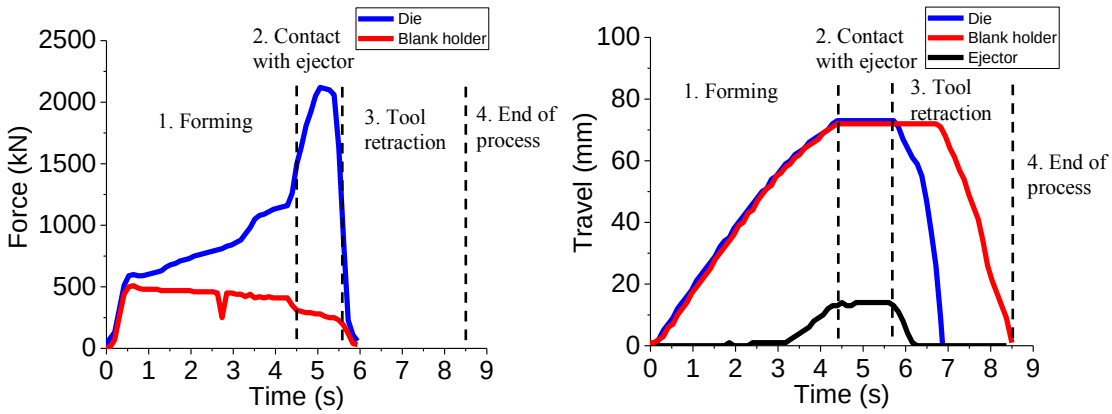

Figure 40: Overview of forming forces and the travel of the main press cylinders.

From the forming loads and travel of the press cylinders, the cycle time of the production process can be evaluated. The forming operation was conducted with an average blank holder force of 439 kN and a total process time of approximately 8.5 s, followed by an idle time of 16s between each formed component. In the idle time, the press operator manually removes the formed component and inserts a new lubricated blank into the forming tools. The process time consists of 4.5s of forming, where the sheet material is formed against the forming die and the draw punch. The travel of the main press cylinder is limited to a stroke length of 73mm,

whereafter contact is made between the draw punch and the counter-holder/ejector, resulting in a rampant increase of the force at the end of the stroke. In the final sequence of the forming operation, the forming tools are retracted, and the forming die is opened for manual removal of the formed component.

4.3.2 Measurement of die temperature

For evaluation of the temperature profile experienced during production of the EGR component, a series of thermographic measurements of the forming die were made during production with an AGEMA Thermovision® 570 thermal imaging camera. An overview of the setup is shown in Figure 41.

Figure 41: Thermographic measurement of the forming die.

The thermal imaging camera was positioned at a distance of 550mm from the forming die. Prior to conducting the measurements, the ambient temperature in the press shop was measured to be approximately 20.5°C. The relative humidity was further assumed to be 50%, as a common default value for thermographic measurements. Evaluation of the emissivity of the forming die was done by conducting reference measurements with a type K thermocouple at a specified reference point on the forming die. With this method an emissivity of 0.25 was determined. With proper calibration of the thermal imaging system, the manufacturer of the thermal imaging camera states the thermographic measurements have a measuring accuracy of ±2°C [233]. The thermographic measurements are, however, highly dependent on the approximated emissivity of

the measured object. The emissivity is, however, highly sensitive to several characteristics of the measured object such as material type, surface finish and the thickness of the oil film on the surface. The remaining oil film on the surface of the die can vary greatly since the sheet metal blanks are lubricated manually by the press operator. The amount of remaining oil on the surface can furthermore accumulate during the test series, resulting in a variable emissivity during testing.

Thermographic measurements were made with the first 50 strokes in the production of the EGR component, see Figure 42, whereafter a stabilization of the temperature profile was achieved. The thermographic image was captured after opening of the forming die and manual removal of the formed component, implying approximately 5-8 seconds between the end of the forming process and capturing of the thermographic image.

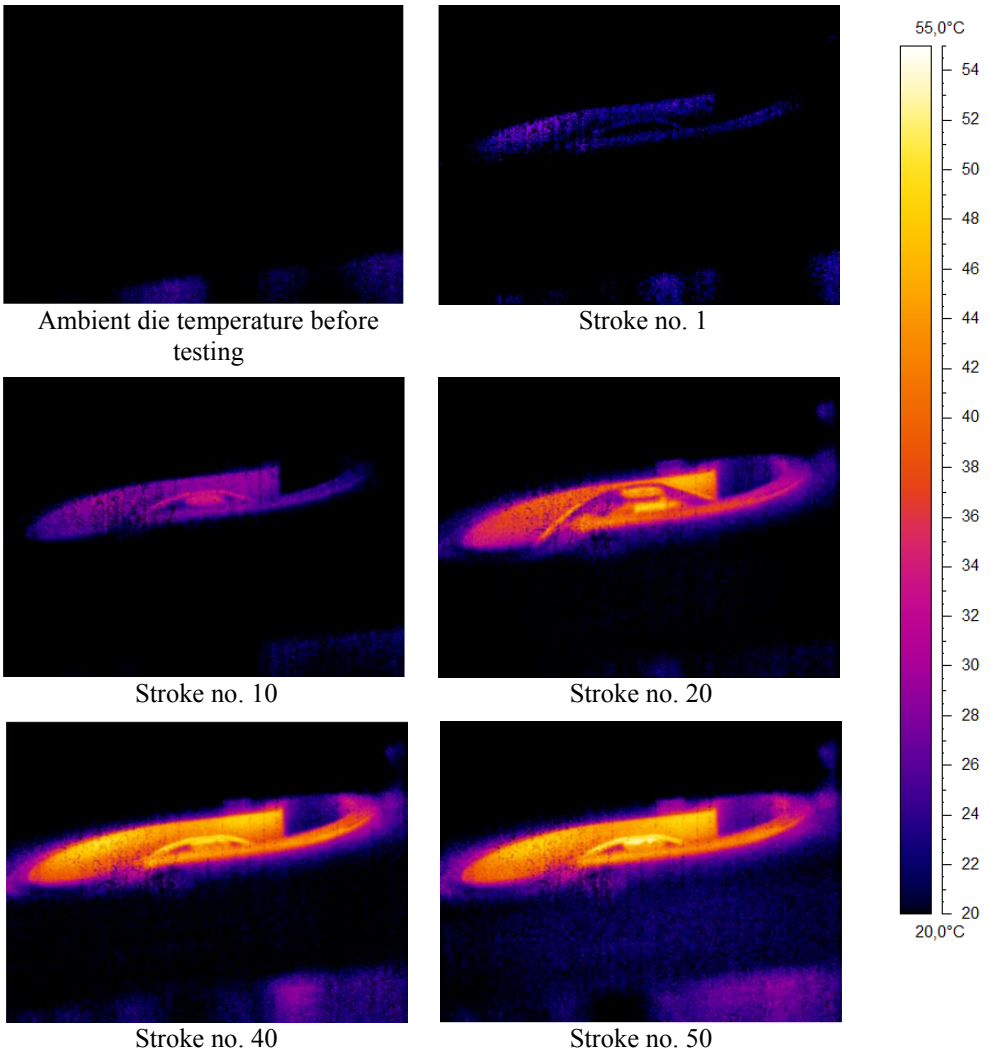

Figure 42: Temperature development in the forming die during the production of the EGR component.

4.3.3 Scanning of tool geometry

A 3D scan of the forming die was made using an ATOS Triple Scan optical scanner, see Figure 43. The optical scanner measures the geometry of the die by triangulation of a fringe pattern that is captured using a two-camera system. For measurement of the forming die, a series of 3mm reference points were placed on the die surface. Since the forming die has a highly polished surface, a thin layer of titanium oxide was sprayed onto the die in order to enhance the definition of the captured surface. Calibration of the optical system was done according to the recommended procedure from the manufacturer, Figure 43a. This involved measurement of a calibration panel from varying distances, positions and different orientations of the camera system. The measurements were carried out with a MV560 (560mm x 420mm x 420mm) lens setup at a measuring distance of approximately 830mm, in a temperature-controlled laboratory with an air temperature of 20.5°C ± 0.5°C. Two separate series of scans were conducted for the blank holder and the forming die, each consisting of 10-12 partial scans that were merged into a final model.

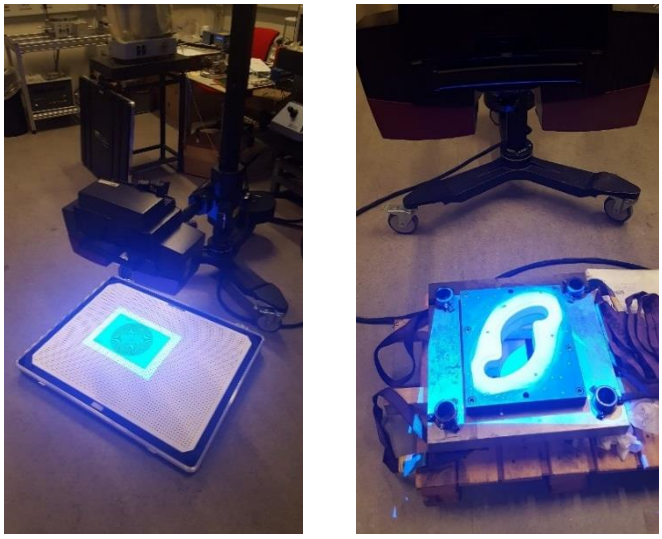

(a) (b)

Figure 43: Photographs from optical scanning showing (a) Calibration of the optical scanner. (b) Scanning of the forming die.

Post-processing of the obtained die geometry was done with the MeshLab software. Post-processing of the scanned die geometry consisted of removal of redundant, scanned features and down sampling of the generated point cloud with a Poisson-disc algorithm, in order to obtain a point cloud with approximately 40.000-50.000 data points. This was done in order to facilitate further processing of the scanned model, while still maintaining an accurate discretization of the die geometry.

A general overview of the drawbead geometry of the forming die is shown in Figure 44, from the 3D scans of the die geometry.

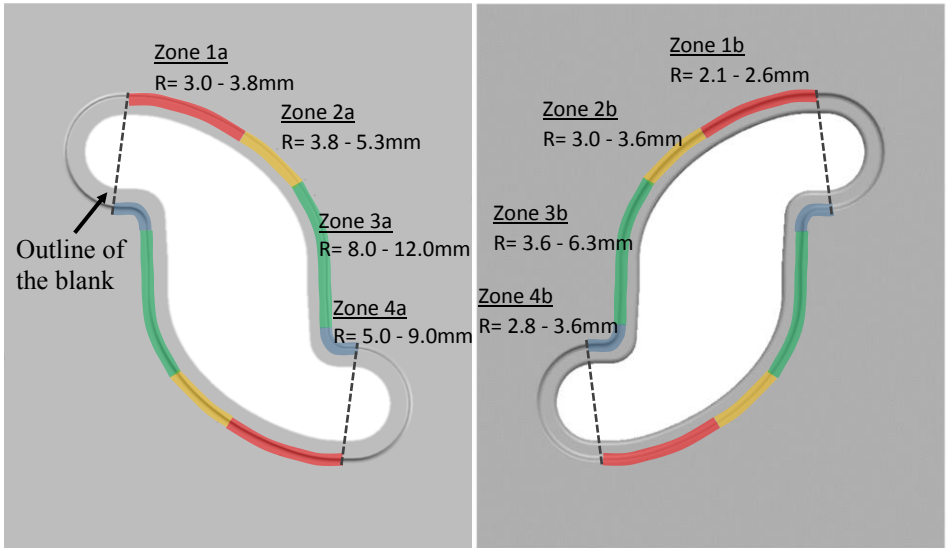

(a) (b)

Figure 44: Overview of the rounding radii of the drawbead geometry on (a) the blank holder and (b) the forming die.

Four zones, grouped by the size of the rounding radii of the drawbead, are identified on the blank holder and the forming die as seen in Figure 44. Zone 1 and zone 2 contain relatively small rounding radii, which results in heavy restraining of the material flow. Zone 3 and zone 4 contain larger rounding radii, resulting in a lesser restriction of the material flow. A sectional view of the drawbead geometry in zone 3 is shown in Figure 45.

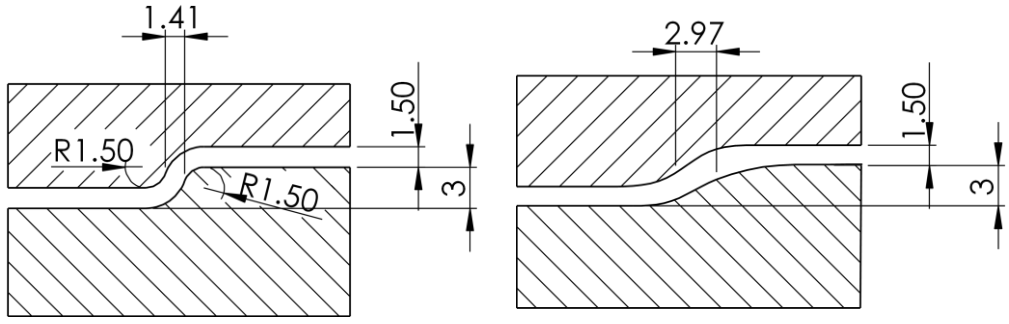

(a) (b)

Figure 45: Sectional view of the drawbead geometry in zone 3 (a) before and (b) after die tryout.

The sectional view of the drawbead geometry, shown in Figure 45, shows the dimensional changes made to the drawbead during the die tryout procedure. The initial rounding radius of the drawbead on the blank holder and on the forming die

is after the die tryout procedure increased and altered to have a gradual transition of the rounding radii. This is done by repeated manual grinding and polishing. The increase in the rounding radii is similarly found to increase the bead gap from being approximately equal to the initial sheet thickness (1.5mm) to 2.97mm. The stepped drawbead geometry, however, maintains the same bead penetration after the die tryout procedure.

4.3.4 Material model

Characterization of the mechanical properties of the EN 1.4301 sheet material was done with a plane strain compression test. The plane strain compression test was selected since the test allows for evaluation of the mechanical properties of materials at substantially higher strains than achievable with tensile testing. In order to satisfy plane strain conditions, the test was conducted with a sheet thickness to tool width ratio of t/w_t = 0.25-0.5. The width of the workpiece material should furthermore be at least five times its thickness. This is essential in order to obtain homogenous deformation and limit the influence of friction during testing. The plane strain compression test was conducted with a series of tools with widths of 2.5, 5 and 10 mm. The test was furthermore conducted with a 5mm stack of sheet material, i.e. 5 sheets, on a 60 ton Mohr & Federhaff hydraulic press. Prior to each test series, the tools were lubricated with a Molycote DX paste.

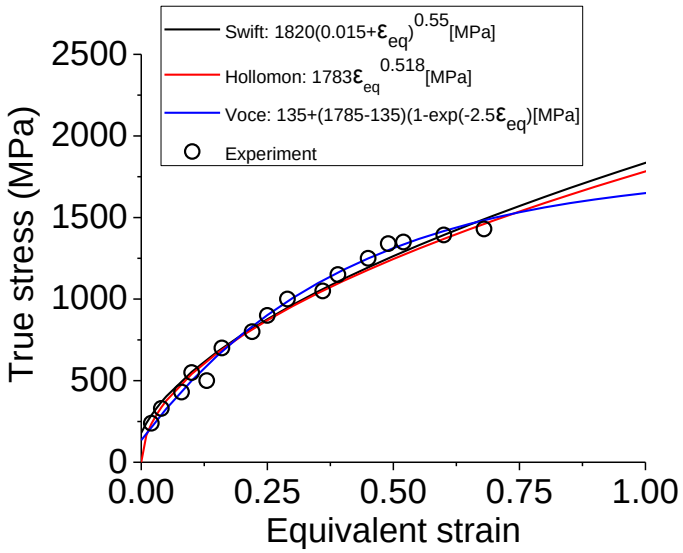

Figure 46: Stress-strain curve for the EN 1.4301 stainless steel.

Figure 46 shows an overview of the experimentally obtained data points, from the plane strain compression test, with curve fitting of common material models. For simulation of the stamping process, the Voce material model is selected since the

model accounts for the saturation of the work hardening behavior of the material, while material models based on power law regression often overestimates the flow stress when extrapolating to higher strains.

4.3.5 Analysis of sheet material flow during forming

The scanned model was imported into LS-DYNA for FE analysis of the stamping process. For the FE analysis, the forming tools were modeled as elastic steel tools with a variable mesh size of 0.5-1mm around the drawbead region, in order to adequately simulate the bending action introduced by the drawbeads. The geometry of the blank was modeled with a quadrilateral mesh with an initial mesh size of 2.5 mm. Adaptive remeshing of the blank was implemented, with three levels of mesh refinement during the simulation. The simulation was set up with a standard shell element formulation (Belytschko-Tsay formulation). Characterization of the strain hardening behavior of the sheet material was done with a plane strain compression test, where a Voce hardening curve of $\sigma_f=135+(1785-135)(1-e^{-2.5\varepsilon eq})$ [MPa] was determined for the material, see Figure 46. The Coulomb friction model was adapted for the FE setup with a friction coefficient of $\mu = 0.1$. The COF was determined by reverse analysis, as shown in section 4.4. With FE analysis the influence of the drawbead geometry on drawing behavior of the stamped component is illustrated in Figure 47 by comparing the outer contour of the flange to the initial blank contour.

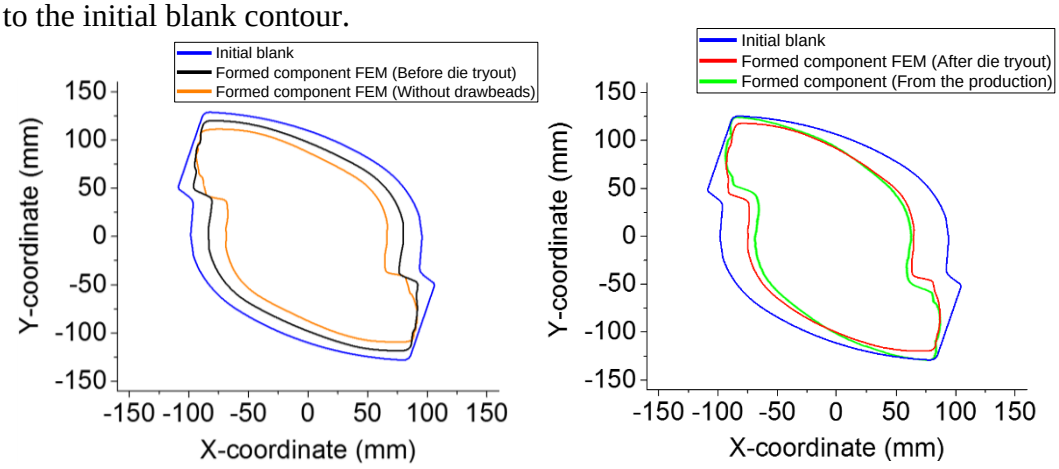

(a) (b)

Figure 47: Contour of the initial blank and the formed component after stamping with (a) the initial drawbead geometry and stamping without drawbeads and (b) stamping with the final drawbead geometry.

Figure 47a shows the restraining action of the drawbeads with the initial drawbead geometry, where the rounding radii of the drawbead is equal to the thickness of the

sheet material along the entire perimeter of the die cavity. This drawbead geometry results in a highly restricted flow of the sheet material. The initial drawbead geometry is furthermore found to introduce a uniform draw-in of the sheet material, throughout the perimeter of the die cavity. Forming the same component without drawbeads, shown in Figure 47a, will conversely result in excessive draw-in of the flange material and will not induce sufficient work hardening of the sheet material. Forming the component without drawbeads will furthermore increase the risk of wrinkling, due to inadequate stretching of the sheet material. Figure 47b shows that the drawbead geometry obtained in the die tryout introduces a variable restriction along the perimeter of the sheet metal blank, seen in the variable sliding length of the sheet material. Figure 48 shows the influence of the drawbead geometry on the shape and thickness of the formed component.

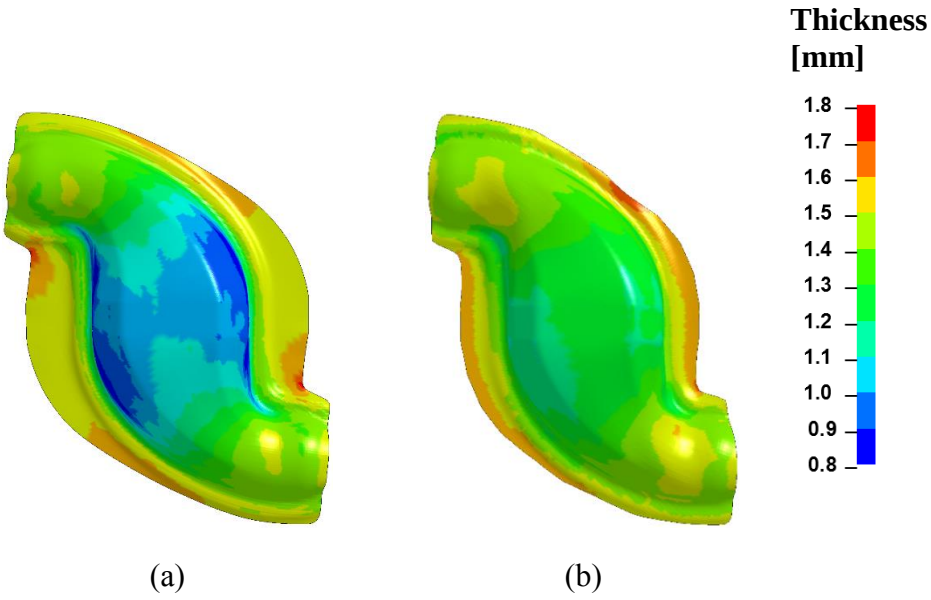

Figure 48: Thickness distribution of the formed component with (a) the initial drawbead geometry and (b) the final drawbead geometry.

Figure 48a showcases the influence of forming the EGR-component with the initial drawbead geometry. The large restriction in the material flow, due to the small rounding radii of the drawbead, results in a large flange remaining after forming and substantial thinning of the component. The large restriction of the material flow greatly exceeds the 20-30% formability guideline for automotive components in stainless steel, and the thinning will possibly also result in fracturing on the top part of the component, where the largest reduction in the thickness is found. The final drawbead geometry, however, results in a variable draw-in of the sheet material ensuring a uniform thickness of the formed component and that the component has a remaining flange that enables proper trimming and TIG-welding in the following production steps.

The analysis of the draw-in characteristics furthermore shows that the drawing behavior of the sheet metal can be approximated well with numerical simulations with the implementation of the scanned forming die. The accuracy of the FE simulation is evaluated by comparison of the outline of the formed component with the simulated result as well as a comparison the forming forces, see Figure 49.

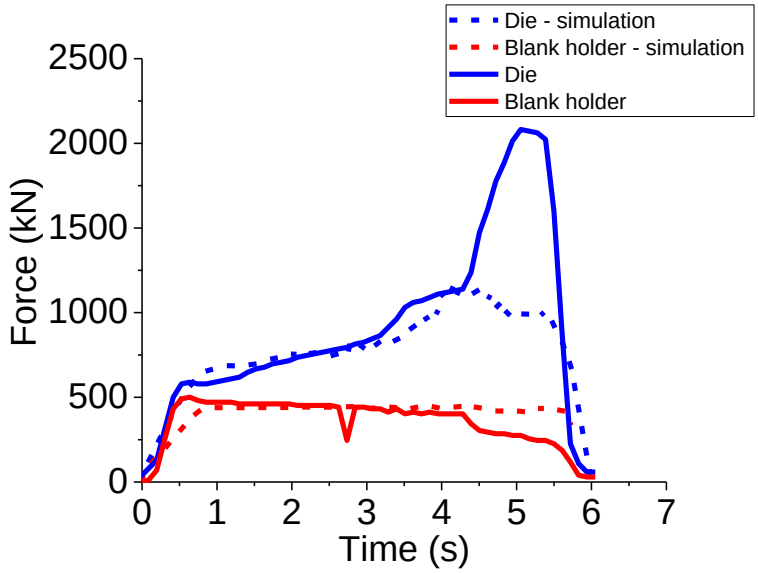

Figure 49: Comparison of the measured and simulated forming forces.

Minor deviations between the numerical results and the formed component are found in Figure 47, most noticeably, at the upper end of zone 1 where the flow of the sheet material is completely restricted and in zone 4 where the flow of the sheet material is underestimated in the simulation. Comparison of the forming forces in Figure 49 shows overall good agreement, however with a deviation at the end of the stroke, where the measured forming force has a rampant increase due to the contact between the draw punch and the counter-holder/ejector.

4.3.6 Analysis of process conditions and wear severity

A large number of models have been developed for the description of friction and wear phenomena, based on either empirical studies or basic principles of contact mechanics [234]. The Archard wear model [235] is the most commonly applied wear model in commercial finite element software for modeling of wear in manufacturing processes. The wear model states that the volume loss w (mm^3) due to wear is governed by the product of the normal force F_N *(N)* and the accumulated sliding length L (mm) and is inversely proportional to the surface hardness H (HRC). The wear coefficient K is determined by the material properties of the contact pair.

$$w = K\frac{F_N L}{H} \tag{3}$$

For adaption of the wear formula into finite element calculations, the wear volume change per unit area at a certain time step $\dot{w}$ is expressed by the normal pressure P *(MPa)* and the relative sliding velocity v_t,

$$\dot{w} = K\frac{P v_t}{H} \tag{4}$$

The total wear volume is obtained by integration of the wear volume rate over time,

$$w = \frac{K}{H}\int_t P v_t dt \tag{5}$$

The integral in Eq. (5) introduces the wear work Z *(MPa·mm)*, which allows for a qualitative evaluation of the wear severity independent of the material properties of the contact pairs, as the wear work is directly proportional to frictional energy dissipated in the contacting surfaces [236]. The wear work is thereby,

$$Z = \int_t P v_t dt \tag{6}$$

Holm [237] and Rabinowicz [238] described wear models with similar structures to Archard's wear model. The models were, however, applied for describing atomic wear in electrical contacts and abrasive wear respectively.

The variable forming conditions introduced by the drawbeads impose different tribological loads on the forming tools. For evaluation of the severity of the forming process, a simulation of the distribution of the contact pressure and the wear work was made, see Figure 50 and Figure 51.

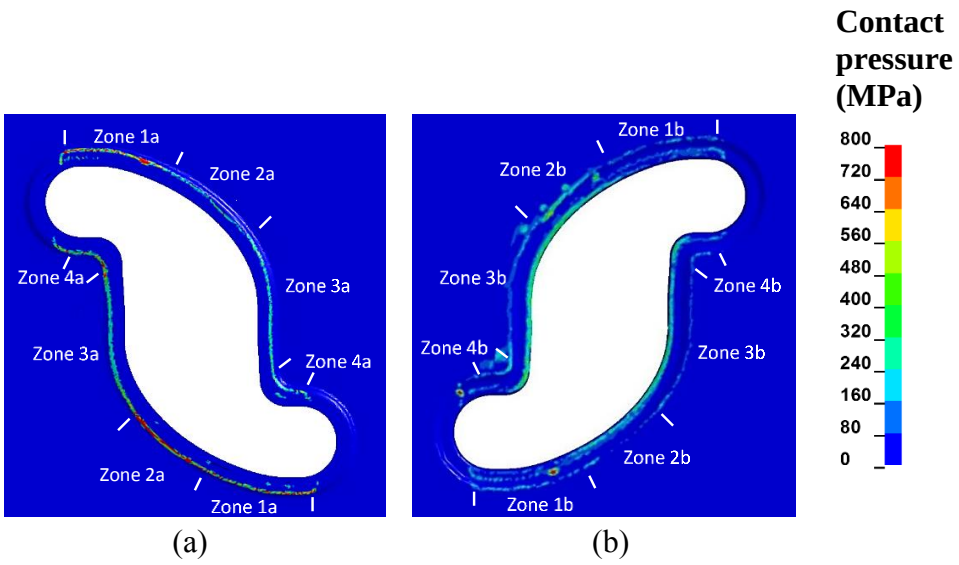

Figure 50: Simulated contact pressure in (a) the blank holder and (b) the forming die during forming.

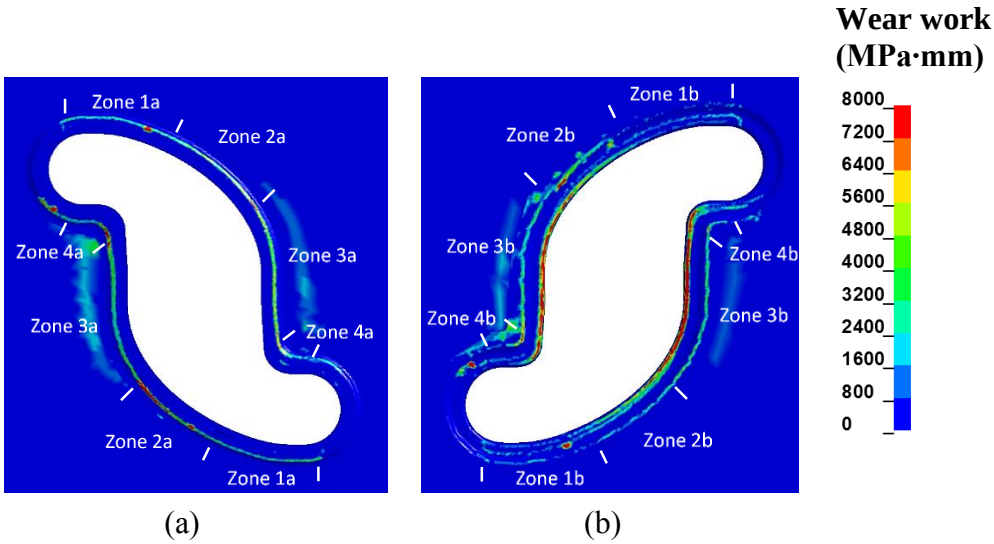

Figure 51: Simulated wear work in (a) the blank holder and (b) the forming die during forming.

For the present study, the wear severity is analyzed by evaluation of the wear work developed in one stroke. This is based on the assumption that no significant changes in the drawbead geometry will occur due to wear in the first 200-300 strokes, where the lubricant performance is evaluated. From the simulated contact pressure distribution, seen in Figure 50, it is confirmed that the zones with smaller rounding radii of the drawbeads are exposed to higher contact pressures. From the wear work in Figure 51, it is similarly seen that the combination of high local contact pressures and moderately long sliding lengths (as seen in Figure 47) result in severe wear conditions in zone 2, with a wear work of more than 8,000 MPa·mm. Another

critical region, in terms of wear, is the die shoulder in zone 3, which is subjected to moderately high contact pressures combined with a very long sliding length at the center of the component. The plane contact between the die and the blank holder, in zone 3, is similarly exposed to increased wear work due to the long sliding length of the sheet material.

The FE model is furthermore used for extraction of central process parameters, like the blank holder pressure, needed for the definition of the experimental testing parameters. An overview of the pressure distribution, when the 439 kN blank holder force is applied, is shown in Figure 52.

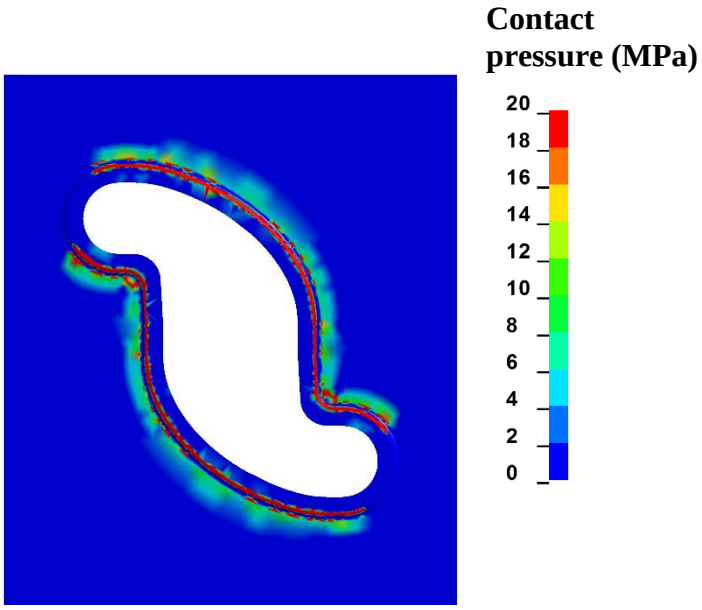

Figure 52: Contact pressure distribution in the forming die after application of the blank holder force.

Simulation of the contact pressure distribution in the forming tools shows that upon application of the blank holder force an average contact pressure of 9 MPa is found in the blank holder region of the forming die. The simulation furthermore shows that the majority of the blank holder force rests on the drawbead geometry when the blank holder force is applied, due to the bending of the sheet material.

4.4 Offline testing

4.4.1 Development of a drawbead tool for simulative testing

For simulative testing of the tribological conditions in the drawbead, a simulative tool has been designed for the UST, see Figure 53.

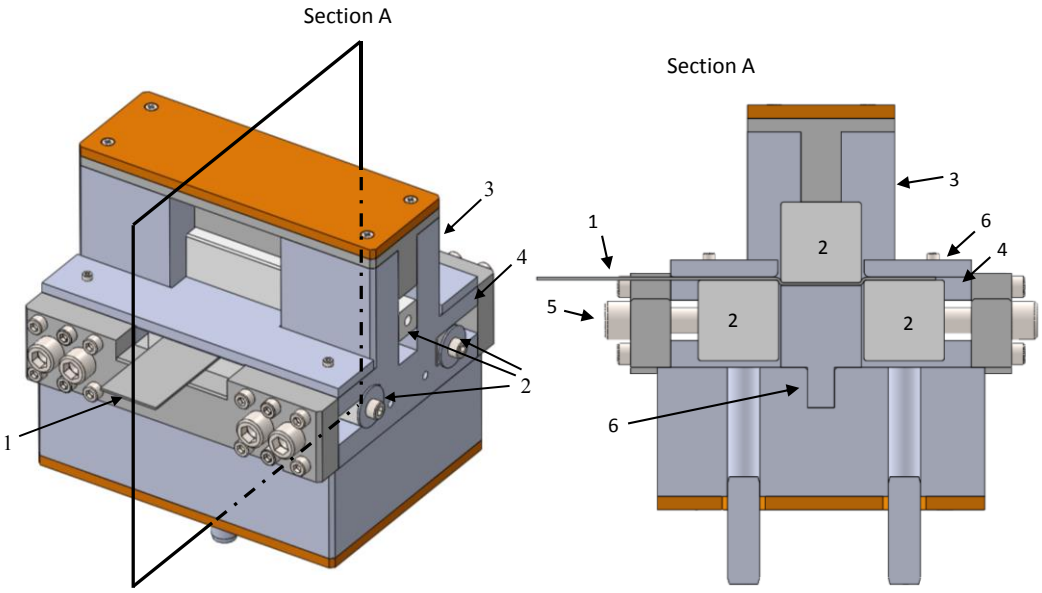

Figure 53: Schematic illustration of the drawbead tool with a cross-sectional view of the main tool components.

With the proposed tool design, the drawbead action can be simulated by drawing strip material (1) through a series of stationary tool pins (2), which are positioned in vertical and horizontal tool grooves (3,4). The center tool pin is kept in place during testing by the vertical axis of the UST, while the outer tool pins are fixed with a set of bolts (5). The positioning of the tool pins can be adjusted in the grooves (3) by the use of shims, thereby allowing a variation of central drawbead parameters such as bead penetration and bead gap. Variation of the tool pin geometry, setup and positioning furthermore enable simulation of different types of drawbeads, e.g. stepped drawbeads, rectangular drawbeads, and semi-circular drawbeads. In order to ensure correct effective rounding radii during forming, three constant gap tools (6) were placed, so that the strip conforms to the curvature of the tool. Back tension can furthermore be imposed on the strip in the stepped drawbead configuration, by force control of the vertical axis (Axis 3) of the tribotester. The general specifications of the tool design are listed in Table 3.

Table 3: Tool design specifications.

Specifications	**Value**
Rounding radii [mm]	1-10
Maximal drawbead restraining force [kN]	50
Bead gap [mm]	0-10
Penetration depth [mm]	0 to full penetration with the specified radii
Sheet thickness [mm]	1-2
Sheet width [mm]	≤60

The proposed tool design allows for a variation of the main drawbead parameters in order to simulate the exact operating conditions in a specific production platform. Along with a variation of the geometrical drawbead parameters, the tool design is made with changeable tool pins, which can be tailored in terms of tool material, hardness and surface topography.

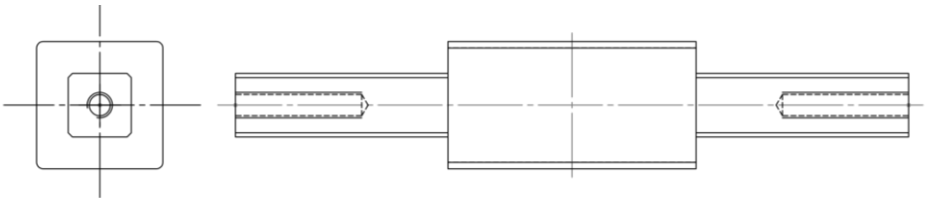

Figure 54: Tool pins for the drawbead tool.

The tool pins are milled with square ends, fitting to the tool groves for positioning of the tools. Each tool, therefore, has four tool surfaces, which can be used for testing as each tool surface progressively deteriorates during the individual test series due to tool wear.

4.4.2 Testing parameters

Based on the analysis of the drawbead geometry and the resulting tribological loads, which the drawbead design introduces, a test setup has been designed to experimentally replicate the drawbead conditions in zone 2, see Figure 51, which is the region with the most severe tribological loads. The presented test setup was made with sheet material of 1 mm thickness. Scaling down the drawbead dimensions with the same factor as the sheet thickness allows to emulate comparable drawing characteristics in terms of surface strains, DBRF and contact pressures in the tool/workpiece interface [239][240]. The testing parameters were furthermore designed to emulate the production parameters of the manually operated press used in production, in terms of process times, sliding length and sliding speed of the forming tools. Two test series were conducted, respectively with uncoated tools and tools with a Tenifer® QPQ surface treatment, in order to analysze of the performance of the two versions of the forming tools used for the production of the EGR component. A summary of the experimental parameters is shown in Table 4.

Table 4 Overview of experimental parameters.

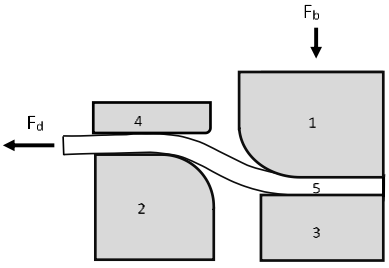

1. Drawbead (entry side)
2. Drawbead (exit side)
3. Blank holder
4. Constant gap tool
5. Sheet material

Tool material	Sleipner, hardened to 60 HRC
Tool surface roughness	Ra = 0.05 μm
Blank holder force, F_b	17 kN
Sliding length	17 mm
Sliding speed	4 mm/s
Idle time	19.5 s
Strip width	30 mm
Bead penetration	2 mm
Bead gap	2 mm
Drawbead entry radius	2 mm
Drawbead exit radius	2.5 mm

The performance of three alternative, environmentally friendly lubricants were analyzed in the presented study. These commercially available lubricants were selected together with the manufacturer of the EGR component, based on the promising tribological performance of the lubricants found in previous studies [13], [241].

Due to a limitation of the minimum test load of the UST, the normal force is increased to 17 kN, corresponding to an average normal pressure of 18,8 MPa. While the increased normal pressure in the planar contact might locally increase the wear rate, the increased normal force will aid with compensation for the die opening force experienced during testing.

4.4.3 2D analysis of the drawbead test

For evaluation of the test conditions, a 2D FE model was developed in LS-DYNA assuming plane strain conditions. An overview of the main components of the 2D model is shown in Figure 55. The FE model consists of two drawbead tools, which are modeled as elastic materials. Discretization of the drawbead tools is done with a quadrilateral mesh with an increasingly refined mesh towards the rounding of the tool (0.02mm element size) in order to ensure proper contact conditions with the strip. For the mechanical simulations, only the main region around the rounding radii of the drawbead tool is discretized in order to limit the number of elements in the simulation and the required computational power for conducting the simulations. The blank holder tool and the constant gap tool are modeled as rigid tools. The blank holder tool is defined with a small draft angle in order to avoid sharp corners and ensure proper contact in the interface. The sheet material used for the 2D simulations is defined by a Voce-formulation of $\sigma_f=135+(1785-135)(1-e^{-2.5\varepsilon_{eq}})$ [MPa] as shown in section 4.3.4.

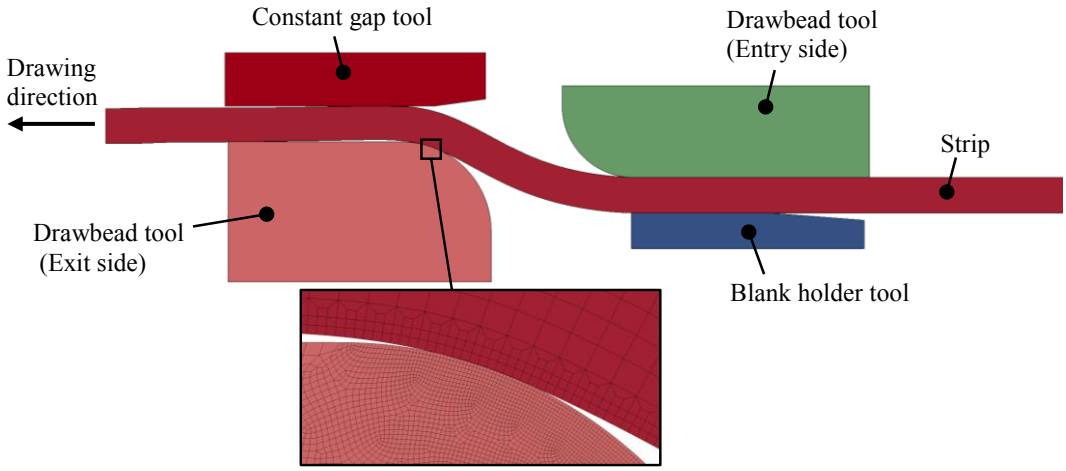

Figure 55: Overview of the setup of the 2D FE model for simulation of the drawbead test.

The COF was determined with reverse analysis, by calibrating the 2D simulation to experimentally determined values of the necessary drawing force required to draw the strip material through the specified drawbead setup with the Iloform BWN 205 lubricant, see Figure 56a.

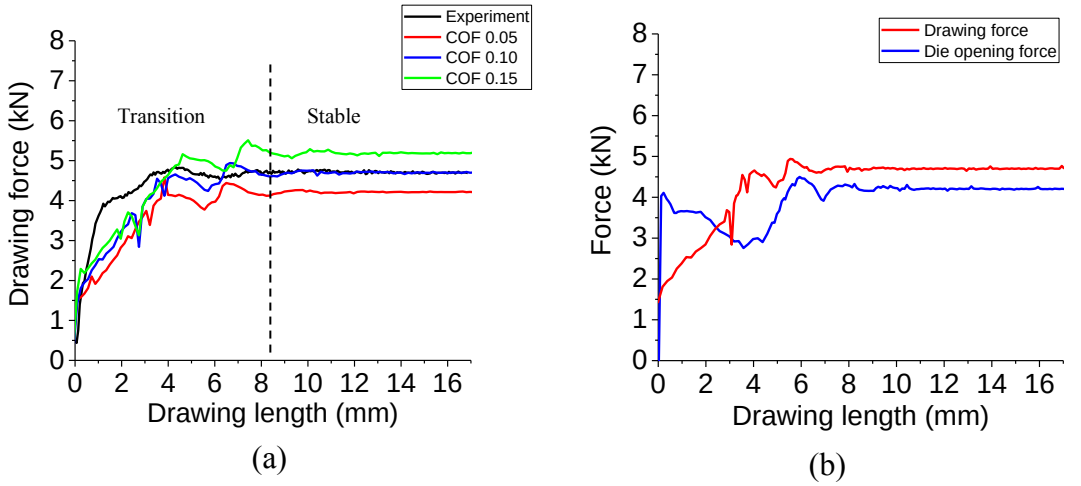

Figure 56: Numerical simulation of the drawbead test with (a) reverse analysis for determination of the COF and (b) simulation of drawbead forces.

The reverse analysis reveals that the numerical simulation which was conducted with an assigned COF of 0.1 to the contacting interfaces between the tools and the workpiece material results in a simulated drawing force which is good agreement with the experimentally measured drawing force. Once the correct COF is determined for the 2D analysis, process conditions such as the drawbead opening force, see Figure 56b, and the contact pressure in the tool/workpiece interface can be evaluated. Due to the cyclic bending of the sheet material induced by the drawbeads, a vertical force component is introduced that can open the forming die if exceeding the BHF [242]. The 2D analysis indicates that the specified drawbead geometry introduces a drawbead opening force of 4.2 kN once the drawing force is stabilized, as shown in Figure 56b.

Analysis of contact pressure distribution on the drawbead tools, shown in Figure 57, reveal a highly localized contact in the tool/workpiece interface, caused by partial penetration of the drawbeads. This results in local peaks in the contact pressure, with 968 MPa and 654 MPa respectively on the drawbead on the exit side and the drawbead on the entry side. Comparison with the 3D simulation presented in section 4.3.6, shows that designed test parameters allow for replication of similar contact conditions as experienced in zone 2 of the forming die. Slightly higher contact pressures are found in the 2D simulation, possibly attributed to the finer mesh discretization and the increased normal force necessary for conducting the experiment.

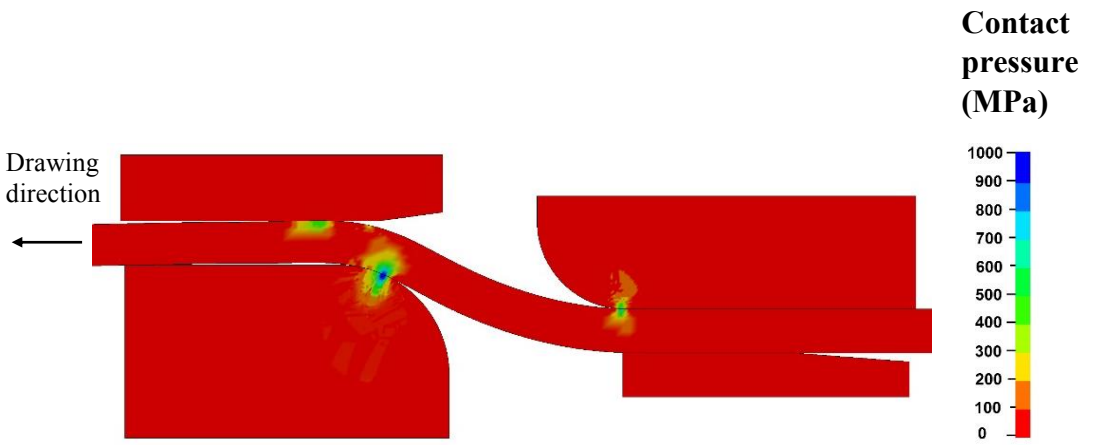

Figure 57: Simulated contact pressure distribution during the drawbead test.

For assessment of the temperature development in the contacting interface during testing, a coupled thermo-mechanical simulation is made with 300 repetitive strokes with the characteristic process times. In the thermo-mechanical model the entire tool geometry was discretized in order to accurately simulate the dissipation of the generated heat in the forming tools from the mechanical work and frictional energy. The analysis of the temperature evolution is based on a 2D setup, where the thermal dissipation through the width of the tool and the tool grooves is neglected. For the coupled mechanical and thermal analysis, a heat transfer coefficient of 50 kW/m^{2}K [216] was furthermore assigned to the contact between the tool and workpiece. An overview of the mechanical and thermal material properties used in the simulation is shown in Table 5.

Table 5: Overview of the thermal and mechanical properties of the tool and workpiece materials.

	Drawbead (Sleipner)	Workpiece (EN 1.4301)
Initial temperature (°C)	20	20
Heat capacity (J/kg·K)	460	500
Thermal conductivity W/(m·K)	20	15
Density (g/cm^3)	7.73	7.90
Young's modulus (GPa)	205	200
Poisson's ratio	0.3	0.3

Figure 58 shows the temperature development in the contact interface between the drawbead tool on the exit side and the sheet metal, where the largest surface temperatures are experienced. Figure 58 furthermore shows a comparison of the simulated tool temperature and the die temperature measured with the thermal imaging camera, see section 4.3.2. The evolution of the generated heat contains three main phases. The peak temperature experienced in the contacting surface is found at the end of each stroke (1), as seen in Figure 58b. A decrease in the peak temperature is thereafter found in the subsequent idle time between each stroke. A sudden drop in the surface temperature of the tools is noted at point (2), where

contact is made with the surface of a new blank with an ambient surface temperature of 20°C. The initiation of the following strokes is seen in point (3).

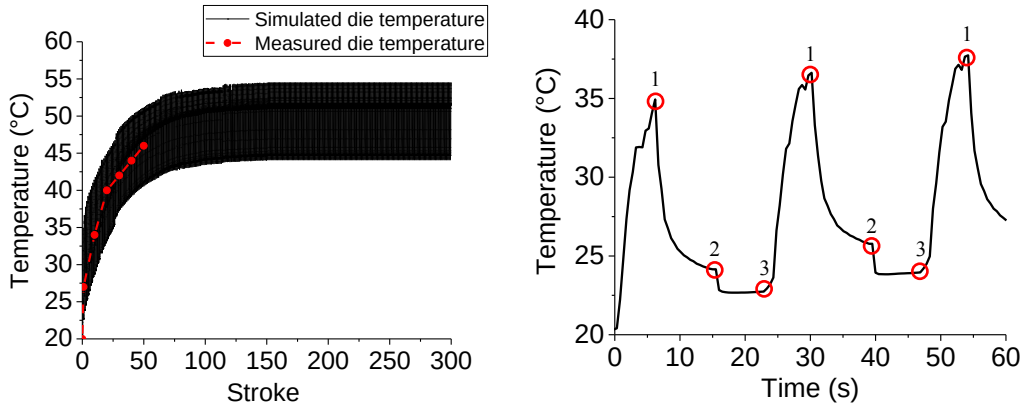

Figure 58: Simulated tool temperature evolution (a) in the first 300 strokes and (b) the tool temperature evolution in the first 3 strokes as a function of time.

The simulation indicates that a steady state is reached after approximately 60 strokes, where the tool temperature stabilizes and varies between 54.2°C and 44.2°C, respectively at the end of the stroke and at the end of the idle time. The measured die temperature, in Figure 42, made with thermal imaging, corresponds well with the average tool temperatures obtained with the thermo-mechanical simulation. The simulation shows that comparable heating and cooling cycles, as experienced in the production, can be obtained experimentally by recreating a comparable drawbead geometry and emulating the industrial forming conditions and process times. The simulation furthermore highlights the influence of the low production rate, due to manual operation of the press, on the temperature evolution in the forming die.

4.4.4 Limits of lubrication with stepped drawbeads

The drawing force measured during testing is shown in Figure 59. The developed tool wear after 300 strokes, with the tested lubricants, is shown in Figure 60 and Figure 61.

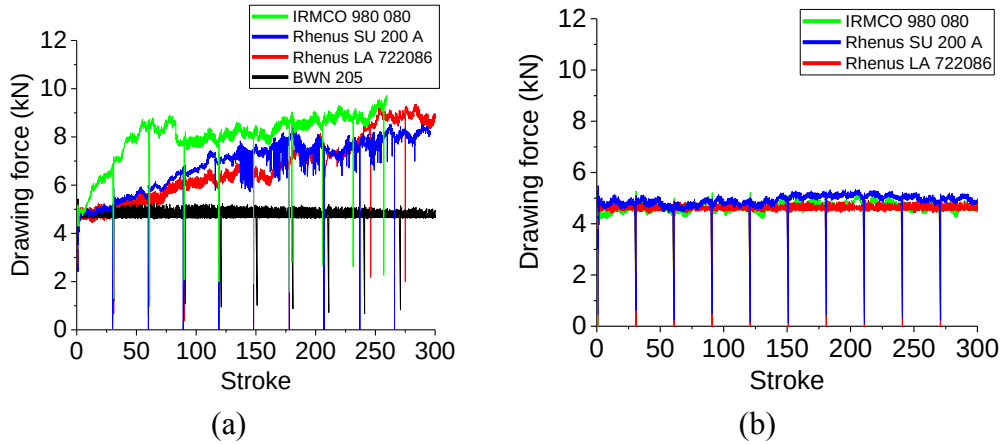

Figure 59: Measured drawing force during testing with (a) the Sleipner tool material without any surface treatment and (b) the Sleipner tool material with a Tenifer® QPQ surface treatment.

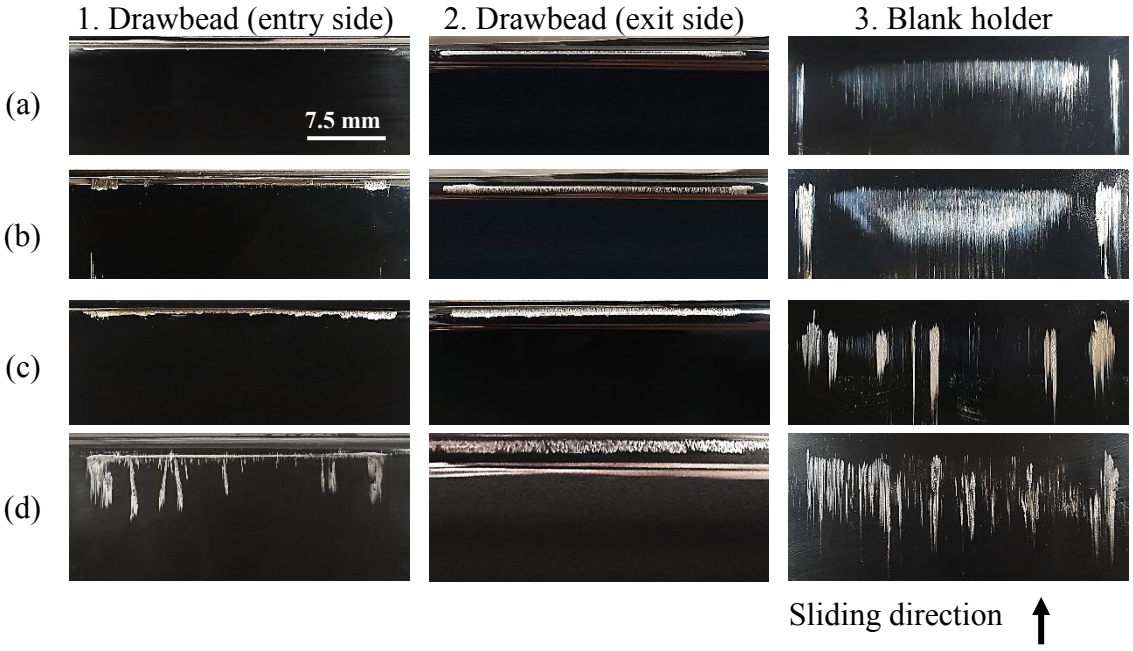

Figure 60: Tool surface, without surface treatment of the tools, after 300 strokes with the tested lubricants: (a) BWN 205, (b) Rhenus LA 72208, (c) Rhenus SU 200 A and (d) IRMCO 980 080.

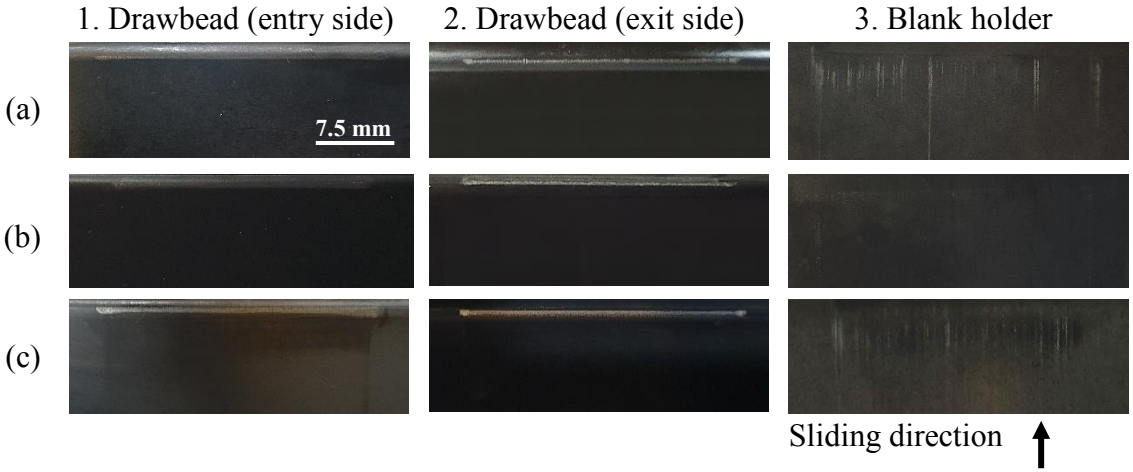

Figure 61: Tool surface, with a Tenifer® QPQ surface treatment, after 300 strokes with the tested lubricants: (a) Rhenus LA 72208, (b) Rhenus SU 200 A and (c) IRMCO 980 080.

From Figure 59 it is seen that the test series with the Rhenus LA 722086, Rhenus SU 200 A and the IRMCO 980 080 lubricants experience a rampant development of the drawing force within the first 50 strokes. This corresponds well with the visible scoring of the tested sheet metal surface, which was observed during the test. Compared with the surface structure of the tool after 300 strokes, see Figure 60, it is seen that a substantial amount of pick-up of workpiece material has accumulated on both the rounding radii of the drawbeads and the plane contact that emulates the contact in the blank holder region of the forming die. The BWN 205 lubricant, which is a highly chlorinated, heavy-duty deep drawing lubricant, has a stable drawing force during testing. The surface structure of the tools, tested with the BWN 205, shows only minor signs of initial run-in wear without any friction junctions formed on the tool. None of the selected, environmentally friendly lubricants could, therefore, replace the BWN 205 when conducting the tests with uncoated tools.

The selected lubricants were, however, found to exhibit a significantly improved tribological performance in the test series conducted with the Tenifer® QPQ treated tools. The test series conducted with the Tenifer® QPQ surface treatment were found to exhibit stable drawing forces and smooth surface structure of the sheet material after testing, for all the tested lubricants. Evaluation of the tool surface indicates only minor signs of abrasive wear without any sign of pick-up of sheet material on the tools. This is seen in Figure 61, where only minor scratches are found on the tool surface due to run-in wear of the iron nitride surface layer formed with the Tenifer® QPQ surface treatment. The presented results indicate that certain, tribologically severe forming operations require a deeper refinement of the tribosystem in order to implement environmentally friendly, non-chlorinated

lubricants. For the EGR component, the combined function of the Tenifer® QPQ surface treatment and an alternative, environmentally friendly forming oil was found to exhibit sufficient tribological integrity to replace the heavy-duty, chlorine-based BWN 205 forming oil.

4.5 Conclusion

In the present chapter, an analysis of the wear conditions in an industrial stamping operation for manufacturing of an EGR component was presented. Based on an analysis of the industrial production platform and the die geometry, a test series was designed for offline replication of industrial forming conditions. Numerical analysis of the tribological loads introduced by the drawbeads showed that specific regions of the forming tool were exposed to increased risk of galling. With an offline simulation of the tribological conditions in the stepped drawbead geometry implemented in the forming die, the presented study showcased an evaluation of the tribological performance of different alternative tribosystems. The study showed that the tribological function of the Tenifer® QPQ surface treatment combined with different forming oils could form the basis for an alternative, environmentally friendly tribosystem for replacement of the hazardous, chlorinated lubricant currently used in production.

Chapter 5 Parametric study of limits of lubrication with semi-circular drawbeads

As seen in the industrial case study, section 4.3, the use of drawbeads for facilitating correct drawing behavior in a stamping operation can introduce varying tribological loads depending on a range of different process and design parameters e.g. drawbead type, sliding length, bead radii and drawbead penetration. This section presents a supplementary study where the influence of different sheet materials with varying mechanical and tribological properties was studied with a variation of the bead penetration.

5.1 Experimental setup

The parametric study is based upon a semi-circular drawbead configuration, see Figure 62, where bead penetrations ranging from partial penetration to full penetration ($H_b = R_{groove\ bead} + R_{drawbead} + t$) are studied.

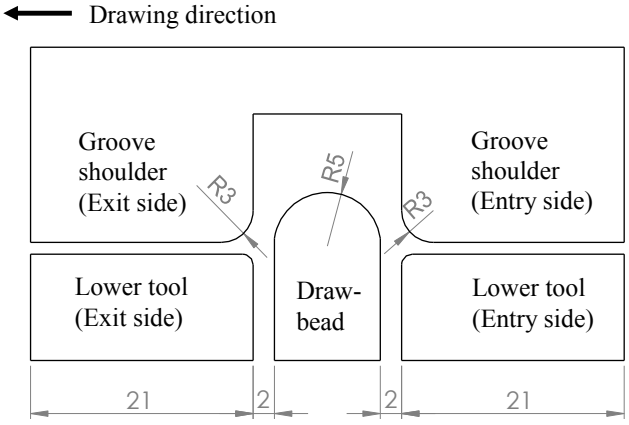

Figure 62: Overview of the semi-circular drawbead tool.

The present drawbead test was conducted on the experimental strip drawing test stand developed at the Institute for Production Engineering and Forming Machines at Technische Universtät Darmstadt, as described by Filzek and Groche [243]. The test stand used for the drawbead test is fully automatic and based on the same working principle as the UST presented in section 2.7.

For the drawbead test, the PL61 Multidraw prelubricant was used with a spray nozzle system for continuous application of 2.5 g/m^2 lubricant film to the surface of the sheet metal during testing. The drawbead tool was made in AISI D2 tool steel

hardened to 59-61 HRC and polished to a surface finish of Ra = 0.05 µm. Two separate test series were conducted with sheet metal of 1.1x50 mm respectively of EN 1.4301 stainless steel and DP 980 with a 10 µm electrogalvanized surface coating. For the drawbead test, a normal force of 10kN was used for the EN 1.4301 stainless steel. 20 kN normal force was applied when testing the DP 980 in order to compensate for a larger die opening force stemming from the greater mechanical strength of the dual phase sheet material. The drawbead test was furthermore conducted with a stroke length of 100mm and a sliding speed of 100 mm/s with an idle time of 1s between each stroke. The EN 1.4301 stainless steel was studied with a bead penetration of respectively 3 mm and 9 mm. The DP 980 was, however, only studied with partial penetrations of 2mm and 3mm, due to a limitation of the maximal drawing force of the test stand.

FE analysis of the test conditions was done with a 2D FE model in LS-DYNA, as also shown in the previous study. Characterization of the mechanical properties of the sheet materials was done by tensile testing, where the following Ludwik formulations were derived: DP 980: $\sigma_f=656 + 1065\cdot\varepsilon_{eq}^{0.282}$ [MPa]. EN 1.4301: $\sigma_f=240 + 1245\cdot\varepsilon_{eq}^{0.45}$ [MPa]. For the FE model, the tool geometry was modeled as elastic materials. Discretization of the drawbead tools was done with a quadrilateral mesh with an element size of 0.03-0.07mm in the tool rounding and the planar contact of the drawbead. Initial characterization of the frictional conditions of the lubricated contact in the tool/workpiece interface was made with a strip drawing test, finding a COF of approximately 0.05 for both material combinations. An overview of the numerical simulations with varying bead penetrations is shown in Figure 63a-d.

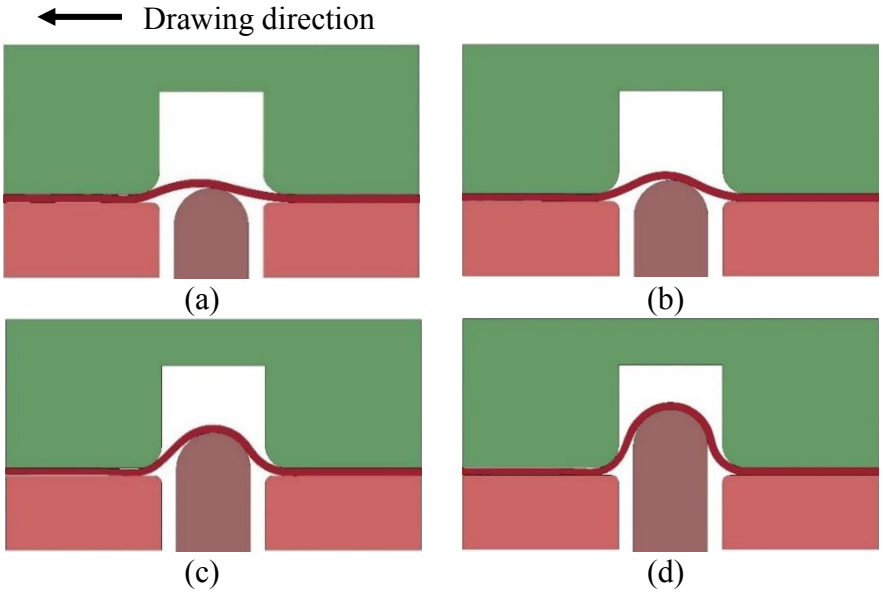

Figure 63: Overview of the sheet metal flow over the drawbead with (a) 2mm bead penetration, (b) 3mm bead penetration, (c) 6mm bead penetration and (d) 9mm bead penetration (full penetration).

5.2 Experimental results

The drawing force measured during testing is shown in Figure 64, and an overview of the surface structure of the drawbead tools after the tests is given by Figure 65-Figure 68.

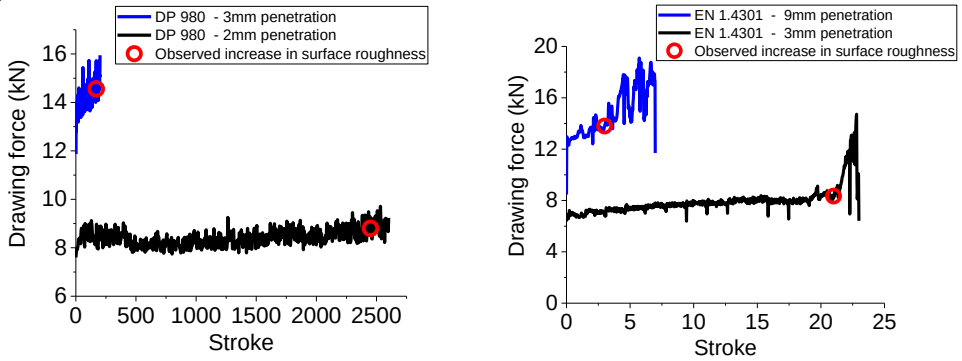

(a) (b)

Figure 64: Measured drawing force during testing for (a) DP980 sheet material with 2mm and 3mm bead penetration (b) EN 1.4301 sheet material with 3mm and 9mm bead penetration.

By visual inspection of the surface structure generated during the test, it was observed that the EN 1.4301 stainless steel had a visible deterioration of the surface after 3 strokes with full penetration of the drawbead, see Figure 66. With bead penetration of 3mm, the threshold sliding length for the EN 1.4301 was 21 strokes, see Figure 65. The DP 980 was found to have a threshold sliding length of 170 strokes with a 3mm bead penetration and 2450 strokes with a 2mm bead penetration, see Figure 67 and Figure 68. Evaluation of the generated surface structure compared to the measured drawing force indicates, that force measurements allow for an accurate evaluation of the point where the breakdown of the lubricant film occurs, where a subsequent deterioration of the surface quality of the sheet material is observed. Measurements of the drawing force are seen to have a larger fluctuation when testing the galvanized DP 980, due to the creation of third body wear particles in the contacting interface during the test.

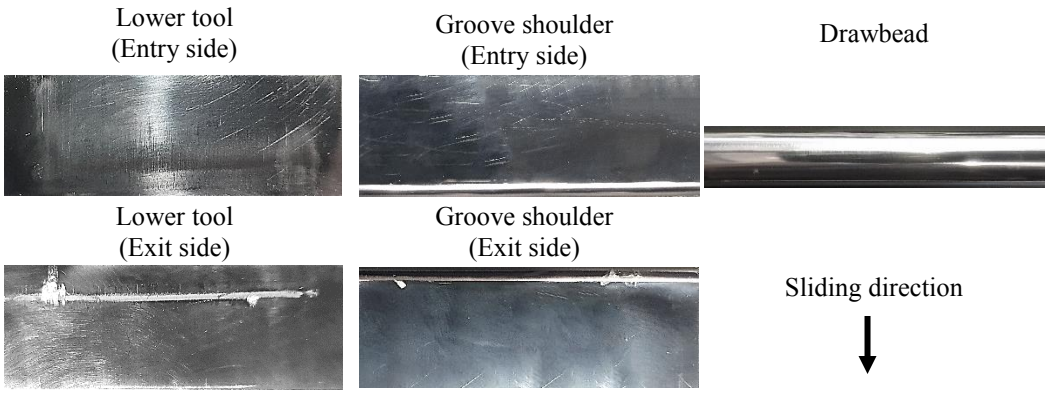

Figure 65: Surface structure of the drawbead tool tested with EN 1.4301 stainless steel and a 3mm bead penetration after 23 strokes.

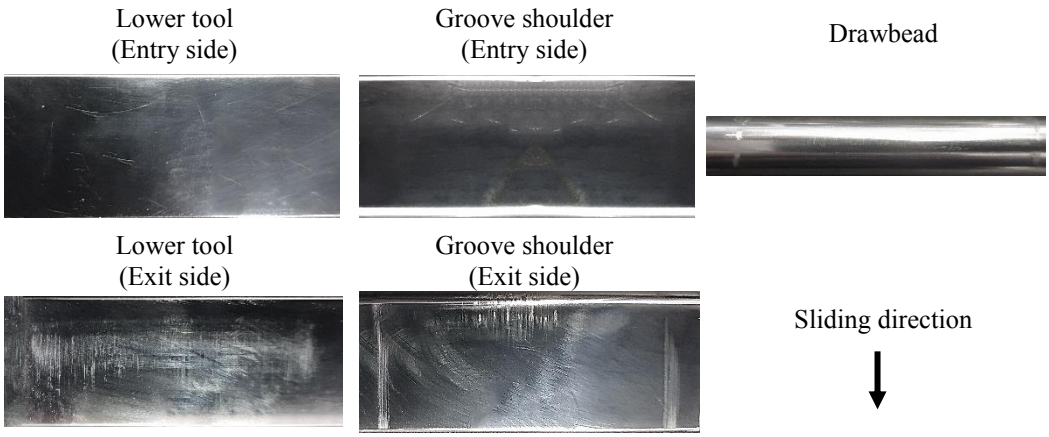

Figure 66: Overview of the surface structure of the drawbead tool tested with EN 1.4301 stainless steel and a 9mm bead penetration after 7 strokes.

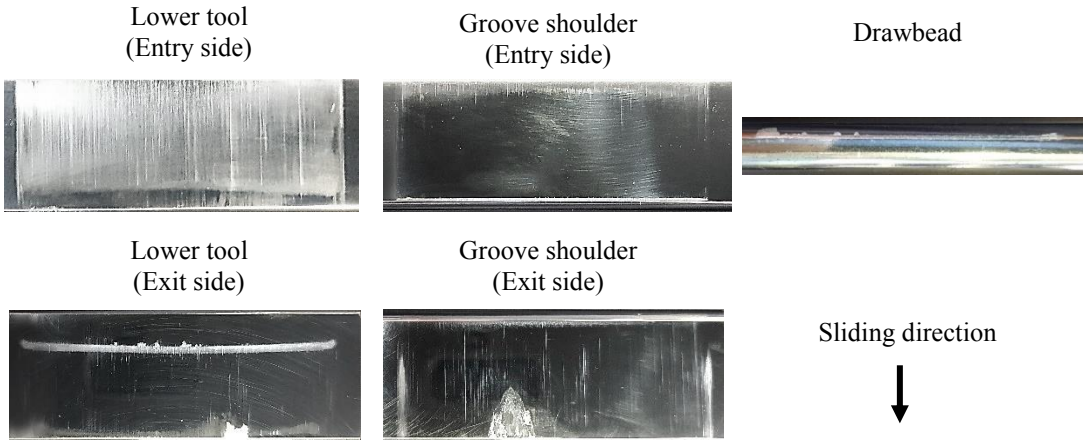

Figure 67: Overview of the surface structure of the drawbead tool tested with DP 980 and a 2mm bead penetration after 2606 strokes.

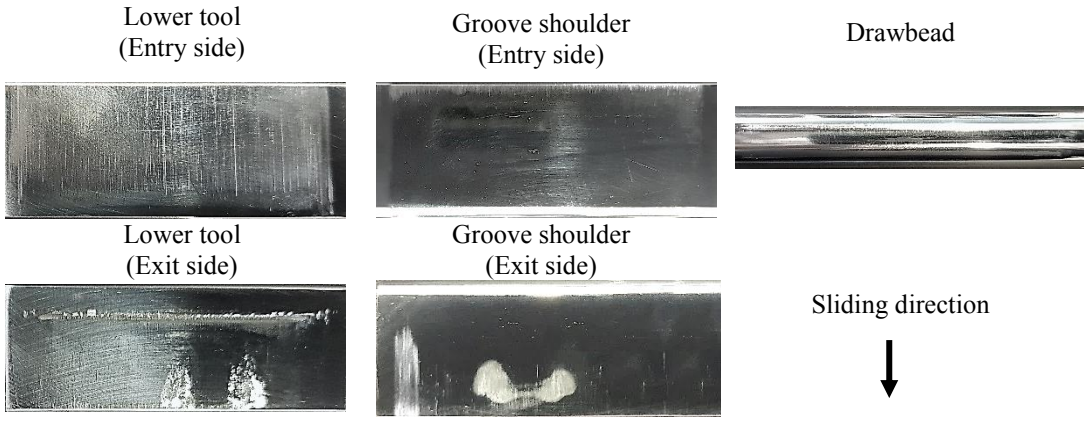

Figure 68: Overview of the surface structure of the drawbead tool tested with DP 980 and a 3mm bead penetration after 201 strokes.

From the overview of the tool surfaces after testing it is seen that the test series conducted with the EN 1.4301 stainless steel experiences severe galling primarily on the rounding of the groove shoulder on the exit side of the tool, for both 3mm and 9mm bead penetrations. The tests conducted with DP 980 are, however, seen to have a concentration of the wear development in the planar contact, on the exit side of the drawbead, between the lower tool and the groove shoulder. The wear development in the test series with the DP 980 is furthermore found to be governed by an accumulation of large third body wear particles from powdering of the electrogalvanized zinc coating of the sheet material. The two test series, therefore, exhibit a fundamental difference in the primary wear mechanism occurring during the test. Several test series reveal large amounts of wear in the tool region in contact with the edge of the sheet material, due to sliding contact with the minor burrs on the edge of the sheet, which are formed during the coil cutting process. The wear caused by irregularities of the edge of the sheet material is therefore not considered in the present study. An overview of the main process parameters of the test series conducted with the DP 980 is shown in Figure 69. The curve regions highlighted in Figure 69 indicate the sequential contact with the groove shoulder (entry side), drawbead, groove shoulder (exit side) and the lower tool. Overviews of the contact area and the distribution of the contact pressure with varying penetrations for the two sheet materials are shown in Figure 70 and Figure 71.

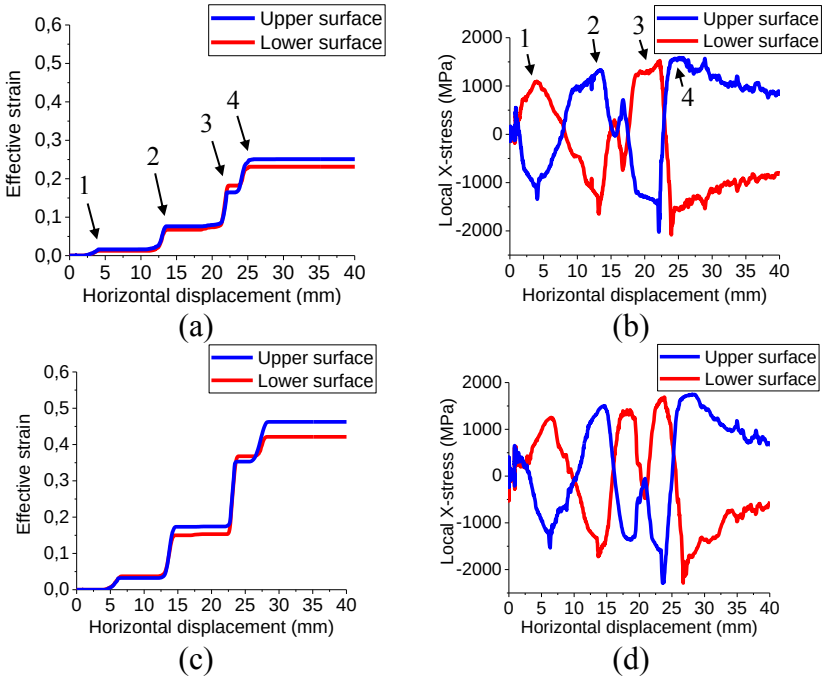

Figure 69: Overview of the forming conditions with the DP 980 sheet material. (a) Strain hardening behaviour of the workpiece material with a 2 mm bead penetration and (b) the corresponding development of the local surface stress in the sheet material. (c) Strain hardening behaviour of the workpiece material with a 3 mm bead penetration and (d) the corresponding development of the local surface stress in the sheet material.

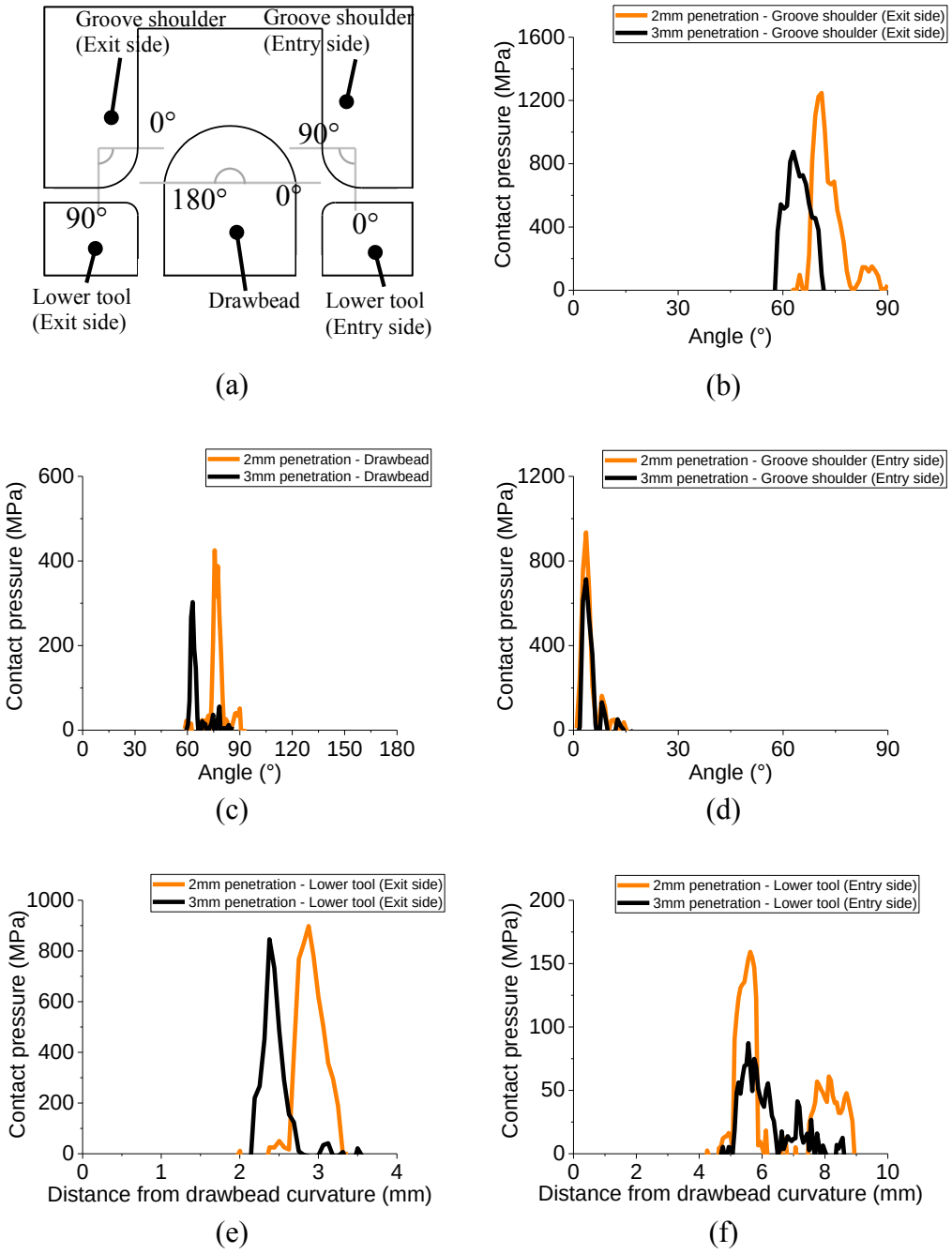

Figure 70: Distribution of the contact pressure when testing DP 980 with varying bead penetrations. (a) Overview of the main tool components. (b) contact pressure in the groove shoulder (exit side), (c) contact pressure in the drawbead, (d) contact pressure in the groove shoulder (entry side), (e) contact pressure in the lower tool (exit side) and (f) contact pressure in the lower tool (entry side).

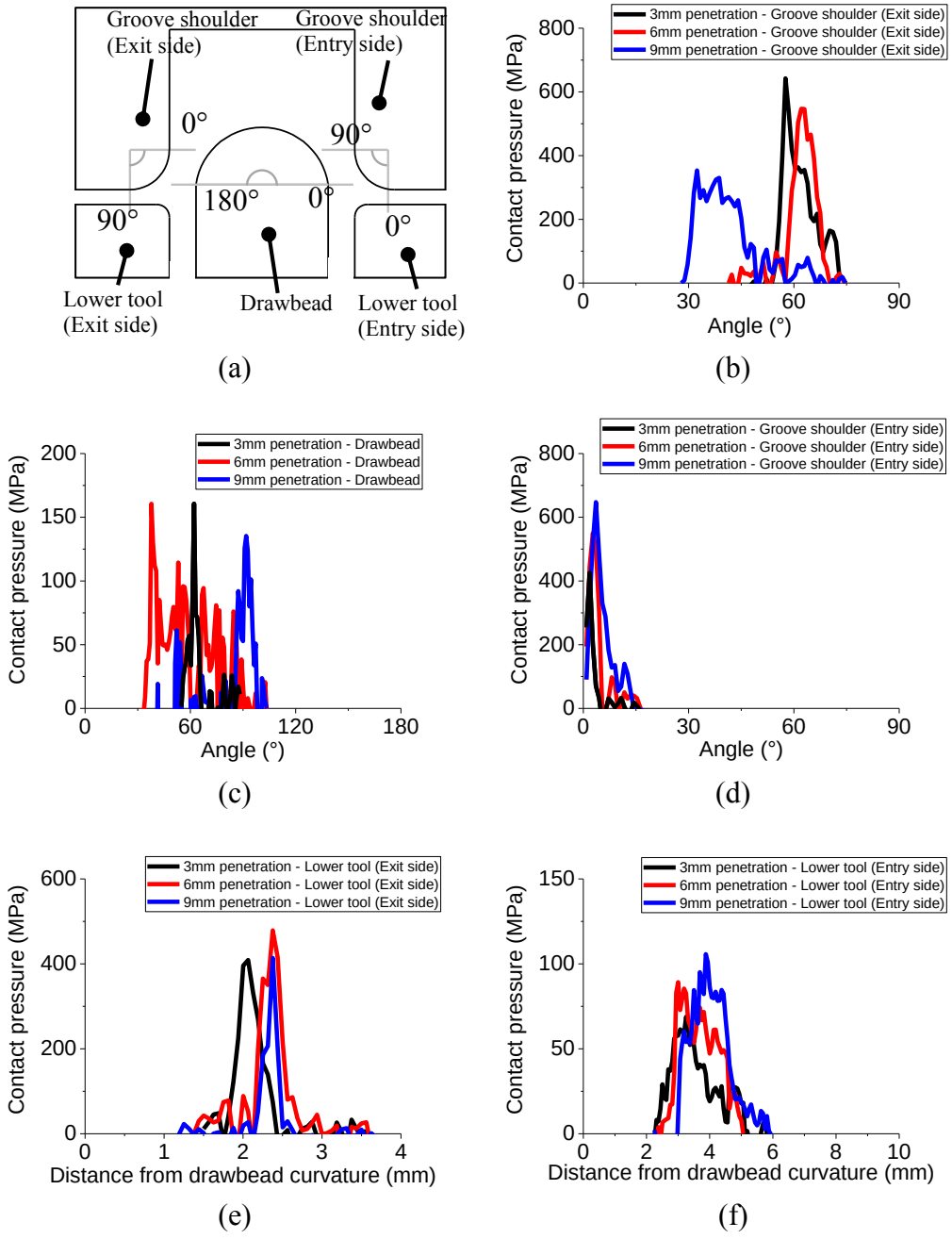

Figure 71: Distribution of the contact pressure when testing EN 1.4301 with varying bead penetrations. (a) Overview of the main tool components. (b) contact pressure in the groove shoulder (exit side), (c) contact pressure in the drawbead, (d) contact pressure in the groove shoulder (entry side), (e) contact pressure in the lower tool (exit side) and (f) contact pressure in the lower tool (entry side).

The overview of the distribution of the contact pressure in the drawbead tool indicates that the highest contact pressures are located in the two groove shoulders and the lower tool towards the exit side. Increased bead penetration is found to either shift or expands the angle of contact between the sheet material and the individual tool component. The most noticeable effect of the bead penetration is seen in the drawbead and the groove shoulder on the exit side, where the increased bead penetration creates a larger area of engagement and a large area for dissipation of the contact forces. Partial bead penetrations are conversely found to create localized contact with high contact pressures. The tests conducted with the EN 1.4301 sheet material exhibits the occurrence of galling focused primarily on the rounding radius of the groove shoulder where the contact pressure is approximately at the highest level. The test series conducted with 9 mm penetration exhibits a substantially shorter sliding length prior to the onset of galling, possibly due to the increased surface expansion of the sheet material caused by the increased DBRF from the deeper bead penetration. The DP 980 exhibits a similar distribution of the contact pressure in the drawbead tool, however, with substantially higher contact pressures due to the greater mechanical strength of the sheet material compared to the stainless steel.

Powdering of the brittle electrodeposited surface coating is the dominant wear mechanism seen in the test series conducted with the DP 980 sheet material. An overview of the accumulation of the galvanized zinc coating after 1990 strokes is shown in Figure 72. In order to maintain the loosely adhered wear particles that accumulated during the test, the overview of the tool surface was captured without any cleaning of the surface.

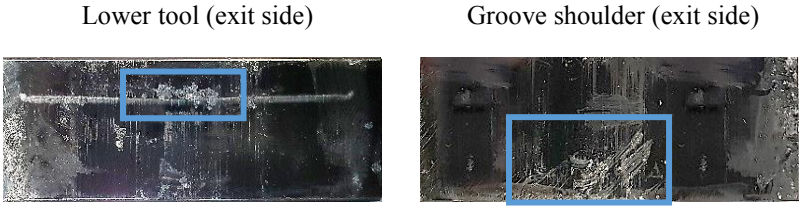

Figure 72: Surface structure of the lower tool and the groove shoulder after 1990 strokes with the DP 980 sheet material and a 2mm bead penetration.

The powdering behavior of stamped parts was previously studied by Rangarajan et al. [244]–[246] who reported that the wear mechanism was highly dependent on the strain state of the sheet material. By analysis of the coating performance in a BUT test, the study concluded that the deterioration of the coating was caused by the bending and unbending strains combined with the influence of the contact pressure and frictional shear stresses. With a drawbead test, Rangarajan [246] furthermore noted a direct correlation between the bead penetration and the mass loss of the

surface coating. The present study exhibits a similar correlation where a substantial decrease in the threshold sliding length is observed when the bead penetration is increased from 2mm to 3mm. While a shallow bead penetration generally increases the contact pressure in the drawbead tool, an increased bead penetration introduces higher surface stresses alternating between tension and compression and a higher straining of the sheet material, see Figure 69. The overview of the tool surface after 1990 strokes indicate an accumulation of third body wear particles occurs during the test, prior to the threshold sliding length where deterioration of the surface of the sheet material is observed. The accumulation of the loosely adhered wear particles is found to be in the same region of the tool surfaces where weld junctions are formed at a later point in the test. The increased sliding length leads to increased lump growth of the loose particles, which were found to adhere strongly to the tool surface after the onset of galling. The accumulation of wear particles is found to occur predominately in the planar contact between the groove shoulder and the lower tool towards the exit side of the tool. The local entrapment of wear particles at the exit side is attributed to the accumulated deterioration of the surface coating during the test, due to cyclic bending and unbending of the sheet material and the sliding contact with the tool surface. The wear behavior of the DP 980 is therefore found to be highly influenced by central drawbead design parameters such as the rounding radius and the bead penetration, which governs central process parameters such as contact pressure and the straining of the sheet material. The different wear characteristics shown in the present study highlights the importance of offline testing of various types of sheet metals, surface coating and lubricants for evaluation of tool life and tribosystem efficiency.

5.3 Conclusion

A supplementary study was conducted for investigation of the wear conditions with a variation of the drawbead geometry and different sheet materials with varying mechanical and tribological properties. Based on an analysis of the limits of lubrication tested with EN 1.4301 stainless steel and DP 980, it was concluded that the tool life was governed by two fundamentally different wear mechanisms. While the EN 1.4301 stainless steel was found to developed pick-up of workpiece material on the groove shoulder towards the exit side of the tool, where high contact pressures are found, the limits of lubrication in test series conducted with the DP980 was governed by the powdering mechanism. The powdering mechanism exhibits a complex wear behavior depending on several parameters such as contact pressure, strain state and the strain path.

Chapter 6 Wear and lubrication in punching and blanking

This chapter presents an investigation of wear and lubrication in severing processes. The current study aims to characterize lubricant properties and performance in punching and blanking operations. For the study, the lubricant application method and the chemical composition of the additive packages of the lubricants are studied for their influence on wear and lubrication.

6.1 Introduction

Severing processes are according to the DIN 8588 [247] subdivided into blanking, wedge-action cutting, tearing and breaking. Blanking is a single stroke shearing operation with closed shear lines, where workpiece material is sheared between a punch and a blanking die. Blanking and punching are the most commonly used severing process in sheet metal forming, often combined with other forming operations as an intermediate or finishing production step. The process sequence of the blanking operation is illustrated in Figure 73.

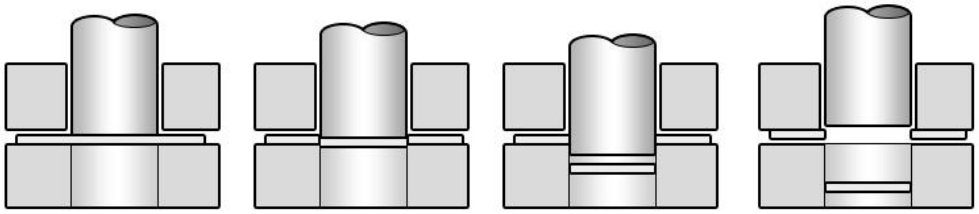

Figure 73: Illustration of the blanking process.

In the first stage blanking operation, initial contact is made between the punch and the sheet material resulting in a large increase in the punch force as the sheet material elastically deforms. The elastic deformation is followed by plastic deformation as the punch penetrates into the die opening and introduces shearing and subsequent crack formation, as the shear strength of the sheet material is exceeded. The propagation of cracks continue along the periphery of the punch and the blanking die until breakthrough of the punch occurs, where a full separation of the sheet material is achieved. During the forward stroke of the blanking operation, a radial flow of lubricant forms a small lubricant reservoir around the periphery of the punch, which enables the formation of a lubricant film between the punch and

the sheet material during the process. The final stage of a blanking operation is the retraction of the punch and stripping of the sheet material. The morphology of the sheared edge consists of four main zones as illustrated in Figure 74:

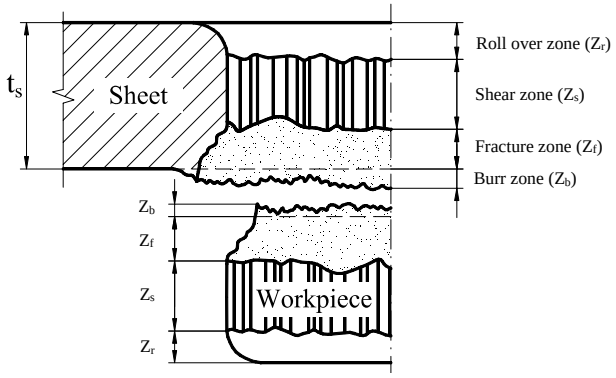

Figure 74: Overview of the different zones of the sheared edge [248].

Material rollover initiates as the sheet material is bent into the shearing gap between the punch and the blanking die, upon initial movement of the punch. At an increased stroke length, the shear zone is formed as the sheet material is plastically deformed into the blanking die, followed by the creation of the fracture zone when the sheet material ruptures. The burr zone is formed due to tearing of the sheet material at the end of the stroke. The size of the burr zone increases with increasing clearances and ductility of the sheet material.

Fine blanking is a high precision process variant of the conventional blanking process, where high dimensional accuracy and smooth shearing edges are obtained by implementation of a vee-ring, a counter punch and a narrow clearance between the punch and the blanking die. Fine blanking is extensively used for manufacturing of components like gears where the surface quality of the sheared surface is of significant importance since it is used as a functional surface. The clearances used in fine blanking is typically 0.5% of the thickness of the sheet material, compared to conventional blanking where a clearance of around 10% of the sheet thickness is normally used. The application of smaller clearances between the punch and the blanking die and the use of a counter punch and a vee-ring introduce high hydrostatic pressures near the deformation zone, which suppress the formation of cracks, leading to the formation of a larger shear zone, while also introducing a larger frictional stress on the punch.

Contrary to most common sheet metal forming operations, the blanking operation generates a new, virgin surface during the process, which combined with the frictional stress exerted on the punch stem during the backstroke creates severe tribological conditions. Sheet materials with high affinity for adhesion with tool steel, such as stainless steels, are therefore prone to cause local pick-up on the punch stem. The formation of local weld junctions on the punch stem causes scoring of the workpiece material in the subsequent strokes and can introduce large tensile stresses in the punch during the backstroke, which can lead to tool failure.

6.2 Tribology in punching and blanking operations

A number of experimental studies [249]–[252] have been conducted for investigation of different process parameters central to the blanking process, such as the influence of wear and tool clearances. Hernandez et al. [253] presented an experimental and theoretical study, where the influence of the blanking clearance on tool life and part quality was investigated. The study outlined a preliminary guideline for the selection of an optimum clearance based on considerations of both cost and part quality. Hambli [254] presented an experimental investigation, where the effect of the interaction between the wear state of the tool, the blanking clearance and the thickness of the sheet material was studied in connection to variations in the blanking force and the geometry of the sheared edge. Millard and Gasnier [255] evaluated the lubricant performance in punching by determining the COF from measurements of the backstroke force and theoretical analysis of the normal stresses exerted on the punch surface. Pfaff [256] reported that the backstroke force in punching is governed by the accumulation of pick-up of wear particles from the workpiece sheet on the punch stem. No further correlation was however found between the development of the wear mechanism and the measured backstroke force, due to scattering of the force measurements, possibly caused by vibrations stemming from the transducer design. Lind et al. [257] proposed that the wear mechanism occurring in a blanking process is characterized by three distinct phases, where abrasive wear, adhesive wear and growth of friction junctions are respectively dominant. Olsson et al. [258]–[260] conducted extensive investigations on wear and lubrication in punching and blanking. The studies showed that the mechanism of lubrication in punching is governed by the lubricant retained on the surface of the punch stem and by the chemical interaction of the lubricant additives with the punch material. This was evaluated by testing punches with different punch tip geometries and surface topographies combined with different lubricant formulations. It was found that a tangential texture on the punch stem combined with a high viscosity lubricant reduced the amount of pick-up developed on the punch stem during testing. In case of efficient, additivated lubricants, however, this lubrication mechanism was of no importance. The studies furthermore showed that the development of the backstroke force gave a good indication of the severity of the developed pick-up on the punch stem and that the punching test requires lubricants which form strong boundary films, such as chlorine-based additives, to avoid excessive wear on the punch stem [261]. Klocke et al. [262] conducted a series of comparative analyses for the characterization of different additives for evaluation of the applicability of non-chlorinated lubricants in fine blanking processes. The study showed that characterization of the

tribochemical effect of single and compound additives enables optimization of the tribosystem for fine blanking processes by utilizing the synergy of the different types of additives. Hogmark et al. [263] studied the wear behavior of AISI D2 tool steel punches with sheet materials of different steel grades. The study concluded that the material properties of the workpiece materials greatly influence the wear profile of the punch tools. Hogmark et al. highlighted material properties of ductility and hard particle phases to be decisive for promotion of adhesion, fatigue and abrasion.

The applicability of tool coatings for prolonging the life of punching tools has furthermore been studied in a number of recent publications investigations [264]–[269]. Klocke and Raedt [270] presented a study, where the formulation and testing of different hard ceramic CVD and PVD coatings were done for cold forging and fine blanking applications. The aim was to minimize the need for hazardous lubricant additives and workpiece pretreatment. Several mechanical and thermal coating properties, such as strong adhesion of the coating to the substrate and high thermal conductivity, were highlighted as critical coating properties in order to withstand the imposed tribological loads of the fine blanking and cold forging processes. Klocke and Raedt furthermore proposed that a low Young's modulus could increase the durability of the tool coating due to reduced tensile stresses in the coating. Kitamura et al. [271] studied the tribological behavior of micro-dimpled punches, by evaluation of the measured backstroke force. They found that a micro-dimpled punch texture made with a pico-second laser could drastically reduce the frictional stress exerted on the punch during the backstroke. For this purpose, the surface texture was optimized in terms of dimple depth, coverage and arrangement.

Many sheet metal forming tribosystems are exposed to high contact temperatures due to the mechanical work and the frictional heat introduced by the forming process. High temperatures can cause severe tribological loads to a tribosystem due to the decomposition of the lubricant additives as well as thinning and evaporation of the lubricant. Analysis of the physiochemical properties of the lubricant additives and the base oil can, therefore, give valuable information about the lubricant behavior in forming processes. Important properties include thermal stability, volatility and the tribological nature of the film-forming additives in the lubricant [272], [273]. Differential thermal analysis (DTA) is a commonly used technique for analysis of the influence of temperature on the physiochemical behavior of organic materials by measurement of heat flow and the change in weight at elevated temperatures, from which the occurrence of exothermic and endothermic reactions can be evaluated. Matveevsky [274]–[278] presented a series of investigations of the performance of different lubricant additives at high temperatures with DTA and different simulative tests. For analysis of the film-

forming action of different lubricant additives, Matveevsky highlighted the importance of two main transition temperature points. At the first transition, the chemically active lubricant additives react with the metal surface resulting in a sharp decrease in the COF. At the second transition, the chemically modified layer loses its lubricating properties due to desorption of polar molecules or melting of chemically reacted tribofilms, which results in a subsequent increase in the COF. Matveevsky furthermore highlighted the possibility of using detected exothermic reactions for evaluation of the critical transition temperatures, where the lubricant additives form a surface film on the metal. Kawamura and Fujita [279] studied the performance of organic sulphur and phosphorus compounds with DTA combined with a cross-pin wear tester. The wear scar diameter of the lubricant containing S-additives increased with increased reactivity of the lubricant additives. The wear scar diameter generated when lubricating with phosphite based EP additives was however found to decrease linearly with increasing reaction starting temperatures. A similar observation was later made by Wan and Xue [280], who studied the performance of P-based lubricant additives for lubrication of aluminum. The study furthermore indicated that the tribochemical reaction between the EP additive and the sliding surface was initiated by a flash temperature generated in the rubbing action. Kawamura [281] later presented a similar correlation between additive reactivity and wear scar diameter with ZDDP additives. DTA was similarly used by Møller et al. [14], [15] for studying the tribological performance of chlorinated paraffin and diakyloplysulfide for ironing of stainless steel. The study concluded that the EP performance of chlorinated paraffins is strongly connected to its high chemical reactivity with chromium.

Punching and blanking processes exhibit severe tribological conditions, where insufficient lubricant quality leads to heavy pick-up of workpiece material on the punch resulting in poor surface quality, reduced dimensional accuracy and a shortened tool life. Hazardous lubricants are therefore often used in order to facilitate stable production conditions. For minimization of the use of hazardous lubricants, the present study aims to evaluate the primary lubricant properties needed to ensure proper lubrication in severing processes, for assessment of the applicability of alternative, environmentally benign lubricants.

6.3 Experimental methods

6.3.1 Punching test

A series of punching tests were conducted with a 1 mm EN 1.4301 stainless steel sheet and Ø2mm PM tool steel AISI M3:2 punches with a 10µm radial clearance between the punch and the blanking die. The narrow clearance results in a high hydrostatic pressure in the shear band region, which induces severe stressing of the lubricant film and promotes a large shear zone similar to the forming conditions of a fine blanking operation. The punches used for the test had a tangential surface texture of Rz = 2.5µm obtained by round grinding. An overview of the chemical composition of the punch material is shown in Table 6. The punching test was conducted on a 320 kN C-frame eccentric press with a stroke rate of 170 RPM and a corresponding punch speed of approximately 45 mm/s. The eccentric press was equipped with an automated pneumatic feeding system that enables continuous drawing of the sheet material from a coil for testing of several consecutive strokes. An overview of the test setup used for the punching test is shown in Figure 75. The blanking force and the backstroke force were acquired during testing with a piezoelectric load transducer.

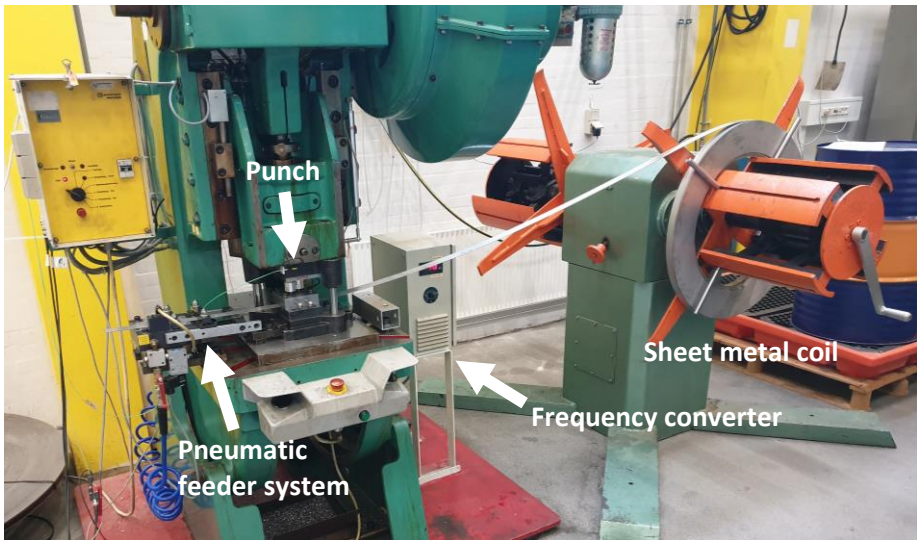

Figure 75: The test setup used for the punching test.

The punching tools used for the present study is based on the tool design proposed by Olsson [16], see Figure 76. For studying the influence of the application method of the lubricant, a lubrication channel was made in the guide plate for a continuous supply of liquid lubricant to the surface of the punch stem during testing.

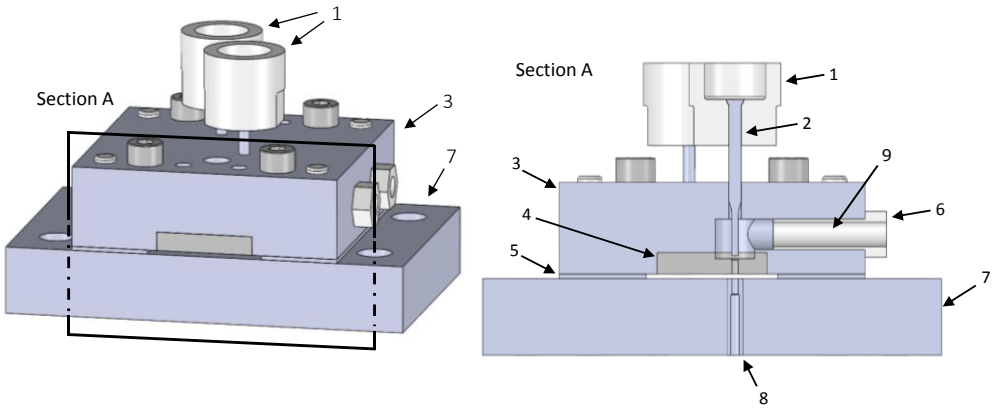

1. Transducer holder
2. Punch
3. Guide plate
4. Stripper plate
5. Spacing plates
6. Pressure gauge connector
7. Die plate
8. Die
9. Lubrication channel

Figure 76: Schematic illustration of the punching tool with a cross-sectional view of the main tool components.

For the present study, the punching tests were conducted with lubricant applied to the surface of the sheet metal by using roller lubricators. A second test series was furthermore conducted where the lubricant was applied on the surface of the punches through the lubrication channels in the punch tool.

Table 6: Chemical composition of the AISI M3:2 punches [282].

Composition (wt%)					
C	**Cr**	**Mo**	**W**	**V**	**Fe**
1.28	4.2	5.0	6.4	3.1	Balance

6.3.2 Four-ball test

Characterization of the wear behavior and the load-bearing capacity of the test lubricants was done with a four-ball test at The Danish Technological Institute. An overview of the test setup used for the four-ball test is shown in Figure 77. Characterization of the wear behavior was studied with a test conducted with a test load of 300N and a test duration of 1 hour with a rotational speed of 1420 RPM. Evaluation of the weld load was done by conducting a series of tests with a 1 minute test duration with increasing test loads until welding of the test specimen was achieved. The load was increased by 200 N per test. Both test series were conducted with Ø12.7mm balls of 100Cr6 and approximately 12 ml of liquid lubricant. The test specimens were cleaned in an ultrasonic bath with a Tickopur TR 13 cleaning agent at 60°C prior to testing. The developed wear scars on the three stationary balls were evaluated with an optical microscope. The average wear scar diameter was determined by measurement of the transversal and the longitudinal wear scar diameter.

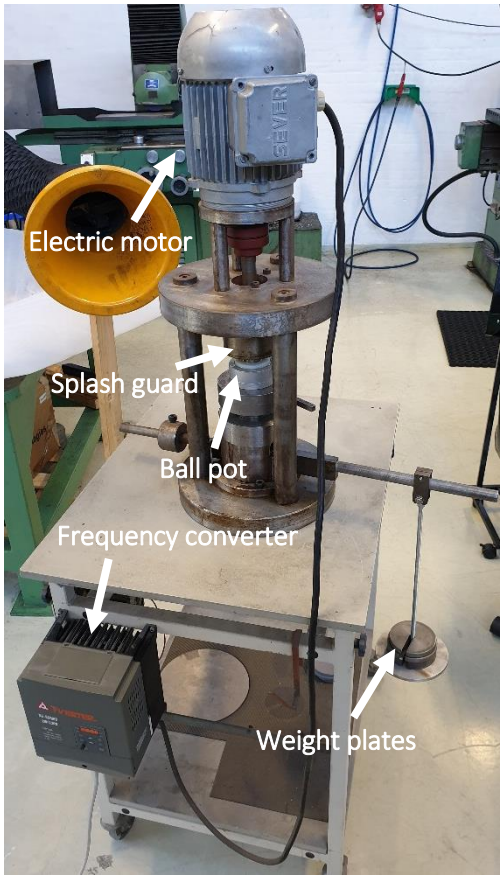

Figure 77: Test setup used for the four-ball test.

6.3.3 High temperature pin-on-disc test

A high temperature pin-on-disc test was carried out on the Bruker Universal Mechanical Tester Tribolab^{TM} at The Polytechnic University of Hauts-de-France. For the test, Ø69.85mm test discs were made of AISI M3:2, hardened to 64 HRC and polished to a circumferential surface finish of Ra = 0.08 µm. The pin was provided with a Ø6.35 ball in 440-C stainless steel with a hardness of 62 HRC. The test was carried out with a constant load of 16N and a rotational velocity of 0.2mm/s. The sliding contact was fully immersed in lubricant during testing. The low sliding velocity used in the test greatly reduces the influence of frictional heating in the sliding contact during testing. An external heat source increased the temperature in the test chamber by 6°C/min to a maximum of 350°C during the test. The slow temperature increase ensured homogenous heating of the workpiece. The temperature in the test chamber was measured with a thermocouple during testing.

6.3.4 Differential thermal analysis (DTA)

The thermal and physiochemical properties of the lubricants were characterized by differential thermal analysis (DTA) with a NETZSCH STA 449 C thermo-microbalance. Two test series were carried out. In the first test series, thermal analysis was performed on 500 mg AISI M3:2 tool steel powder mixed with the test lubricants. In the second case, the thermal analysis was carried out with 75 mg of each test lubricant separately. Each sample was transferred into an alumina crucible and heated to 550°C, with a 10°C/min heating rate. The tests were carried out in an argon atmosphere with a gas flow of 50 ml/min and in dry air with a gas flow of 43 ml/min of nitrogen and 7 ml/min of oxygen.

The morphological features of the AISI M3:2 powder were studied with SEM. Figure 78 shows an overview of the shape and the range of the particle size of the AISI M3:2 powder used for the DTA. The AISI M3:2 powder, which was created with gas atomization, reveals a powder consisting primarily of sphere-like particles with a low aspect ratio. The particle size of the powder ranges from 0.005-0.4mm.

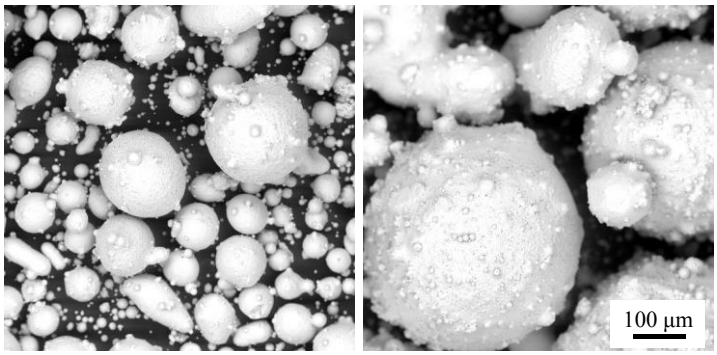

Figure 78: SEM micrograph of the AISI M3:2 powder used for the DTA.

6.3.5 Analysis of lubricant composition with XRF

Six commercially available lubricants with different additive formulations were selected for the presented punching experiment. An overview of the selected lubricants is shown in Table 7.

Table 7: General overview of the lubricants used for the blanking experiment.

Name	Lubricant manufacturer	Description	Kinematic viscosity at 40°C (cSt)
Illoform TDN 81	Castrol	Highly chlorinated paraffin oil	170
Illoform PN 226	Castrol	Medium chlorinated paraffin oil with S-, P-, ester-additives, and ZDDP	67
SF 125 A	Rhenus	Mineral oil with Ca-, S-additives and triphenyl phosphate	125
Montgomery DB 4265	FUCHS	Mineral oil with calcium carbonate and S-additives. Diluted 1:6 with water.	2
DROSERA MS 5	Total	Multipurpose machine oil containing triphenyl phosphate	5
Paraffin Oil	Carl Roth	Pure, high viscosity paraffin oil	75

A preliminary evaluation of the elemental composition of the different lubricants was made with X-ray fluorescence (XRF). This was done in order to characterize the overall lubricant content since the exact lubricant formulation is normally not disclosed by the manufacturer [283]. Detailed knowledge about the specific additive package of the different lubricants is valuable in order to understand the function of the lubricant in the forming operations. The composition of the lubricants were evaluated with an Oxford Maxxi 6 X-ray fluorescence analyzer, where the most common elements used in lubricant additives (EP, AW, FM) were surveyed, see Table 8.

Table 8: Elemental composition of the lubricants used for the blanking experiment. Values are given in counts per second (CPS) in an X-ray fluorescence analyzer.

	Elements (CPS)							
	Ba	Br	Ca	Cl	P	S	Mo	Zn
Illoform TDN 81	-	-	-	6631	113	142	-	-
Illoform PN 226	-	-	61	4381	87	153	-	2400
SF 125 A	-	-	4049	-	49	556	-	-
Montgomery DB 4265	-	-	793	-	18	16	-	-
DROSERA MS 5	-	-	-	-	11	-	-	-
Paraffin oil	-	-	-	-	-	-	-	-

No calibration standards were available for the different lubricant additives, meaning that an exact quantification of each lubricant additive was not possible. Evaluation of the counts per second (CPS) for each element allows for a qualitative evaluation of the elemental composition of the lubricants as well as giving a relative comparison of the quantity of each element. The XRF measuring technique has limited applicability for determining the content of elements with low atomic mass. Commonly used lubricant additives such as Mg and B compounds are there not detectable with the specified test setup. The XRF analysis is therefore used as a preliminary survey method for evaluation of the content of common film-forming additives like Cl, P and S in the lubricants.

6.4 Numerical modeling of the punching process

Axisymmetric FE analysis of the punching operation was made with a coupled thermo-mechanical model with the commercial software LS-DYNA. An overview of the modeled tool setup is shown in Figure 79, and the input parameters are included in Table 9.

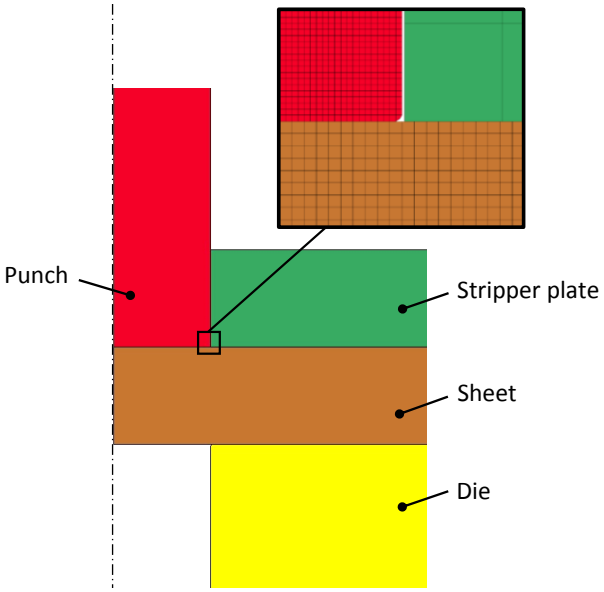

Figure 79: Numerical model with the initial mesh shown in the detail.

Table 9: Input parameters for numerical simulation.

	Punch (AISI M3:2)	**Blanking Die (1.3343 HSS)**	**Sheet material (EN 1.4301)**
Initial temperature (°C)	20	20	20
Heat capacity (J/kg·K)	420	460	500
Thermal conductivity W/(m·K)	24	27	15
Heat transfer coefficient (kW/m²·K)	50	50	50
Density (g/cm³)	7.73	8.12	7.90
Elastic modulus (GPa)	230	217	200
Poisson's ratio	0.3	0.3	0.3

In the FE model, the forming tools were modeled as rigid steel tools, whereas the sheet material was modeled as an elastoplastic material characterized by a Ludwig formulation $\sigma_f = 1339\varepsilon^{0.594}+231$ [MPa], which was determined by tensile testing. The sheet material was discretized with a quadrilateral mesh with an element size of 0.025mm. A COF 0.1 was furthermore assigned to all the contacting interfaces. For the FE analysis of the punching operation, a rounding radius of 0.002mm was applied to the edge of the punch and the edge of the die in order to avoid localized damage due to sharp contact in the interfaces between tools and the sheet material. A remeshing algorithm was furthermore applied in the numerical model to compensate for the large localized deformation of the mesh in the shear band region. Ductile fracture of the sheet material was modeled with a simple critical shear stress criterion, where element deletion was initiated at a shear stress of 1300 MPa. Comparison of the punch force and the morphology of the sheared edge indicates that the applied fracture model gives an accurate description of the ductile fracture occurring in the punching process, see Figure 80. For evaluation of the developed punch temperature, the thermal coupling is maintained between the punch surface and the sheared surface after element deletion.

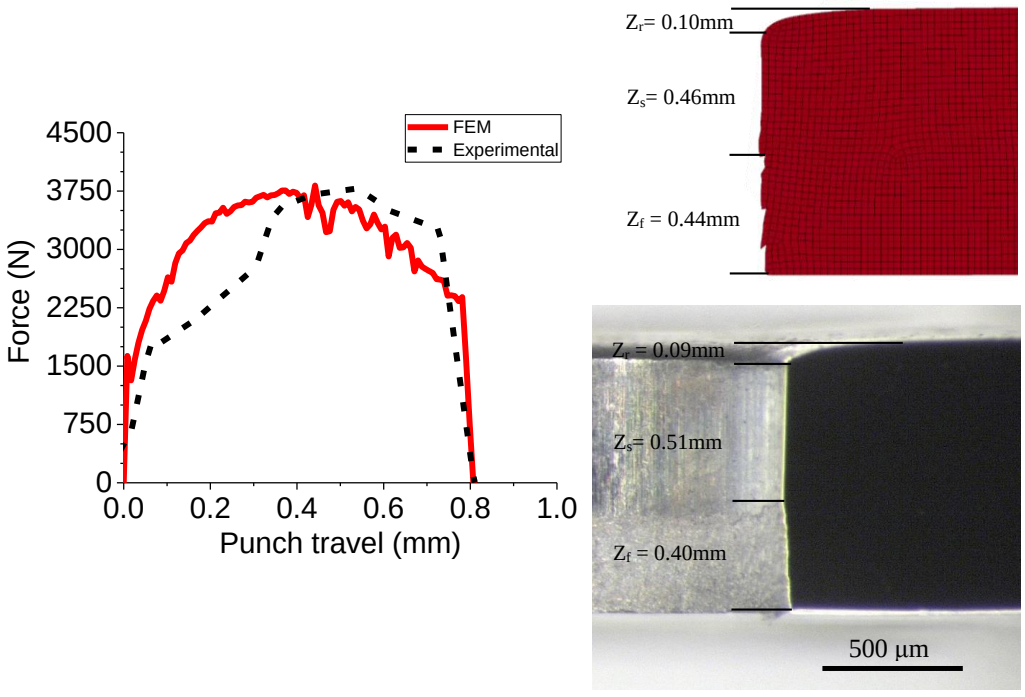

Figure 80: Comparison of the experimental results with the numerical simulation with (a) the punch force and (b) the morphology of the sheared surface.

A cross section of the sheared surface is shown in Figure 80 compared to the sheared surface obtained with numerical simulation with the specified fracture model. Comparison of the actual sheared surface with the results from the numerical simulations indicate a reasonable accuracy of the FE model, where minor deviations are primarily found in the size of the shear zone and the fracture zone. Comparison of the measured blanking force and the results from the numerical simulation indicate a similar development of the force exerted on the punch during the punching process. A further correlation cannot be made due to the limitation of the sampling speed of the data acquisition unit used in the experimental setup.

6.5 Experimental results

6.5.1 Punching tests

The punching test was conducted with a number of different liquid lubricants for evaluation of the lubricant performance. Figure 81 shows the results of the punching test, plotting the backstroke force as a function of the number of strokes for the tested lubricants. Dry conditions are also included for reference.

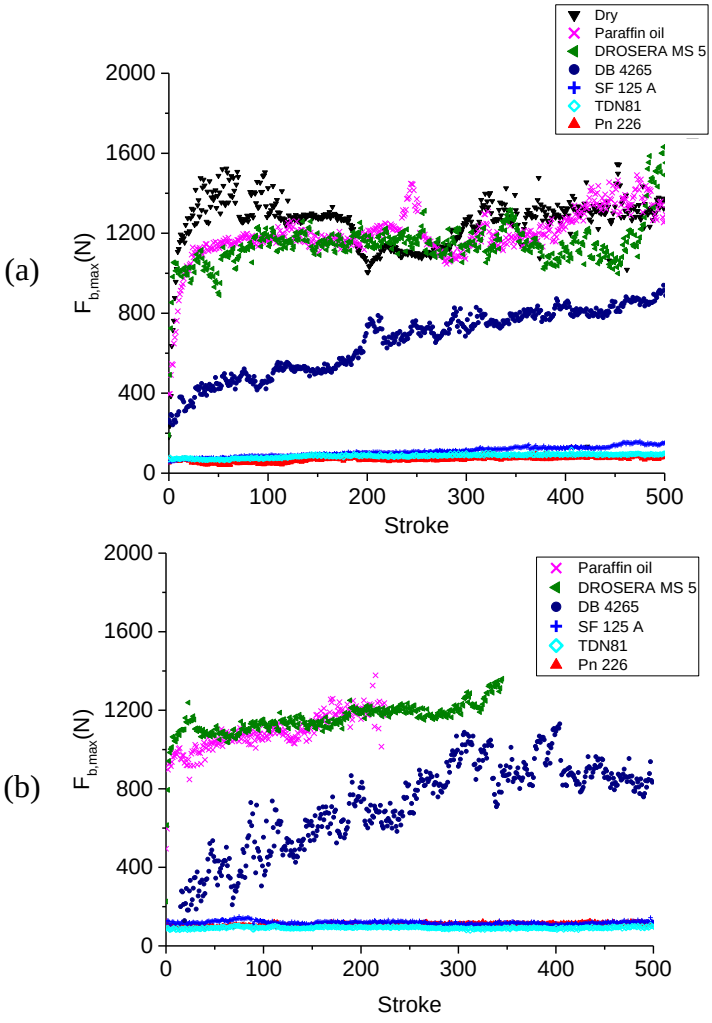

Figure 81: Backstroke force as a function of the number of strokes for the tested lubricants and under dry conditions when (a) applying the lubricant to the surface of the sheet material with roller lubricators and (b) application of the lubricant via the lubricant channels.

Inspection of the surface structure of the punches after testing was done with an FEI Inspect™ S50 SEM, Figure 82.

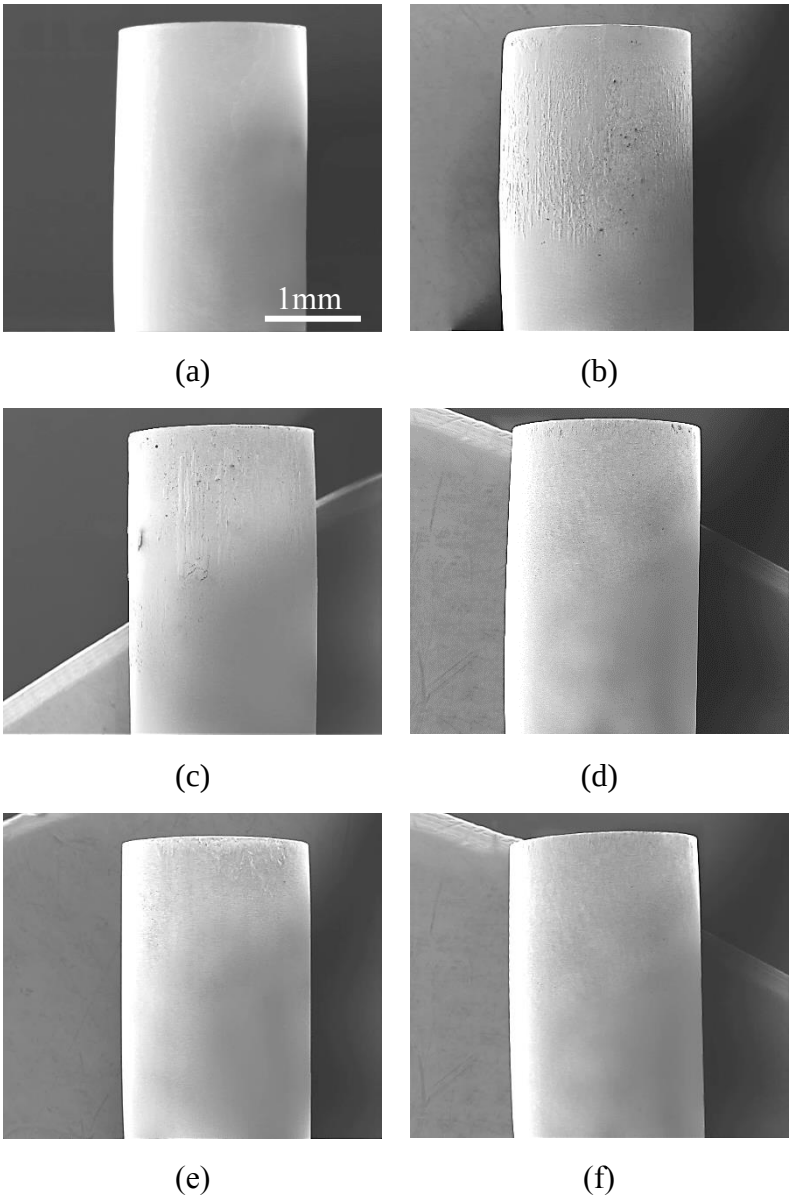

Figure 82: SEM micrographs of the punch surface of (a) a new punch and (b-f) punches after testing with different lubricants: (b) DB 4265, (c) Drosera MS 5, (d) Pn226, (e) SF125 and (f) TDN81.

The development of the backstroke force under dry conditions is found to reach saturation approximately within the first 30 strokes. In the subsequent strokes, the backstroke force is found to fluctuate around an average value of approximately 1300N. The stabilization of the backstroke force is attributed to a saturation of the pick-up of workpiece material on the punch surface. The test series conducted with the low viscosity oil Drosera MS 5 and the pure paraffin oil were found to exhibit

similar performance. The DB 4265 lubricant, containing Ca- and S- based lubricant additives, exhibits a gradually increasing backstroke force within the first 500 strokes. The DB 4265 lubricant is based on a suspension of solid particles in the base oil, which inhibits direct metal-to-metal contact between the punch and the sheet material [284]–[286]. This mechanism of lubrication is found to retard the adhesive wear that accumulates on the punch stem. Common characteristics of the lubricants, which exhibited poor performance in the punch test, are low viscosities and either a low content of film-forming additives or no additives at all, as evaluated with XRF. The two chlorinated paraffin oils, TDN81 and Pn 226, were found to exhibit excellent lubricating ability in the punching test with a consistently low backstroke force throughout the 500 strokes. The SF 125 A lubricant, containing Ca-, P- and S-additives, was found to have comparable performance, however, with a small increase in the backstroke force after approximately 250 strokes.

From inspection of the surface structure of the punches after testing, it is seen that the three highly additivated lubricants, which resulted in low backstroke forces in the punching test, have resulted in minor levels of pick-up of workpiece material around the punch tip. In contrast to this, the test series conducted with the DB 4265 and the Drosera MS 5 lubricants are found to have a large amount of accumulated pick-up of workpiece material on the punch stems, corresponding to a large increase in the measured backstroke force during the test. This development of the wear mechanism was previously described by Olsson et al. [287].

An overview of the development of the backstroke force during the punching test is shown in Figure 83 and Figure 84, for the Drosera MS 5 and the Pn226 lubricants, for respective representation of poor and excellent lubricating ability in the punching test.

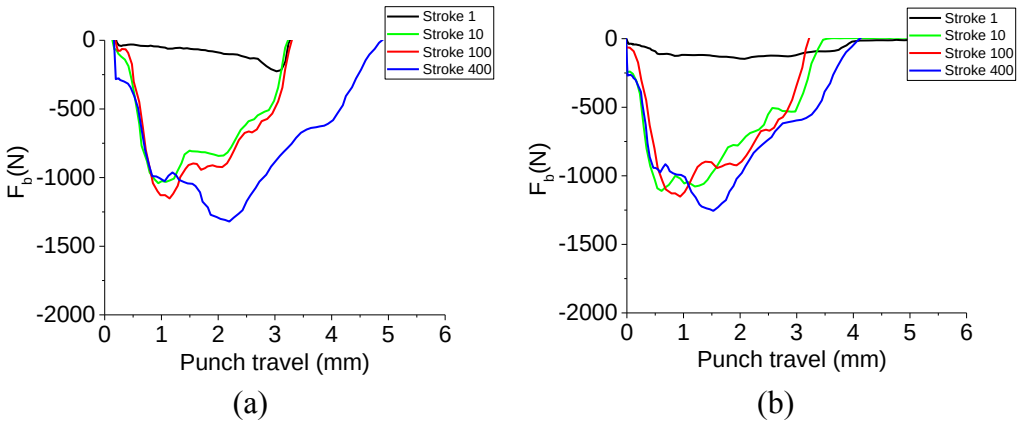

Figure 83: Development of the backstroke force with the Drosera MS 5 lubricant applied on (a) the surface of the punch and (b) applied on the surface of the sheet material with roller lubricators.

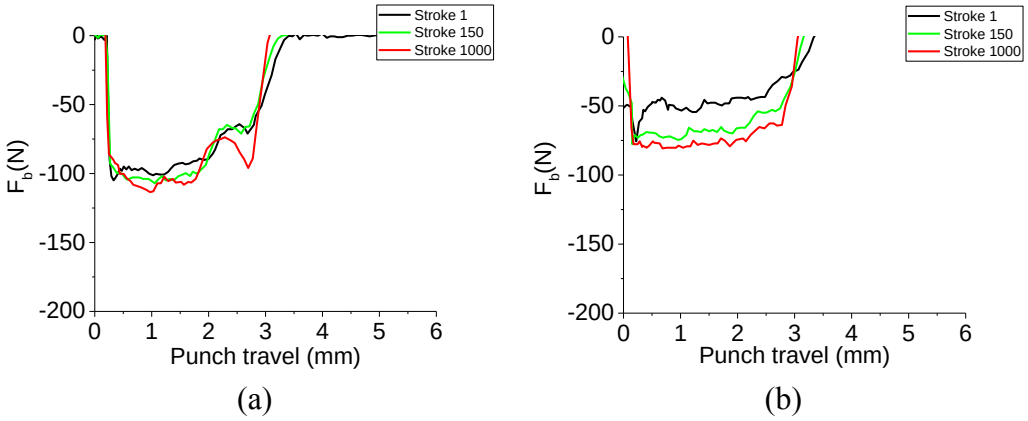

Figure 84: Development of the backstroke force with the Pn 226 lubricant applied on (a) the surface of the punch and (b) applied on the surface of the sheet material with roller lubricators.

As highlighted in the previously in the study, the Drosera MS 5 reveals substantially higher levels of the measured backstroke force during testing, due to the pick-up of workpiece material on the punch stem. The Drosera MS 5 furthermore showcases a broadening of the load curve as pick-up of workpiece material gradually covers a larger part of the punch surface after a number of successive strokes [287]. The Pn226 lubricant is, however, found to introduce a uniform backstroke force within a punch travel of approximately 3mm. This behavior is attributed to the minor levels of pick-up developed only at the punch tip region, as seen in the SEM micrograph in Figure 82.

Comparison of the two methods of applying the lubricant for the test reveals a similar development of the backstroke force across all test series. This indicates that the lubricant efficiency in the punching test is primarily governed by the tribological properties of the additive package of the lubricants and that the application method has no noticeable impact in the present study. While similar wear behavior is found with the two lubricant application methods, further testing is still required in order to evaluate the possibility for minimization of the required lubricant dosage for the punching test.

6.5.2 Four-ball test

An overview of the wear characteristics and the determined weld load for the tested lubricants is shown in Figure 85a and Figure 85b, respectively. Micrographs of the developed wear scars are shown in Appendix A.

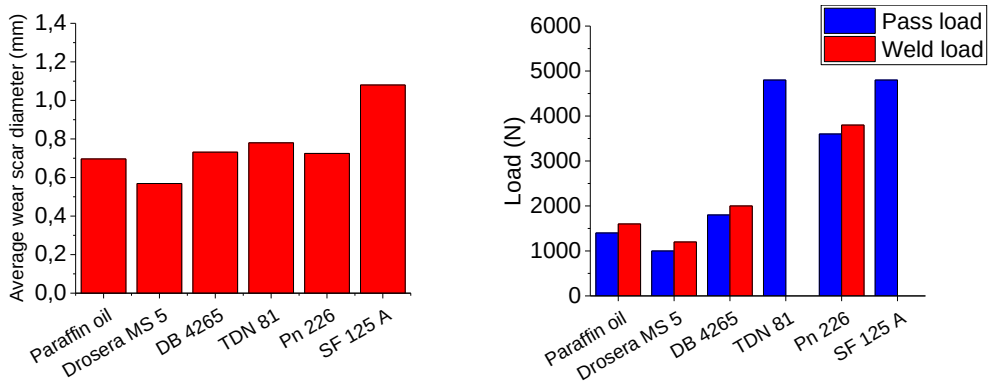

(a) (b)

Figure 85: Wear behavior and the load-bearing capacity of the tested lubricants in the four-ball test. The results are shown by (a) developed wear scar diameter and (b) the weld load and the pass load.

From Figure 85a it is seen that the wear scar diameters generated during the four-ball test range from 0.57-0.73 mm for most of the tested lubricants. The test with SF 125 A is however found to result in a substantially larger wear scar diameter. While the different lubricants exhibited a widely varying performance in the punching test, the developed wear scar diameter indicates a comparable wear development in the four-ball test. Evaluation of the load-bearing capacity, however, reveals a substantial difference in the tribological properties of the lubricants. The tested lubricants with high weld loads in the four-ball test correspond to the lubricants with excellent results in the punching test; namely those lubricants, which inhibited adhesive wear on the punch stem. Conversely, the lubricants with low weld loads, in the range of 1600-2000 N, are those providing poor lubrication in the punching test. The weld load of TDN 81 and SF 125 A could not be determined for the present study as the loads were found to exceed the maximum capacity of the experimental equipment. The lubricants with high load bearing capacities are found to form tribofilms in the interface between the workpiece and the punch, which retards the mechanism of adhesive wear on the punch surface, as e.g. seen with the chlorinated paraffin oil. The load-bearing capacity of the lubricant is therefore identified as one of the primary tribological lubricant properties for punching and blanking processes, where the affinity for adhesion of workpiece material to the punch poses a major tribological issue.

6.5.3 High temperature pin-on-disc test

The influence of thermal conditions on the tribological properties of the lubricants was studied with the high temperature pin-on-disc test. The main results are summarized in Figure 86, where an average COF of two test repetitions is shown as a function of temperature.

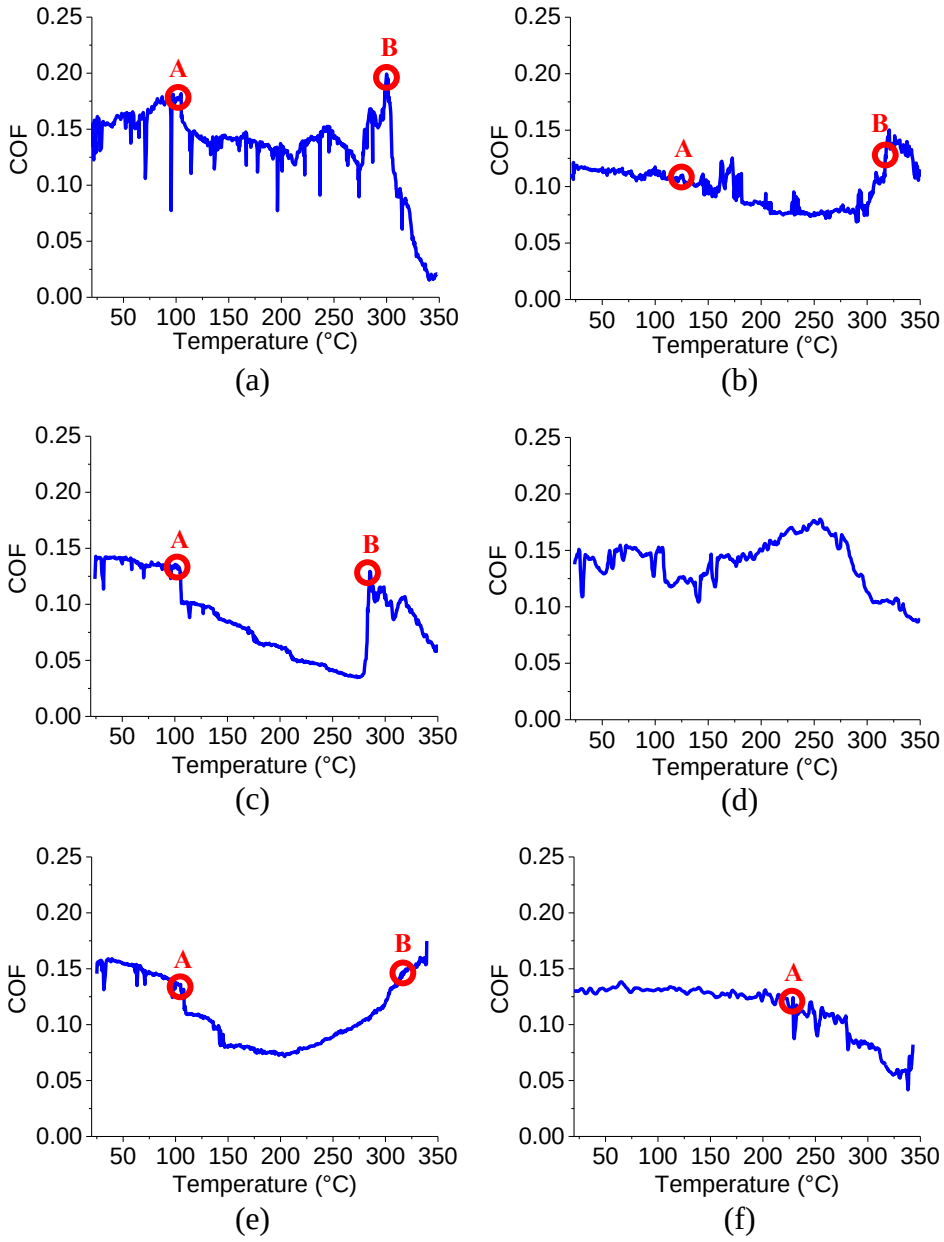

Figure 86: COF as a function of the test temperature in pin-on-disc testing with (a) TDN81, (b) SF 125 A, (c) Pn226, (d) Paraffin oil, (e) Drosera MS 5 and (f) DB4265.

All the additivated lubricants with known boundary lubrication properties are in the pin-on-disc test found to exhibit a temperature interval, where a significantly lower COF is measured due to thermal activation of the lubricant additives. This temperature interval is defined by point (A), where the active additive species in the lubricant are adsorbed on the surface of the metal, forming a tribofilm that lowers the COF and point (B), where a loss of the lubricating properties occurs due to thermal degradation of the lubricant. These transition temperatures indicate the working range of the lubricant, where properties of boundary lubrication are exhibited. The pure paraffinic base oil is conversely found to have an increasing COF at elevated temperatures due to thinning of the lubricant. After the initial increase in friction, a large decrease in the measured COF is seen at approximately 270°C, when nearing the boiling point of the lubricant, as seen in the following DTA results in section 6.5.4.

Inspection of the generated surface structure of the discs and an analysis of the surface composition was made with EDX with the Zeiss Supra 35 field emission gun SEM. Several test specimens exhibit the formation of a solid layer of lubricant residue adjacent to the wear scar after testing. This behavior was most pronounced with the specimens lubricated with the DB 4265 and the PN 226 lubricants, see Figure 87. An EDX analysis was therefore made on the surface of the test specimen after rinsing with ethanol in order to remove the majority of remnants of liquid lubricant without removal of weakly adhered lubricant species, see Table 10. A second EDX analysis was furthermore conducted for analysis of the surface composition after cleaning of the surface with acetone in an ultrasonic cleaning bath in order to ensure fully cleaned surfaces, see Figure 88 and Table 11. This was done in order to evaluate the presence of chemically reacted surface film without the influence of residue lubricant on the surface.

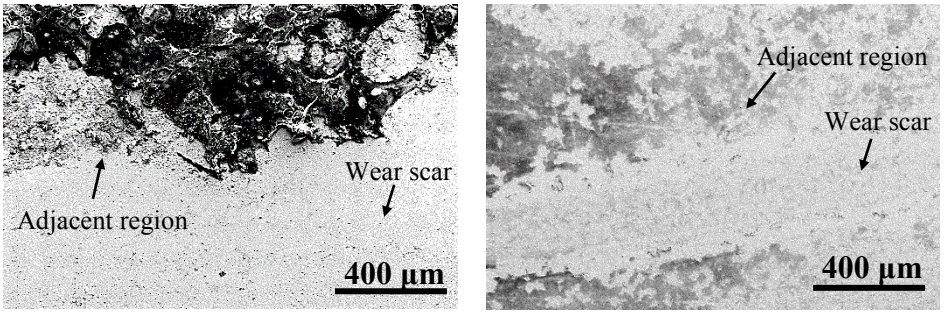

(a) (b)

Figure 87: SEM micrographs of the surface of the test specimen after pin-on-disc testing and rinsing with ethanol. The tested lubricants are (a) DB 4265 and (b) Pn 226.

Table 10: EDX analysis of the test specimens after rinsing with ethanol.

		Element (wt%)					
Lubricant	**Location**	**C**	**Cl**	**P**	**S**	**Ca**	**Other**
Illoform TDN 81	Adjacent region	22.6	0.7	-	-	-	76.7
	Wear scar	12.5	0.4	-	-	-	87.1
Illoform PN 226	Adjacent region	61.5	0.8	1.8	-	0.3	35.6
	Wear scar	10.2	0.5	-	-	-	89.3
Montgomery DB 4265	Adjacent region	61.0	-	0.3	1.3	1.8	35.6
	Wear scar	26.7	-	-	-	-	73.3
SF 125 A	Adjacent region	32.1	-	-	17.3	0.2	50.6
	Wear scar	11.7	-	-	8.0	-	80.1
DROSERA MS 5	Adjacent region	11.1	-	-	-	-	88.9
	Wear scar	6.3	-	-	-	-	93.7
Paraffin oil	Adjacent region	5.1	-	-	-	-	94.9
	Wear scar	5.0	-	-	-	-	95.0

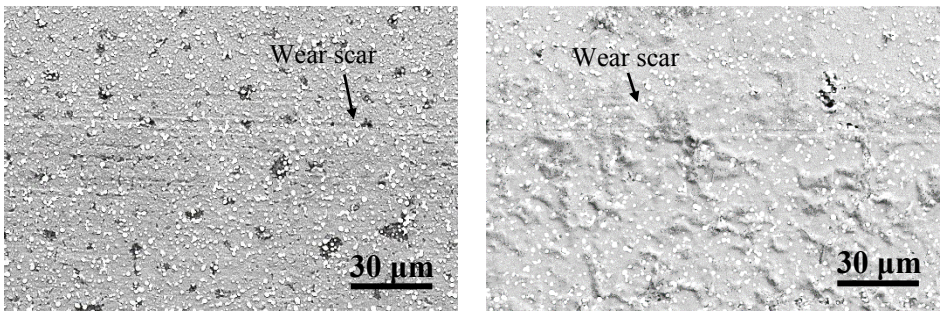

(a) (b)

Figure 88: SEM micrographs of the surface structure of the test specimen after pin-on-disc testing and cleaning with acetone. The tested lubricants are (a) DB 4265 and (b) Pn 226.

Table 11: EDX analysis of the test specimens after cleaning with acetone.

		Element (wt%)					
Lubricant	**Location**	**C**	**Cl**	**P**	**S**	**Ca**	**Other**
Illoform TDN 81	Wear scar	11.1	0.4	-	-	-	88.5
Illoform PN 226	Wear scar	13.7	0.5	0.6	-	-	85.2
Montgomery DB 4265	Wear scar	16.6	-	-	-	-	83.4
SF 125 A	Wear scar	18.3	-	-	7.1	0.6	74.0
DROSERA MS 5	Wear scar	11.1	-	-	-	-	88.9
Paraffin oil	Wear scar	7.1	-	-	-	-	92.9

Evaluation of the surface composition of the test specimens, cleaned with ethanol, indicate the presence of lubricant species in the wear scar and the adjacent regions for all the additivated lubricants. The region adjacent to the wear scar are in all cases found to contain a high concentration of the remaining lubricant species, indicating the gradual removal of the surface species in the generated wear scar during the

test, due to the sliding contact with the tool pin. TDN 81, Pn 226 and SF 125 A indicate the presence of a surface film even after contact with an aggressive solvent like acetone. Both lubricants with additive packages based on chlorinated paraffins exhibit the presence of minor levels of Cl in the wear scar, where iron chlorides are commonly reported to be the main surface constituents with Cl-based EP additives [288]. The test series conducted with the DB 4265 lubricant does not exhibit the presence of any lubricant species on the tool surface after cleaning with acetone. This is indicative of the function of the lubricant, which is based on a separation of the contacting bodies of the tribosystem via a suspension of solid particles in the lubricant, as seen in Figure 87.

Exceeding point (B) results in loss of the tribological function of the lubricant due to thermal degradation caused by desorption of polar molecules and melting of chemically reacted tribofilms [289]. Analyzing the surface composition of the test specimen after the lubricant has undergone thermal decomposition could, therefore, render the analyzed surface as unrepresentative of the surface generated during testing. A supplementary study was therefore conducted with a pin-on-disc test, conducted at room temperature where the developed wear scar is only influenced by frictional heating from the sliding contact without an external heating source, see Appendix B.

6.5.4 Differential thermal analysis (DTA)

Evaluation of the lubricant properties at elevated temperatures was furthermore done with a DTA, see Figure 89. The DTA was conducted in dry air as well as in an inert argon atmosphere in order to study the influence of oxygen on the lubricant additives and to conversely limit the oxidative degradation of the lubricants.

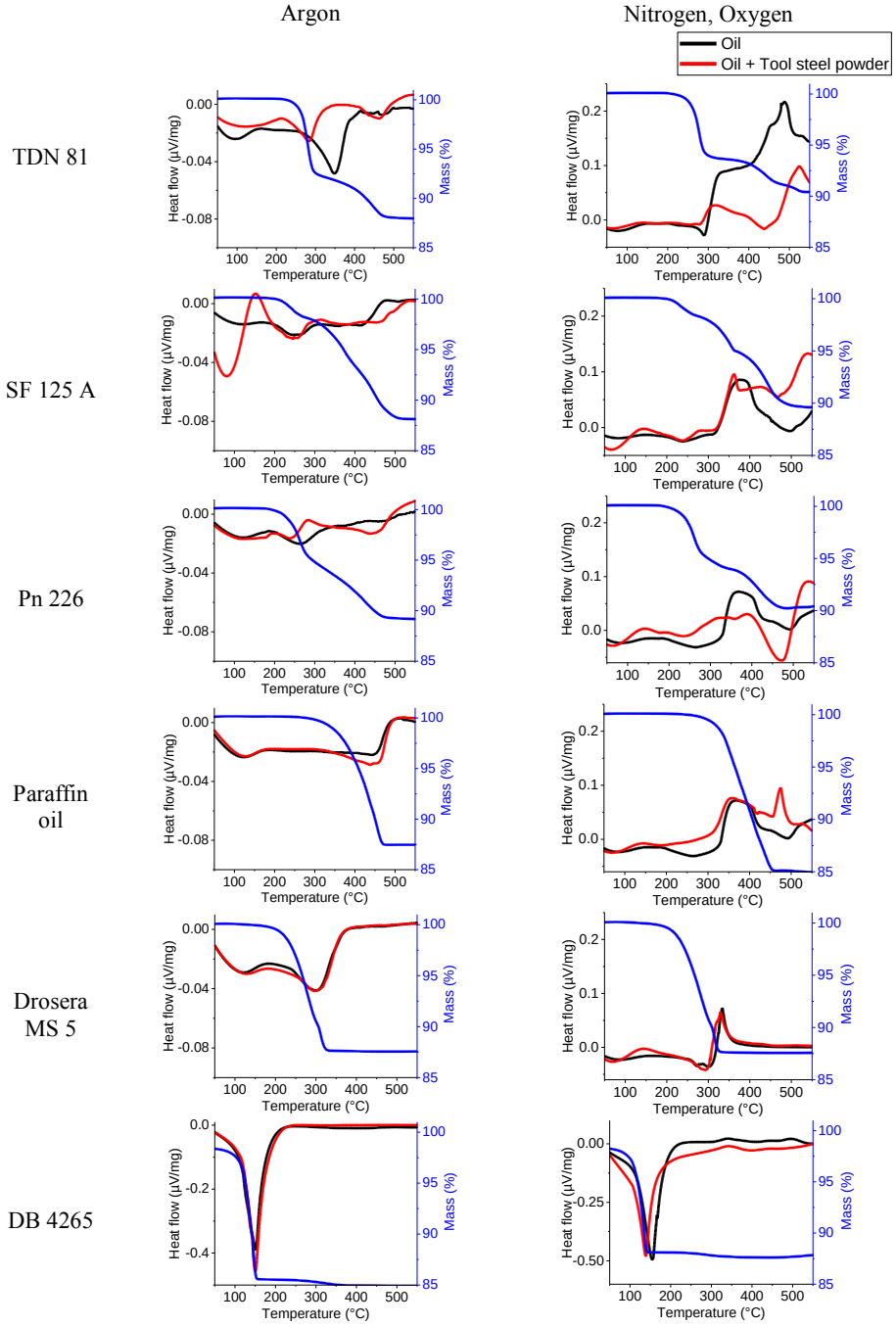

Figure 89: DTA thermograms of the tested lubricants.

The thermograms established from testing the pure lubricants and the tool steel powder and lubricant mixtures were used for assessment of the transition temperatures, where activation of the lubricant additives was initiated. This was evaluated by superposition of the two thermograms [279]. A summary of the critical transition temperatures is shown in Table 12.

Table 12: Overview of the transition temperatures of the tested lubricants.

	Temperature of initial chemical reaction [°C]	**Temperature of lubricant breakdown [°C]**	**Temperature interval of the first exothermic peak [°C] (Ar)**	**Temperature interval of the first exothermic peak [°C] (N, O)**
Illoform TDN 81	101	287	151-256	-
Illoform PN 226	104	285	223-339	89-338
SF 125 A	109	309	125-195	108-212
Montgomery DB 4265	229	-	-	-
DROSERA MS 5	105	319	-	90-226
Paraffin oil	-	-	-	94-369

The thermogram for Pn 226 and tool steel powder mixture reveals an exothermic peak at a temperature of 223-339°C in the inert Ar atmosphere. The first exothermic peak in dry air is, however, seen in the temperature range of 89-339°C. The widening of the temperature range of the exothermic peak is possibly due to the influence of oxygen on the compound additive package of the lubricant, as certain groups of lubricant additives, e.g. certain S-based additives, only exhibit a tribological function with the presence of oxygen [262]. The thermogram for the pure paraffinic base oil reveals an initial exothermic peak in the temperature range of 94-369°C in dry air, while no major reaction peaks were found in Ar. This behaviour is attributed to the oxidative degradation of the lubricant at elevated temperatures with the presence of oxygen. This is indicative of the sensitivity of the DTA technique towards a range of different physical and chemical phenomena occurring simultaneously during the heating cycle, highlighting the importance of assessing the lubricants in varying atmospheres for evaluation of the thermal stability and the tribological properties of the lubricant. Additives such as antioxidants are commonly used in commercially available lubricants for sacrificial oxidation in order to retard the oxidative degradation of the lubricant. The use of antioxidant additives, therefore, influences the thermal stability of the lubricant without a direct influence on the tribological properties. Assessment of the thermal properties of the lubricant in an inert atmosphere, therefore, allows for separation

of the effect of lubricant additives commonly found in the compound additive packages in commercially available lubricants. The DTA is therefore used as a supplementary technique for assessment of the lubricant properties at elevated temperatures. This encompasses a supplementary method for determining the transition temperatures of the film forming additives and the thermal stability of the lubricant.

The DB 4265 lubricant exhibits a lower COF at temperatures above 229°C. The DTA thermogram of the DB 4265 lubricant reveals a large endothermic peak as the added dilutent in the lubricant is evaporated. A further increase of the test temperature indicates a minor decrease in the mass of the test sample. This is seen at a test temperature of approximately 224°C, where a corresponding decrease of the COF is measured in the pin-on-disc test. The decrease in the COF is therefore attributed to evaporation of the liquid lubricant constituents, where the suspended solid particles in the lubricant remain on the surface of the test specimen. This corresponds well with the observed surface film remaining on the test specimen after the pin-on-disc test, see Figure 87a. ZDDP is a common AW additive, found in the additive package of the Pn226 lubricant. Tse et al. [290] reported that the ZDDP compound undergoes irreversible thermal degradation at a temperature of approximately 220°C, evaluated by in-situ high-pressure and high-temperature infrared spectroscopy. In the present study, the Pn226 lubricant exhibits a low COF in the temperature interval between 104-285°C. The Pn226 lubricant is furthermore seen to have a temperature range where a lower COF is exhibited similar to the TDN 81 lubricant, which also has an additive package based on chlorinated paraffins. A similar correlation is seen with the SF 125 A and the Drosera MS 5 lubricants, which both contain triphenyl phosphate as an AW additive [291], [292].

.

6.5.5 Numerical simulation of tool and interface temperature

Punching operations are commonly found to develop highly localized temperature fields and transient temperature peaks, which makes it difficult to characterize the process temperatures with conventional measurement techniques, e.g. thermocouples or thermographic measurements. Assessment of the temperature development in the forming tool and the sheet material during the punching operation in the present study is therefore done with a coupled thermo-mechanical FE simulation. The simulated temperature field during the punching operation is shown in Figure 90a, where point 1 and point 2 are highlighted. Point 1 is inside the punch 0.42 mm from the punch edge, while point 2 is at the center of the shear band region.

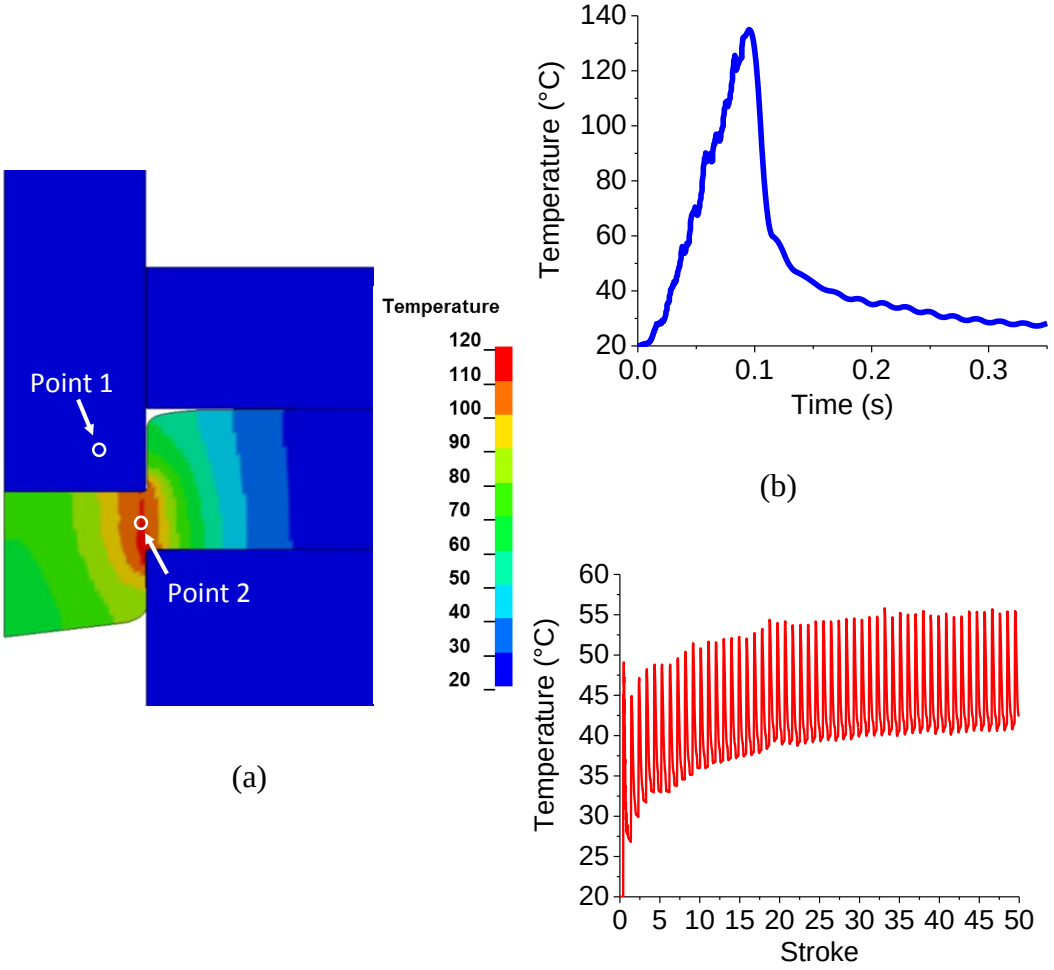

Figure 90: Thermo-mechanical FE simulation of temperature showing (a) the temperature distribution in the tools and workpiece in the first stroke, (b) temperature development in point 2 during the first stroke, and (c) temperature development in point 1 during the first 50 strokes.

The temperature development in the sheared surface, see Figure 90b, shows a high temperature peak during the forward punch stroke, followed by a rapid dissipation of the generated heat after approximately 0.1s. The peak temperature ranges locally between 135-150°C in the shear band region. Figure 90c shows the development of the punch temperature in point 1 during the first 50 strokes. The transient temperature peak and the short time of contact between the punch and the sheet material result in minor heat transfer to the punch, which is found to stabilize after approximately 40 strokes. The peak temperature in the interface between the punch and the sheet material governs the tribological behaviour of the lubricant, as seen in the pin-on-disc test and the DTA. The lubricants providing excellent lubrication in the punching test are therefore characterized by having high load bearing capacities combined with an applicable thermal working range, where the peak temperature in the punching process ensures the activation of the lubricant additives in the punch/workpiece interface in order to inhibit the development of pick-up of workpiece material.

6.6 Conclusion

In this chapter, the performance of different lubricants was evaluated with a process test which emulates the tribological conditions of a fine blanking operation. A clear correlation between the developed punch wear and the measured backstroke force was confirmed in accordance with literature. Assessment of process temperatures was done with numerical analysis. Analysis of the physiochemical properties of the tested lubricants revealed that an applicable temperature range and a high load-bearing capacity are central lubricant properties necessary for ensuring sufficient lubricating ability for punching and blanking operations.

Chapter 7 Conclusion and future work

This thesis presented a study on process monitoring in sheet metal forming using AE for online evaluation of wear and frictional conditions. From a series of different simulative forming tests, a methodology for evaluation of process conditions was derived, based primarily on time domain analysis. In the different laboratory tests, application of the AE measurements was found to describe different tribological process phenomena such as fluctuations in the measured COF, analysis of wear severity and the condition of tool coatings. The derived methodology was furthermore applied for monitoring of formings conditions in a deep drawing operation, where the AE technique could indicate the occurrence of process deviations due to tool wear. Further testing is, however, required for validation of the applicability of AE as a process monitoring technique in industrial production environments, where the influence of noise e.g. from parallel production processes could pose a bigger issue. This could possibly imply a further refinement of the derived testing methodology, in terms of the required signal filtering and feature extraction. For online process monitoring of industrial forming processes with complex forming geometries, the adaption of multi-channel systems could furthermore be applied for evaluation of source location. Application of the multi-channel AE system could thereby support a fully condition-based tool maintenance schedule where damage localization and severity is continuously monitored.

The study furthermore presented an analysis of an industrial production platform for stamping of an EGR component, where the use of chlorinated paraffin oil was previously deemed necessary in order to facilitate stable production conditions. The forming die, used in the described production platform, was designed with a stepped drawbead feature, which greatly influences drawing characteristics of the component and central tribological parameters such as surface expansion, contact pressure, and sliding length. The drawbead design implemented in the forming die was based entirely on a trial and error procedure, where dimensional changes were made manually to the drawbead during the die tryout stage in the production of the forming tools. A 3D scan of forming the tools was therefore made for characterization of the implemented drawbead design. Characterization of the production process was made with numerical analysis with the scanned die geometry. Based on the numerical analysis, critical die regions were extracted in terms of the developed wear work, indicative of the severity of the tribological conditions introduced locally by the drawbead geometry. Further characterization

of the production conditions was carried out by measurement of load, travel and the die temperature profile for extraction of experimental test parameters. A drawbead tool was designed, for offline replication of the industrial forming conditions. With the designed drawbead tool, a series of tests were carried out for evaluation of the performance of alternative, environmentally friendly tribosystems. The tests concluded that no other lubricant could replace the highly chlorinated BWN 205 lubricant when tested with an untreated tool steel material. A combination of a Tenifer® QPQ surface treatment and a range of different environmentally benign deep drawing lubricants were, however, found to provide sufficient tribological performance in order to replace the BWN 205 lubricant.

The wear behavior in drawbeads, with varying drawbead geometries and different workpiece materials with different mechanical and tribological properties, were investigated in a supplementary study. In a semi-circular drawbead geometry, the EN 1.4301 stainless steel was found to develop a substantial amount of galling at the groove shoulder radius, where the obtained contact pressure is at the highest levels. The primary wear mechanism, seen when testing the DP 980 workpiece material, was based on powdering of the electrogalvanized workpiece coating. The limits of lubrication was thereby governed by an accumulation of third body particles from the electrogalvanized workpiece coating in the planar contact of the drawbead. The different wear mechanisms observed during testing highlights the importance of offline simulative tests for evaluation of wear behavior and tribosystem efficiency.

Since the physical design of drawbeads is often based on a trial and error approach, the use of drawbeads in industrial forming dies often imply a large variety of different drawbead types and geometries, each tailored to the specific product geometry. Extended testing of the limits of lubrication of various drawbead types and geometries, combined with different lubricants, sheet materials, tool materials and tool coatings can, therefore, prove to be valuable for tool designers for estimation of the tribological loads, tool life and costs linked to manufacturing and maintenance of tools. The use of tool coatings such as DLC, CrN and TiAlN have in recent years been implemented extensively in forming industry for extending the tool life of forming tools exposed to severe tribological conditions. Further analysis of the limits of lubrication with such tool coatings, used in tribologically severe processes could therefore be valuable for assessment of tribosystem efficiency in processes which often require hazardous lubricants. Further work could similarly be conducted based on automated production lines with high production rates and high tool temperatures, for assessment of tribosystems efficiency with increased thermal stressing of the lubricants.

The study furthermore analyzed the tribological function of commercial forming lubricants for characterization of the central lubricant properties needed for lubrication in punching and blanking operations. This was done based on an analysis of physiochemical lubricant properties combined with a process test. With a process test that emulates the forming conditions in fine blanking operations, the tribological efficiency of different commercially available forming lubricants were studied. A clear correlation between the developed punch wear and the measured backstroke force was confirmed in accordance with literature and the previous work conducted at DTU-MEK. The study found that an applicable temperature range and a high load-bearing capacity are central lubricant properties necessary for ensuring sufficient lubricating ability for punching and blanking operations. It was furthermore explored that the influence of the lubricant application method, had no noticeable impact on the lubricating ability of the commercially available forming lubricants. The results of the analysis indicated that punching and blanking operations introduce severe tribological conditions where only lubricants with strong boundary interaction in the interface of the tribosystem can minimize the pick-up of workpiece material on the punch stem during testing.

Analysis of the tribological properties of new, environmentally friendly tribosystems for fine blanking operations, however, requires further investigation of the chemical function of the different types of film-forming additives, additive synergy and the influence of parameters such as additive concentration, lubricant dosage, tool coatings and sheet thickness. Analysis of lubricant dosage, tool coatings and sheet thickness, combined with further testing of the influence of the lubricant application method could possibly yield a reduction of the minimum amount of lubricant necessary for punching and blanking operations.

Bibliography

[1] *European Parliament, Council (2006) REACH, EC Regulation No. 1907/2006 of the European Parliament and of the Council.* , Retrieved April 11, 2019.

[2] "Ministry of Environment, Government of Japan http://www.env.go.jp/en/laws/policy/basic/index.html." , Retrieved April 11, 2019.

[3] "Ministry of Environment, Government of Japan http://www.env.go.jp/en/laws/recycle/01.pdf." , Retrieved April 11, 2019.

[4] J. M. Herdan, "Lubricating oil additives and the environment - An overview," *Lubrication Science*, vol. 9, no. 2. pp. 161–172, 1997.

[5] N. Bay, A. Azushima, P. Groche, I. Ishibashi, M. Merklein, M. Morishita, T. Nakamura, S. Schmid, and M. Yoshida, "Environmentally benign tribo-systems for metal forming," *CIRP Ann. - Manuf. Technol.*, vol. 59, no. 2, pp. 760–780, 2010.

[6] N. Bay, T. Nakamura, and S. Schmid, "Green Lubricants for Metal Forming," *Proc. 4th Int. Conf. Tribol. Manuf. Process.*, vol. 1, pp. 4–33, 2010.

[7] T. Wakabayashi, "Technological Aspects and Future Trends in Lubricating Oils," *Japanese J. Tribol.*, vol. 48, no. 2, pp. 206–213, 2003.

[8] N. Bay, D. D. Olsson, and J. L. Andreasen, "Lubricant test methods for sheet metal forming," *Tribol. Int.*, vol. 41, pp. 844–853, 2008.

[9] H. Ike, "Report on Metal Forming Tribology Research in Japan with Special Focus on Environmental Aspects," *Proceed. Int. Conf. Tribol. Manuf. Process.*, pp. 229–238, 2004.

[10] F. Klocke, T. Maßmann, K. Bobzin, E. Lugscheider, and N. Bagcivan, "Carbon based tool coatings as an approach for environmentally friendly metal forming processes," *Wear*, vol. 260, no. 3, pp. 287–295, 2006.

[11] C. T. White and J. W. Mintmire, "The Future of Metalworking Fluids Additives," *Stle*, vol. 71, no. 3, pp. 36–45, 2015.

[12] C. Skak, J. O. Rasmussen, M. Nilsson, M. M. Pedersen, and T. Mathiesen, “Mapping and development of alternatives to chlorinated lubricants in the metal industry (KLORPARAFRI),” *Danish Environ. Prot. Agency*, no. 1039, 2005.

[13] E. Ceron, “New tribo-systems for sheet metal forming of advanced high strength steels and stainless steels,” PhD Thesis, 2014.

[14] I. . Petrushina, E. Christensen, R. . Bergqvist, P. . Møller, N. . Bjerrum, J. Høj, G. Kann, and I. Chorkendorff, “On the chemical nature of boundary lubrication of stainless steel by chlorine- and sulfur-containing EP-additives,” *Wear*, vol. 246, no. 1–2, pp. 98–105, 2000.

[15] P. B. Møller, I. M. Petrushina, E. Christensen, N. J. Bjerrum, J. Høj, G. Kann, J. L. Andreasen, and N.Bay, “Chemical Interactions between Extreme Pressure Lubricants and Stainless Steel during Ironing Procedure,” *Nord. ’98 Proc. 8th Int. Conf. Tribol.*, vol. 2, pp. 7–10, 1998.

[16] D.D. Olsson, “Limits of Lubrication in Sheet Metal Forming of Stainless Steel,” PhD Thesis, 2003.

[17] “DIN 8580:2003-09 Fertigungsverfahren - Begriffe, Einteilung.” .

[18] “DIN 8582:2003-09 Fertigungsverfahren Umformen - Einordnung; Unterteilung, Begriffe, Alphabetische Übersicht.” .

[19] K.-H. Grote and E. K. Antonsson, Eds., *Springer Handbook of Mechanical Engineering*. Springer Berlin Heidelberg, 2009.

[20] “DIN 50320 Verschleiß - Begriffe, Systemanalyse von Verschleißvorgängen, Gliederung des Verschleißgebietes,” 1979.

[21] “ASTM G40 - Standard terminology relating to wear and erosion,” 2013.

[22] E. Van der Heide, A. J. Huisin‘t Veld, and D. J. Schipper, “The effect of lubricant selection on galling in a model wear test,” *Wear*, vol. 250, no. 251, pp. 973–979, 2001.

[23] K. G. Budinski and S. T. Budinski, “Interpretation of galling tests,” *Wear*, vol. 332–333, pp. 1185–1192, 2015.

[24] M. Torbacke, Å. K. Rudolphi, and E. Kassfeldt, *Lubricants: Introduction to Properties and Performance*. John Wiley & Sons, Ltd, 2014.

[25] D. Tabor, “Mechanism of boundary lubrication,” *Proc. R. Soc. London. Ser. A*, vol. 212, no. 1111, pp. 498–505, 1952.

[26] K. Komvopoulos, N. Saka, and N. P. Suh, “The Mechanism of Friction in Boundary Lubrication,” *J. Tribol.*, vol. 107, no. 4, pp. 452–462, 1985.

[27] S. M. Hsu and R. S. Gates, “Boundary lubricating films: Formation and lubrication mechanism,” *Tribol. Int.*, vol. 38, no. 3, pp. 305–312, 2005.

[28] I. Minami, “Molecular Science of Lubricant Additives,” *Appl. Sci.*, vol. 7, no. 5, p. 445, 2017.

[29] T. Sakurai, K. Sato, and Y. Yamamoto, “Reaction between Chlorine Extreme Pressure Additives and Metal Surfaces at High Temperatures,” *Bull. Japan Pet. Inst.*, vol. 7, pp. 17–24, 1965.

[30] T. Sakurai and K. Sato, “Chemical Reactivity and Load Carrying Capacity of Lubricating Oils Containing Organic Phosphorus Compounds,” *ASLE Trans.*, vol. 13, no. 4, pp. 252–261, 1970.

[31] Q. Xue and L. Weimin, “Tribochemistry and the development of AW and EP oil additives — a review,” *Lubr. Sci.*, vol. 7, no. 1, pp. 81–92, 1994.

[32] A. G. Papay, “Antiwear and extreme-pressure additives in lubricants,” *Lubr. Sci.*, vol. 10, no. 3, pp. 209–224, 1998.

[33] K. Matsumoto, “Surface chemical and tribological investigations of phosphorus-containing lubricant additives,” ETH Zürich, 2003.

[34] N. Bay, O. Wibom, and P. A. F. Martins, “Testing of friction and lubrication in bulk metal forming,” in *Int. Mech. Engn. Conf. and Exhibition*, 1998, pp. 1–19.

[35] J. Filzek, “Friction behavior of new lubricants for sheet metal forming,” *Int. Colloq. Tribol. Automot. Ind. Lubr.*, 2006.

[36] C. G. Wall, “Laboratory evaluation of sheet metal forming lubricants,” *Lubr. Eng.*, vol. 40, no. 3, 1984.

[37] H. D. Nine, “Drawbead Forces in Sheet Metal Forming,” *Mech. Sheet Met. Form.*, pp. 179–211, 1978.

[38] H. D. Nine, “Assessment of lubricants for aluminum forming,” *SAE Tech. Pap.*, 1978.

[39] H. D. Nine, “Testing lubricants for sheet metal forming,” in *Metallurgical Society of AIME*, 1983, pp. 31–46.

[40] D.D. Olsson, N. Bay, and J. L. Andreasen, “Direct friction measurement in draw bead testing,” in *International Conference on Technology of Plasticity*, 2005, pp. 1811–1817.

[41] N. M. Wang and V. C. Shah, “Drawbead design and performance,” *J. Mater. Shap. Technol.*, vol. 9, no. 1, pp. 21–26, 1991.

[42] G. M. Dalton and J. A. Schey, “Effects of Bead Finish Orientation on Friction and Galling in the Drawbead test,” *SAE Tech. Pap.*, no. 897, pp. 123–133, 1992.

[43] G. M. Dalton and J. A. Schey, “Effects of Bead Surface Preparation on Friction in the Drawbead Test,” *SAE Int. Conf.*, pp. 29–39, 1991.

[44] M. Vermeulen and H. Hobleke, “Functionality and Characterisation of Textured Sheet Steel Products,” *Adv. Tech. Assess. Surf. Topogr.*, pp. 249–305, 2003.

[45] H. R. Zonker, N. C. Whittle, R. A. Hoffman, and M. M. Teichman, “Tool material performance during draw bead deformation of aluminum sheet,” in *SAE Technical Papers*, 1996, pp. 125–133.

[46] R. P. Hunz, C. Collison, and K. McCrea, “Lubricant performance of various extreme pressure compounds as measured by the SLT horizontal draw-bead simulator,” *Lubr. Eng.*, vol. 46, no. 9, pp. 549–552, 1990.

[47] J. M. Lanzon, M. J. Cardew-Hall, and P. D. Hodgson, “Characterising frictional behaviour in sheet metal forming,” *J. Mater. Process. Technol.*, vol. 80–81, pp. 251–256, 1998.

[48] J. A. Schey, “Speed effects in drawbead simulation,” *J. Mater. Process. Technol.*, vol. 57, no. 1–2, pp. 146–154, 1996.

[49] Y. Joshi, P. Christiansen, I. Masters, N. Bay, and R. Dashwood, “Numerical Modelling of Drawbeads for Forming of Aluminium Alloys,” *J. Phys. Conf. Ser.*, vol. 734, no. 3, pp. 1–4, 2016.

[50] J. A. Schey, “Friction in sheet forming with soft and hard tooling,” *Steel Res.*, vol. 69, no. 4–5, pp. 148–153, 1998.

[51] J. A. Schey and S. W. A. Watts, “Transient Tribological Phenomena in Drawbead Simulation,” *SAE Spec. Publ.*, no. 897, pp. 143–149, 1992.

[52] J. H. Jang, W. T. Kim, C. J. Van Tyne, and Y. H. Moon, “Experimental analysis on the frictional behaviour of drawbeads in sheet metal forming,” *Steel Res. Int.*, vol. 78, no. 12, pp. 884–889, 2007.

[53] A. Wihlborg and L. Gunnarsson, “A frictional study of uncoated EBT steel sheets in a bending under tension friction test,” *Wear*, vol. 237, no. 1, pp. 129–136, 2000.

[54] D. Schmoeckel, M. Prier, and J. Staeves, “Topography Deformation of Sheet Metal during the Forming Process and Its Influence on Friction,” *CIRP Ann.*, vol. 46, no. 1, pp. 175–178, 1997.

[55] M. J. Alinger and C. J. Van Tyne, “Evolution of the tribological characteristics of several forming die materials,” *J. Mater. Process. Technol.*, vol. 111, no. 1–3, pp. 20–24, 2001.

[56] P. Groche and G. Nitzsche, “Reduction of Friction in Deep Drawing of Aluminium Alloys by Generating Local Hydrostatic-Pressure Lubrication,” *Proc. Inst. Mech. Eng. Part B J. Eng. Manuf.*, vol. 220, no. 1, pp. 43–48, 2006.

[57] L. R. Sanchez, “Experimental Investigation of Friction Effects Enhanced by Tool Geometry and Forming Method on Plane Strain Sheet Metal Forming,” *Tribol. Trans.*, vol. 42, no. 2, pp. 343–352, 1999.

[58] M. Littlewood, “Effect of surface finish and lubrication on frictional variations involved in sheet-metal-forming process,” *Sheet Met. Ind.*, vol. 41, no. 452, 1964.

[59] J. M. Lanzon, M. J. Cardew-Hall, and P. D. Hodgson, “Characterising frictional behaviour in sheet metal forming,” *J. Mater. Process. Technol.*, vol. 80–81, pp. 251–256, 1998.

[60] H. Y. Kim, B. C. Hwang, and W. B. Bae, “An experimental study on forming characteristics of pre-coated sheet metals,” *J. Mater. Process. Technol.*, vol. 120, no. 1–3, pp. 290–295, 2002.

[61] M. Jonasson, T. Pulkkinen, L. Gunnarsson, and E. Schedin, “Comparative study of shotblasted and electrical-discharge-textured rolls with regard to frictional behavior of the rolled steel sheet surfaces,” *Wear*, vol. 207, no. 1–2, pp. 34–40, 1997.

[62] G. Ferran, A. . de Moura, and L. . Moreira, “Computer aided development of a bending–drawing test for thin metallic sheets,” *J. Mater. Process. Technol.*, vol. 80–81, pp. 531–537, 1998.

[63] G. J. Coubrough, M. J. Alinger, and C. J. Van Tyne, “Angle of contact between sheet and die during stretch-bend deformation as determined on the bending-under-tension friction test system,” *J. Mater. Process. Technol.*, vol. 130–131, pp. 69–75, 2002.

[64] P. Carlsson, U. Bexell, and M. Olsson, “Tribological behaviour of thin organic permanent coatings deposited on hot-dip coated steel sheet — a laboratory study,” *Surf. Coatings Technol.*, vol. 132, pp. 169–180, 2000.

[65] J. A. Schey and M. McLean, “Critical evaluation of test methods for sheet metalworking lubrication,” in *ASME*, 1988, vol. 10, pp. 25–32.

[66] P. K. Saha and W. R. D. Wilson, “Friction in forming electro-galvanized steel sheet with tool steel and carbide coated tools,” in *ASME*, 1993, vol. 67, pp. 209–218.

[67] J. L. Andreasen, D. D. Olsson, K. Chodnikiewicz, and N. Bay, “Bending under tension test with direct friction measurement,” *Proc. Inst. Mech. Eng. Part B J. Eng. Manuf.*, vol. 220, no. 1, pp. 73–80, 2006.

[68] E. Ceron and N. Bay, “Determination of Friction in Sheet Metal Forming by Means of Simulative Tribo-Tests,” *Key Eng. Mater.*, vol. 549, no. 549, pp. 415–422, 2013.

[69] E. Ceron, P. A. F. Martins, and N. Bay, “Thermal Analysis of Bending Under Tension Test,” *Procedia Eng.*, vol. 81, pp. 1805–1810, 2014.

[70] E. Ceron, M. Olsson, and N. Bay, “Lubricant Film Breakdown and Material Pick-Up in Sheet Forming of Advanced High Strength Steels and Stainless Steels when Using Environmental Friendly Lubricants,” *Adv. Mater. Res.*, vol. 966–967, no. 966–967, pp. 219–227, 2014.

[71] E. Üstünyagiz, M. H. Sulaiman, P. Christiansen, C. V. Nielsen, and N. Bay, “A Study on DLC Tool Coating for Deep Drawing and Ironing of Stainless Steel,” *Key Eng. Mater.*, vol. 767, pp. 181–188, 2018.

[72] S. Fukui, T. Ohi, H. Kudo, I. Takita, and J. Seiko, “Some aspects of friction in metal-strip drawing,” *Int. J. Mech. Sci.*, vol. 4, no. 4, pp. 297–312, 1962.

[73] H. R. Le and M. P. F. Sutcliffe, “Measurements of friction in strip drawing under thin film lubrication,” *Tribol. Int.*, vol. 35, no. 2, pp. 123–128, 2002.

[74] S. Aleksandrović, M. Dordević, M. Stefanović, V. Lazić, D. Adamović, and D. Arsić, “Different ways of friction coefficient determination in stripe ironing test,” *Tribol. Ind.*, vol. 36, no. 3, pp. 293–299, 2014.

[75] K. Dohda and N. Kawai, “Compatibility Between Tool Materials and Workpiece in Sheet-Metal Ironing Process,” *J. Tribol.*, vol. 112, no. 2, p. 275, 1990.

[76] K. Dohda, H. Kubota, and Y. Tsuchiya, “Application of DLC Coating to Ironing Die,” *JSME International Journal Series A*, vol. 48, no. 4. pp. 286–291, 2005.

[77] T. Takaki, S. Ito, K. Kitamura, K. Yagishita, and J. Shibata, “Evaluation of anti-galling property of sulfurized olefins with overbased calcium sulfonates on stainless steel by cup internal ironing test,” in *Procedia Engineering*, 2017, vol. 207, pp. 2292–2297.

[78] J. L. Andreasen and N. Bay, “A Strip Reduction Test for Measurement of Lubricity in Ironing,” in *19th IDDRG Biennial Congress*, 1996, pp. 435–444.

[79] J. L. Andreasen, N. Bay, and L. De Chiffre, “Quantification of galling in sheet metal forming by surface topography characterisation,” *Int. J. Mach. Tools Manuf.*, vol. 38, no. 5–6, pp. 503–510, 1998.

[80] J. L. Andreasen, N. Bay, M. Andersen, E. Christensen, and N. Bjerrum, “Screening the performance of lubricants for the ironing of stainless steel with a strip reduction test,” *Wear*, vol. 207, no. 1–2, pp. 1–5, 1997.

[81] S. Gazvoda, J. L. Andreasen, and D. D. Olsson, “Strip reduction testing of lubricants developed during ENFORM project,” 2001.

[82] J. L. Andreasen, K. Krebs, G. Kann, and N. Bay, “Quantitative Evaluation of Lubricants and Tool Surfaces for Ironing of Stainless Steel,” *Proc. 1st Int. Conf. Tribol. Manuf. Process. ’97, Gifu*, pp. 358–363, 1997.

[83] S. Christiansen and L. De Chiffre, “Topographic characterization of progressive wear on deep drawing dies,” *Tribol. Trans.*, vol. 40, no. 2, pp. 346–352, 1997.

[84] B. Wadman, J. Eriksson, M. Olsson, E. Schedin, E. Madsen, and N. Bay, “Influence of surface texture on the galling characteristics of lean duplex and austenitic stainless steels,” *Proc. Duplex World 2010*, pp. 1211–1220, 2010.

[85] E. Üstünyagiz, C. V. Nielsen, P. Christiansen, P. A. F. Martins, and N. Bay, “Continuous Strip Reduction Test Simulating Tribological Conditions in Ironing,” in *Procedia Engineering*, 2017, vol. 207, pp. 2286–2291.

[86] S. L. Semiatin, “Forming and Forging,” in *ASM Handbook*, vol. 14, no. 3, ASM International, 1993.

[87] B. N. Maker, “On Drawbeads in Sheet Metal Forming,” *SAE Tech. Pap.*, no. 724, pp. 1–5, 2000.

[88] W. F. Hosford and R. Caddell, *Metal Forming*. Cambridge University Press, 2011.

[89] Z. Q. Lin, Y. X. Bao, G. L. Chen, and G. Liu, “Study on the drawbead setting of the large deformation and bending area in a cover panel,” *Proc. NUMISHEET*, vol. 99, pp. 264–268, 1999.

[90] S. S. Tufekci, C.-T. Wang, G. L. Kinzel, and T. Altan, “Estimation and control of drawbead forces in sheet metal forming,” *SAE Trans.*, vol. 103, no. 5, pp. 738–747, 1994.

[91] S. G. Xu, M. L. Bohn, and K. J. Weinmann, “Drawbeads in Sheet Metal Stamping - A Review,” *SAE Tech. Pap.*, 1997.

[92] V. A. Zharkov, *Theory and practice of deep drawing*. Mechanical Engineering Publications, 1995.

[93] VDI 3141, “Einfließwulste und Ziehstäbe in Stanzerei-Großwerkzeugen.” 1990.

[94] D. A. Smith, *Handbook of Die Design*, 3rd ed. Society of Manufacturing Engineers, 1990.

[95] P. Groche and M. Christiany, “Evaluation of the potential of tool materials for the cold forming of advanced high strength steels,” *Wear*, vol. 302, no. 1–2, pp. 1279–1285, 2013.

[96] C. Weidemann, “The blankholding action of draw beads,” in *Proc. 10th Biennial Congress of IDDRG*, 1978, pp. 79–85.

[97] S. Kluge, “Spannungsüberlagerung durch Einsatz von Ziehstaben Beim Umformen unregelmäßiger Blechteile,” *Blech Rohre Profile*, vol. 39, pp. 117–123, 1992.

[98] T. B. Stoughton, “Model of drawbead forces in sheet metal forming,” in *Proceedings of the 15th biennial IDDRG Congress*, 1988, pp. 205–215.

[99] N.-M. Wang, “A mathematical model of drawbead forces in sheet metal forming,” *J. Appl. Metalwork.*, vol. 2, no. 3, pp. 193–199, 1982.

[100] M. R. Herderich, “Experimental determination of the blankholder forces needed for stretch draw die design,” *SAE Spec. Publ.*, no. 825, 1990.

[101] L. R. Sanchez and K. J. Weinmann, “An analytical and experimental study of the flow of sheet metal between circular drawbeads,” *J. Manuf. Sci. Eng. Trans. ASME*, vol. 118, no. 1, pp. 45–54, 1996.

[102] B. S. Levy, “Development of a predictive model for draw bead restraining force utilizing work of Nine and Wang,” *J. Appl. Metalwork.*, vol. 3, no. 1, pp. 38–44, 1983.

[103] J. M. Yellup and M. J. Painter, “The prediction of strip shape and restraining force for shallow drawbead systems,” *J. Appl. Metalwork.*, vol. 4, no. 1, pp. 30–38, 1985.

[104] N. Triantafyllidis, B. Maker, and S. K. Samanta, “An Analysis of Drawbeads in Sheet Metal Forming: Part I—Problem Formulation,” *J. Eng. Mater. Technol.*, vol. 108, no. 4, p. 321, 1986.

[105] F.-K. Chen and J.-H. Liu, “Analysis of an equivalent drawbead model for the finite element simulation of a stamping process,” *Int. J. Mach. Tools Manuf.*, vol. 37, no. 4, pp. 409–423, 1997.

[106] P. Chabrand, F. Dubois, and J. C. Gelin, “Modelling drawbeads in sheet metal forming,” *Int. J. Mech. Sci.*, vol. 38, no. 1, pp. 59–77, 1995.

[107] L. Shuhui, L. Zhongqin, X. Weili, and B. Youxia, “An improved equivalent drawbead model and its application,” *J. Mater. Process. Technol.*, vol. 121, no. 2–3, pp. 308–312, 2002.

[108] M. G. Lee, K. Chung, R. H. Wagoner, and Y. T. Keum, “A numerical method for rapid estimation of drawbead restraining force based on non-linear, anisotropic constitutive equations,” *Int. J. Solids Struct.*, vol. 45, no. 11–12, pp. 3375–3391, 2008.

[109] T. Meinders, B. D. Carleer, H. J. M. Geijselaers, and J. Huétink, “The implementation of an equivalent drawbead model in a finite-element code for sheet metal forming,” *J. Mater. Process. Technol.*, vol. 83, no. 1–3, pp. 234–244, 1998.

[110] E. Ceron and N. Bay, “A methodology for off-line evaluation of new environmentally friendly tribo-systems for sheet metal forming,” *CIRP Ann. - Manuf. Technol.*, vol. 62, no. 1, pp. 231–234, 2013.

[111] E. Ceron and N. Bay, “Testing and Prediction of Limits of Lubrication in Sheet Metal Forming,” *Proc. Int. Deep Draw. Res. Gr. Conf.*, 2012.

[112] A. E. Tekkaya, W. Homberg, and A. Brosius, *60 Excellent inventions in metal forming*. Springer Berlin Heidelberg, 2015.

[113] “ICFG Document: Lubrication aspects in cold forging of aluminium and aluminium alloys,” *Wire*, vol. 46, no. 1, pp. 2–12, 1996.

[114] N. Bay, “Trends and Visions in Metal Forming Tribology,” in *10th International Conference on Technology of Plasticity*, 2011.

[115] K. L. Friis, P. S. Nielsen, and N. Bay, “Testing and modelling of industrial tribo-systems for sheet metal forming,” in *9th International Conference on Technology of Plasticity*, 2008, pp. 417–422.

[116] P. Jewvattanarak, N. Mahayotsanun, S. Mahabunphachai, S. Ngernbamrung, and K. Dohda, “Tribological effects of chlorine-free lubricant in strip drawing of advanced high strength steel,” *Proc. Inst. Mech. Eng. Part J J. Eng. Tribol.*, vol. 230, no. 8, pp. 974–982, 2016.

[117] K. P. Rao and C. L. Xie, “A comparative study on the performance of boric acid with several conventional lubricants in metal forming processes,” *Tribol. Int.*, vol. 39, no. 7, pp. 663–668, 2006.

[118] F. Sgarabotto and A. Ghiotti, “Frictional Behaviour of Environmentally Friendly Lubricants for Sheet Metal Forming Processes,” *Key Eng. Mater.*, vol. 504–506, pp. 537–542, 2012.

[119] T. Takaki, K. Kitamura, and J. Shibata, “Development of chloride-free oil with sulfur-based EP additive for cold forming of stainless steel,” *Mech. Eng. J.*, vol. 5, no. 2, pp. 17-00449-17-00449, 2018.

[120] M. Djordjevic, D. Arsic, S. Aleksandrovic, V. Lazic, D. Milosavljevic, R. Nikolic, and V. Mladenovic, "Comparative study of an environmentally friendly lubricant with conventional lubricants in strip ironing test," *J. Balk. Tribol. Assoc.*, vol. 22, no. 1A, 2016.

[121] W. Rehbein, "Friction and wear measurement of additives by strip drawing test and SRV," *Tribol. Und Schmierungstechnik*, vol. 61, no. 2, pp. 65–72, 2014.

[122] M. Tolazzi, M. Meiler, and M. Merklein, "Tribological Investigations on Coated Steel Sheets Using the Dry Film Lubricant Drylube E1," *Adv. Mater. Res.*, vol. 6–8, pp. 565–572, 2005.

[123] H. Kim, J. Sung, F. E. Goodwin, and T. Altan, "Investigation of galling in forming galvanized advanced high strength steels (AHSSs) using the twist compression test (TCT)," *J. Mater. Process. Technol.*, vol. 205, no. 1–3, pp. 459–468, 2008.

[124] H. Kim, J. H. Sung, R. Sivakumar, and T. Altan, "Evaluation of stamping lubricants using the deep drawing test," *Int. J. Mach. Tools Manuf.*, vol. 47, no. 14, pp. 2120–2132, 2007.

[125] H. Kim, T. Altan, and Q. Yan, "Evaluation of stamping lubricants in forming advanced high strength steels (AHSS) using deep drawing and ironing tests," *J. Mater. Process. Technol.*, vol. 209, no. 8, pp. 4122–4133, 2009.

[126] S. Chandrasekharan, H. Palaniswamy, N. Jain, G. Ngaile, and T. Altan, "Evaluation of stamping lubricants at various temperature levels using the ironing test," *Int. J. Mach. Tools Manuf.*, vol. 45, no. 4–5, pp. 379–388, 2005.

[127] M. Meiler, M. Pfestorf, M. Geiger, and M. Merklein, "The use of dry film lubricants in aluminum sheet metal forming," *Wear*, vol. 255, no. 7–12, pp. 1455–1462, 2003.

[128] L. Kirkhorn, O. Gutnichenko, S. Bihagen, and J.-E. Ståhl, "Minimum quantity lubrication (MQL) with carbon nanostructured additives in sheet metal forming," *Procedia Manuf.*, vol. 25, pp. 375–381, 2018.

[129] R. Matsumoto and K. Osakada, "Measurement of Friction in Cold Upsetting with Mist Lubrication," *Mater. Trans.*, vol. 45, no. 9, pp. 2891–2896, 2004.

[130] O. Sandberg, "Advanced low-friction tool steel for metal processing: Properties and industrial experiences," *Int. J. Microstruct. Mater. Prop.*, vol. 3, no. 2–3, pp. 391–400, 2008.

[131] Y. Jimbo and A. Azushima, "Effect of carbide properties of roll materials on lubricity in cold sheet rolling of low-carbon steel," *Int. J. Mach. Tools Manuf.*, vol. 41, no. 3, pp. 347–360, 2001.

[132] A. Azushima and Y. Jimbo, “Effect of carbide properties on lubrication characteristics of roll in cold sheet rolling,” *Tetsu To Hagane-journal of the Iron and Steel Institute of Japan*, vol. 81, no. 12. pp. 1150–1155, 1995.

[133] K. Tamaoki, K. ichi Manabe, S. Kataoka, and T. Aizawa, “Electroconductive ceramic tooling for dry deep drawing,” *J. Mater. Process. Technol.*, vol. 210, no. 1, pp. 48–53, 2010.

[134] K. Tamaoki, K. Manabe, S. Kataoka, and T. Aizawa, “Continuous Dry Cylindrical and Rectangular Deep Drawing by Electroconductive Ceramic Dies,” *J. Manuf. Sci. Eng.*, vol. 135, no. 3, pp. 1–7, 2013.

[135] S. Kataoka, M. Murakawa, T. Aizawa, and H. Ike, “Tribology of dry deep-drawing of various metal sheets with use of ceramics tools,” *Surf. Coatings Technol.*, vol. 177–178, pp. 582–590, 2004.

[136] J. P. Dan, H. J. Boving, and H. E. Hintermann, “Hard coatings,” *J. Phys. IV*, vol. 85, pp. 933–941, 1993.

[137] I. J. R. Baumvol, “New trends in hard coatings technology,” *Nucl. Inst. Methods Phys. Res. B*, vol. 85, no. 1–4, pp. 230–235, 1994.

[138] V. Diciuc and A. Kazek-Kęsik, “The structure and formation of functional hard coatings: A short review,” in *MATEC Web of Conferences*, 2017, vol. 112, pp. 1–7.

[139] K. Vercammen, H. Haefke, Y. Gerbig, A. Van Hulsel, E. Pflüger, and J. Meneve, “Comparative study of state-of-the-art diamond-like carbon films,” *Surf. Coatings Technol.*, vol. 133–134, pp. 466–472, 2000.

[140] M. Murakawa, N. Koga, and T. Kumagai, “Deep-drawing of aluminum sheets without lubricant by use of diamond-like carbon coated dies,” *Surf. Coatings Technol.*, vol. 76–77, pp. 553–558, 1995.

[141] M. Murakawa and S. Takeuchi, “Evaluation of tribological properties of DLC films used in sheet forming of aluminum sheet,” *Surf. Coatings Technol.*, vol. 163–164, pp. 561–565, 2003.

[142] K. Taube, “Carbon-based coatings for dry sheet-metal working,” *Surf. Coatings Technol.*, vol. 98, no. 1–3, pp. 976–984, 1998.

[143] F. Sgarabotto and A. Ghiotti, “Tribological behaviour of PVD coatings for sheet metal forming tools: Laboratory and industrial evaluation,” *Key Eng. Mater.*, vol. 504–506, pp. 543–548, 2012.

[144] A. Ghiotti and S. Bruschi, “Tribological behaviour of DLC coatings for sheet metal forming tools,” *Wear*, vol. 271, no. 9–10, pp. 2454–2458, 2011.

[145] B. Sresomroeng, V. Premanond, P. Kaewtatip, A. Khantachawana, N. Koga, and S. Watanabe, "Anti-adhesion performance of various nitride and DLC films against high strength steel in metal forming operation," *Diam. Relat. Mater.*, vol. 19, no. 7–9, pp. 833–836, 2010.

[146] P. N. Silva, J. P. Dias, and A. Cavaleiro, "Performance of W-TI-(N) coated pins in lubricated pin-on-disk tests," *Surf. Coatings Technol.*, vol. 202, no. 11, pp. 2338–2343, 2008.

[147] J. H. C. de Souza and M. Liewald, "Analysis of the tribological behaviour of polymer composite tool materials for sheet metal forming," *Wear*, vol. 268, no. 1, pp. 241–248, 2010.

[148] J. D. Bressan, G. A. Battiston, R. Gerbasi, D. P. Daros, and L. M. Gilapa, "Wear on tool steel AISI M2, D6 and 52100 coated with Al2O3 by the MOCVD process," *J. Mater. Process. Technol.*, vol. 179, no. 1–3, pp. 81–86, 2006.

[149] L. Wang, X. Nie, J. Housden, E. Spain, J. C. Jiang, E. I. Meletis, A. Leyland, and A. Matthews, "Material transfer phenomena and failure mechanisms of a nanostructured Cr-Al-N coating in laboratory wear tests and an industrial punch tool application," *Surf. Coatings Technol.*, vol. 203, no. 5–7, pp. 816–821, 2008.

[150] J. L. Mo and M. H. Zhu, "Sliding tribological behaviors of PVD CrN and AlCrN coatings against Si3N4 ceramic and pure titanium," *Wear*, vol. 267, no. 5–8, pp. 874–881, 2009.

[151] J. L. Mo, M. H. Zhu, B. Lei, Y. X. Leng, and N. Huang, "Comparison of tribological behaviours of AlCrN and TiAlN coatings-Deposited by physical vapor deposition," *Wear*, vol. 263, no. 7–12 SPEC. ISS., pp. 1423–1429, 2007.

[152] S. Sivarajan and R. Padmanabhan, "Improvement of Tribology in Sheet Metal Forming of High-Strength Steel Sheets by PVD-Coated Dies," *Mater. Perform. Charact.*, vol. 7, no. 3, pp. 320–328, 2018.

[153] T. Sato and T. Besshi, "Anti-galling evaluation in aluminum sheet forming," *J. Mater. Process. Technol.*, vol. 83, no. 1–3, pp. 185–191, 1998.

[154] K. Tamaoki, S. Kataoka, K. Kanda, S. Tanako, and T. Teranish, "Study of Deep Drawing Using Diamond Coated Tools," *J. Mater. Test. Res. Assoc. Japan*, vol. 53, no. 4, pp. 247–253, 2008.

[155] M. Liljengren, K. Kjelsson, T. Johansson, and N. Asnafi, "Die materials, hardening methods and surface coatings for forming of high, extra high & ultra high strength steel sheets (HSS, EHSS, UHSS)," in *The International Deep Drawing Research Group*, 2006, pp. 597–603.

[156] A. Azushima, J. Miyamoto, and H. Kudo, “Effect of Surface Topography of Workpiece on Pressure Dependence of Coefficient of Friction in Sheet Metal Forming,” *CIRP Ann. - Manuf. Technol.*, vol. 47, no. 1, pp. 479–482, 1998.

[157] R. Balbach and K. Lange, “Influence of Various Surface Microstructures on the Tribology in Aluminium Sheet Metal Forming,” *CIRP Ann. - Manuf. Technol.*, vol. 36, no. 1, pp. 181–184, 1987.

[158] N.Bay and T. Wanheim, “Contact Phenomena under Bulk Plastic Deformation Conditions,” *3rd Int. Conf. Technol. Plast.*, vol. 4, pp. 1667–1691, 1990.

[159] L. Lazzarotto, L. Dubar, A. Dubois, P. Ravassard, and J. Oudin, “Three selection criteria for the cold metal forming lubricating oils containing extreme pressure agents,” *Journal of Materials Processing Technology*, vol. 80–81. pp. 245–250, 1998.

[160] J. Staeves, “Beurteilung der Topografie von Blechen in Hinblick auf die Reibung bei der Umformung,” 1998.

[161] G. Ngaile, M. Gariety, and T. Altan, “Enhancing Tribological Conditions in Tube Hydroforming by Using Textured Tubes,” *J. Tribol.*, vol. 128, no. 3, p. 674, 2006.

[162] M. F. El-Menshawy and M. S. Ahmed, “Monitoring and control of the electro-discharge texturing process for steel cold mill work rolls,” *Manuf. Eng. Trans.*, pp. 470–475, 1985.

[163] B. Podgornik and J. Jerina, “Surface topography effect on galling resistance of coated and uncoated tool steel,” *Surf. Coatings Technol.*, vol. 206, no. 11–12, pp. 2792–2800, 2012.

[164] M. Geiger, U. Popp, and U. Engel, “Excimer Laser Micro Texturing of Cold Forging Tool Surfaces - Influence on Tool Life,” *CIRP Ann.*, vol. 51, no. 1, pp. 231–234, 2002.

[165] M. Vermeulen and J. Scheers, “Micro-hydrodynamic effects in EBT textured steel sheet,” *Int. J. Mach. Tools Manuf.*, vol. 41, no. 13–14, pp. 1941–1951, 2001.

[166] H. L. Costa and I. M. Hutchings, “Development of a maskless electrochemical texturing method,” *J. Mater. Process. Technol.*, vol. 209, no. 8, pp. 3869–3878, 2009.

[167] V. Franzen, J. Witulski, A. Brosius, M. Trompeter, and A. E. Tekkaya, “Textured surfaces for deep drawing tools by rolling,” *Int. J. Mach. Tools Manuf.*, vol. 50, no. 11, pp. 969–976, 2010.

[168] R. S. Eriksen, M. Arentoft, J. Grønbæk, and N. Bay, “Manufacture of functional surfaces through combined application of tool manufacturing processes and Robot Assisted Polishing,” *CIRP Ann. - Manuf. Technol.*, vol. 61, no. 1, pp. 563–566, 2012.

[169] T. Mizuno and M. Okamoto, “Effects of lubricant viscosity at pressure and sliding velocity on lubricating conditions in the compression-friction test on sheet metals,” *Journal of Lubrication Technology*, vol. 104, no. 1. p. 53, 1982.

[170] H. Kudo, M. Tsubouchi, H. Takada, and K. Okamura, “An Investigation into Plasto-Hydrodynamic Lubrication with a Cold Sheet Drawing Test,” *CIRP Ann. - Manuf. Technol.*, vol. 31, no. 1, pp. 175–180, 1982.

[171] A. Azushima, S. Yoneyama, T. Yamaguchi, and H. Kudo, “Direct Observation of Microcontact Behavior at the Interface between Tool and Workpiece in Lubricated Upsetting,” *CIRP Ann. - Manuf. Technol.*, vol. 45, no. 1, pp. 205–210, 1996.

[172] J. Bech, N. Bay, and M. Eriksen, “A Study of Mechanisms of Liquid Lubrication in Metal Forming,” *CIRP Ann. - Manuf. Technol.*, vol. 47, no. 1, pp. 221–226, 1998.

[173] S. W. Lo and W. R. D. Wilson, “A theoretical model of micro-pool lubrication in metal forming,” *J. Tribol. ASME*, vol. 121, no. 4, pp. 731–738, 1999.

[174] A. Azushima, “FEM Analysis of Hydrostatic Pressure Generated Within Lubricant Entrapped Into Pocket on Workpiece Surface in Upsetting Process,” *J. Tribol.*, vol. 122, no. 4, pp. 822–827, 2000.

[175] A. Stephany, H. R. Le, and M. P. F. Sutcliffe, “An efficient finite element model of surface pit reduction on stainless steel in metal forming processes,” *J. Mater. Process. Technol.*, vol. 170, no. 1–2, pp. 310–316, 2005.

[176] A. Mousavi, M. Schomacker, and A. Brosius, “Macro and micro structuring of deep drawing’s tools for lubricant free forming,” in *Procedia Engineering*, 2014, vol. 81, pp. 1890–1895.

[177] R. Krux, W. Homberg, M. Kalveram, M. Trompeter, M. Kleiner, and K. Weinert, “Die Surface Structures and Hydrostatic Pressure System for the Material Flow Control in High-Pressure Sheet Metal Forming,” *Adv. Mater. Res.*, vol. 6–8, pp. 385–392, 2005.

[178] A. Godi, J. Grønbæk, and L. De Chiffre, “Off-line testing of multifunctional surfaces for metal forming applications,” *CIRP J. Manuf. Sci. Technol.*, vol. 11, pp. 28–35, 2015.

[179] T. Claesson, J. Laring, K. Nonås, and J. Stahre, “Effects of tool die surface topography on friction and galling in sheet metal forming,” in *Proceedings of Swedish Production Symposium*, 2009, pp. 213–219.

[180] J. Berglund, C. A. Brown, B.-G. Rosén, and N. Bay, “Milled die steel surface roughness correlation with steel sheet friction,” *CIRP Ann.*, vol. 59, no. 1, pp. 577–580, 2010.

[181] M. H. Sulaiman, P. Christiansen, and N. Bay, “Influence of tool texture on friction and lubrication in strip reduction,” in *Procedia Engineering*, 2017, vol. 207, pp. 2263–2268.

[182] E. Van der Heide, A. J. Huisin‘t Veld, and D. J. Schipper, “The effect of lubricant selection on galling in a model wear test,” *Wear*, vol. 250, no. 251, pp. 973–979, 2001.

[183] B. Podgornik, J. Vižintin, and S. Hogmark, “Improvement in galling performance through surface engineering,” *Surf. Eng.*, vol. 22, no. 4, pp. 235–238, 2006.

[184] I. Ubhayaratne, Y. Xiang, M. Pereira, and B. Rolfe, “An audio signal based model for condition monitoring of sheet metal stamping process,” in *Proceedings of the 2015 10th IEEE Conference on Industrial Electronics and Applications, ICIEA 2015*, 2015, pp. 1267–1272.

[185] I. Ubhayaratne, M. P. Pereira, Y. Xiang, and B. F. Rolfe, “Audio signal analysis for tool wear monitoring in sheet metal stamping,” *Mech. Syst. Signal Process.*, vol. 85, pp. 809–826, Feb. 2017.

[186] C. Teymuri Sindi, M. Ahmadi Najafabadi, and M. Salehi, “Tribological behavior of sheet metal forming process using acoustic emission characteristics,” *Tribol. Lett.*, vol. 52, no. 1, pp. 67–79, 2013.

[187] D. Dornfeld, “Application of acoustic emission techniques in manufacturing,” *NDT E Int.*, vol. 25, no. 6, pp. 259–269, 1992.

[188] S. Y. Liang and D. A. Dornfeld, “Characterization of Sheet Metal Forming Using Acoustic Emission,” *J. Eng. Mater. Technol.*, vol. 112, no. 1, p. 44, 1990.

[189] T. Jayakumar, C. K. Mukhopadhyay, S. Venugopal, S. L. Mannan, and B. Raj, “A review of the application of acoustic emission techniques for monitoring forming and grinding processes,” *Journal of Materials Processing Technology*, vol. 159, no. 1. pp. 48–61, 2005.

[190] B. A. Behrens, I. El-Galy, T. Huinink, and C. Buse, “Online monitoring of deep drawing process by application of acoustic emission,” in *10th International Conference on Technology of Plasticity*, 2011.

[191] T. Skåre and F. Krantz, “Wear and frictional behaviour of high strength steel in stamping monitored by acoustic emission technique,” *Wear*, vol. 255, no. 7–12, pp. 1471–1479, 2003.

[192] R. F. Z. S. Mostafavi, C.T. Sindi, F. Pashmforoush, “Acoustic Emission Waves from the Onset of Galling between Tool and Sheet Material,” *Mater. Eval.*, vol. 71, pp. 1335–1342, 2013.

[193] C. Mechefske, G. Sun, and J. Sheasby, “Using acoustic emission to monitor sliding wear,” *Insight*, vol. 44, no. 8, pp. 490–497, 2002.

[194] F. Saeidi, S. A. Shevchik, and K. Wasmer, “Automatic detection of scuffing using acoustic emission,” *Tribol. Int.*, vol. 94, pp. 112–117, 2016.

[195] I. A. Rastegaev, D. L. Merson, and A. Vinogradov, “Real time acoustic emission methodology in effective tribology testing,” *Int. J. Microstruct. Mater. Prop.*, vol. 9, no. 3–5, pp. 360–373, 2014.

[196] A. Hase, H. Mishina, and M. Wada, “Correlation between features of acoustic emission signals and mechanical wear mechanisms,” *Wear*, vol. 292–293, pp. 144–150, 2012.

[197] L. Wang and R. J. K. Wood, “Acoustic emissions from tribological contacts,” *Tribol. Int.*, vol. 42, pp. 1629–1637, 2009.

[198] M. Oda and H. Toshiaki, “Tribological evaluation of boriding metal by acoustic emission technique,” *Japan Soc. Mech. Eng.*, vol. 61, no. 328–334, 1995.

[199] K. Matsuoka, D. Forrest, and T. Ming-Kai, “On-line wear monitoring using acoustic emission,” *Wear*, vol. 162–164, no. PART A, pp. 605–610, 1993.

[200] R. J. Boness, “Wear detection and analysis using acoustic emission techniques,” *Natl. Conf. Publ. - Inst. Eng. Aust.*, no. 90, pp. 33–37, 1990.

[201] T. Hisakado, H. Suda, and M. Sekine, “Relation between lubricated wear of ceramics and acoustic emission characteristics,” *Tribol. Trans.*, vol. 41, no. 2, pp. 209–216, 1998.

[202] G. Stadler, P. Bergmann, I. Gódor, and F. Grün, “Wear detection in tribological systems based on acoustic emissions,” in *International Multidisciplinary Scientific Conference*, 2016, pp. 1–12.

[203] C. L. Jiaa and D. A. Dornfeld, “Experimental studies of sliding friction and wear via acoustic emission signal analysis,” *Wear*, vol. 139, no. 2, pp. 403–424, 1990.

[204] P. Tian, Y. Tian, L. Shan, Y. Meng, and X. Zhang, “A correlation analysis method for analyzing tribological states using acoustic emission, frictional

coefficient, and contact resistance signals," *Friction*, vol. 3, no. 1, pp. 36–46, 2015.

[205] C. W. Cho and Y. Z. Lee, "Wear-life evaluation of CrN-coated steels using acoustic emission signals," *Surf. Coatings Technol.*, vol. 127, no. 1, pp. 59–65, 2000.

[206] T. Hisakado and T. Warashina, "Relationship between friction and wear properties and acoustic emission characteristics: iron pin on hardened bearing steel disk," *Wear*, vol. 216, no. 1, pp. 1–7, 1998.

[207] J. Yan, Y. Heng-Hu, Y. Hong, Z. Feng, L. Zhen, W. Ping, and Y. Yan, "Nondestructive Detection of Valves Using Acoustic Emission Technique," *Advances in Materials Science and Engineering*, vol. 2015. pp. 1–9, 2015.

[208] B.-A. Behrens, S. Hübner, and K. Wölki, "Acoustic emission—A promising and challenging technique for process monitoring in sheet metal forming," *J. Manuf. Process.*, vol. 29, pp. 281–288, 2017.

[209] A. Terchi and Y. H. J. Au, "Acoustic emission signal processing," *Measurement and Control*, vol. 34, no. 8. pp. 240–244, 2001.

[210] P. Srinivasa Pai and P. K. Ramakrishna Rao, "Acoustic emission analysis for tool wear monitoring in face milling," *Int. J. Prod. Res.*, vol. 40, no. 5, pp. 1081–1093, 2002.

[211] D. Crivelli and S. Bland, "Structural health monitoring via acoustic emission," *Reinf. Plast.*, vol. 60, no. 6, pp. 390–392, 2016.

[212] K. M. Holford, "Acoustic Emission in Structural Health Monitoring," *Key Eng. Mater.*, vol. 413–414, no. 413–414, pp. 15–28, 2009.

[213] A. Dubois, L. Dubar, P. Picart, and J. Oudin, "Identification of the bulk behavior in the near-contact-surface of steel workpieces," *J. Mater. Eng. Perform.*, vol. 5, no. 6, pp. 734–742, 1996.

[214] K. Le Mercier, M. Dubar, K. Mocellin, A. Dubois, and L. Dubar, "Quantitative analysis of galling in cold forging of a commercial Al-Mg-Si alloy," in *Procedia Engineering*, 2017, vol. 207, pp. 2298–2303.

[215] A. Dubois, D. Patalier, P. Picart, and J. Oudin, "Optimization of the upsetting-sliding test parameters for the determination of friction laws at medium and high contact pressures," *J. Mater. Process. Technol.*, vol. 62, no. 1–3, pp. 140–148, 1996.

[216] D. D. Olsson, N. Bay, and J. L. Andreasen, "Prediction of limits of lubrication in strip reduction testing," *CIRP Ann. - Manuf. Technol.*, vol. 53, no. 1, pp. 231–234, 2004.

[217] ASTM International, “ASTM E2374 - Standard Guide for Acoustic Emission System Performance Verification.” 2004.

[218] N. N. Hsu and F. R. Breckenridge, “Characterization and calibration of acoustic emission sensors,” *Mater. Eval.*, vol. 39, no. 1, pp. 60–68, 1981.

[219] K. Jemielniak, “Some aspects of acoustic emission signal pre-processing,” *J. Mater. Process. Technol.*, vol. 109, no. 3, pp. 242–247, 2001.

[220] M. H. Sulaiman, P. Christiansen, and N. Bay, “A study of DLC coatings for ironing of stainless steel,” in *Journal of Physics: Conference Series*, 2017, vol. 896, no. 1, pp. 1–7.

[221] V. V Shanbhag, B. F. Rolfe, N. Arunachalam, and M. P. Pereira, “Understanding the source of acoustic emission signals during the wear of stamping tools,” in *IOP Conference Series: Materials Science and Engineering*, 2018, vol. 418, no. 1, pp. 1–8.

[222] V. V. Shanbhag, P. M. Pereira, F. B. Rolfe, and N. Arunachalam, “Time series analysis of tool wear in sheet metal stamping using acoustic emission,” in *Journal of Physics: Conference Series*, 2017, vol. 896, no. 1, pp. 1–8.

[223] V. V. Shanbhag, B. F. Rolfe, N. Arunachalam, and M. P. Pereira, “Investigating galling wear behaviour in sheet metal stamping using acoustic emissions,” *Wear*, vol. 414–415, pp. 31–42, 2018.

[224] M. A. Najafabadi, M. Salehi, M. R. Morowati, M. Hasani, S. A. Ebrahimian, and C. Sindi-Teymuri, “Investigation of the Deep Drawing Process by Means of Acoustic Emission Characteristics,” *Mater. Eval.*, vol. 76, no. 11, pp. 1525–1531, 2018.

[225] M. Christiany and P. Groche, “Reproducibility of Wear Tests and the Effect of Load on Tool Life in Sheet Metal Forming,” *Adv. Mater. Res.*, vol. 1018, pp. 293–300, 2014.

[226] Ö. N. Cora, A. Agcayaz, K. Namiki, H. Sofuoglu, and M. Koç, “Die wear in stamping of advanced high strength steels - Investigations on the effects of substrate material and hard-coatings,” *Tribol. Int.*, vol. 52, pp. 50–60, 2012.

[227] H. Hoffmann, C. Hwang, and K. Ersoy, “Advanced wear simulation in sheet metal forming,” *CIRP Ann. - Manuf. Technol.*, vol. 54, no. 1, pp. 217–220, 2005.

[228] M. Eriksen, “The influence of die geometry on tool wear in deep drawing,” *Wear*, vol. 207, no. 1–2, pp. 10–15, 1997.

[229] M. P. Pereira, W. Yan, and B. F. Rolfe, “Sliding distance, contact pressure and wear in sheet metal stamping,” *Wear*, vol. 268, no. 11–12, pp. 1275–1284, 2010.

[230] X. Z. Wang, S. H. Masood, and M. E. Dingle, “An Investigation on Tool Wear Prediction in Automotive Sheet Metal Stamping Die Using Numerical Simulation,” in *Proceedings of the International MultiConference of Engineers and Computer Scientists*, 2009, vol. II.

[231] X. Z. Wang and S. H. Masood, “Investigation of die radius arc profile on wear behaviour in sheet metal processing of advanced high strength steels,” *Mater. Des.*, vol. 32, no. 3, pp. 1118–1128, 2011.

[232] K. Ersoy-Nürnberg, G. Nürnberg, M. Golle, and H. Hoffmann, “Simulation of wear on sheet metal forming tools-An energy approach,” *Wear*, vol. 265, no. 11–12, pp. 1801–1807, 2008.

[233] “AGEMA Thermovision® 570 Operating Manual.” 1997.

[234] H. C. Meng and K. C. Ludema, “Wear models and predictive equations: their form and content,” *Wear*, vol. 181–183, no. PART 2, pp. 443–457, 1995.

[235] J. F. Archard and W. Hirst, “The Wear of Metals under Unlubricated Conditions,” *Proc. R. Soc. A Math. Phys. Eng. Sci.*, vol. 236, no. 1206, pp. 397–410, 1956.

[236] K. Ersoy, G. Nuernberg, G. Herrmann, and H. Hoffmann, “Advanced Prediction of Tool Wear by Taking the Load History into Consideration,” *AIP Conf. Proc.*, vol. 907, pp. 697–702, 2007.

[237] R. Holm, *Electric Contacts*. Almqvist & Wiksells Boktryckeri AB, 1946.

[238] E. Rabinowicz, *Friction and Wear of Materials*. John Wiley, 1965.

[239] H.-C. Shih, “Evaluation of zinc coating adhesion in stamping advanced high strength steel,” in *Proceedings of the ASME International Mechanical Engineering Congress and Exposition*, 2014, vol. 2A, pp. 1–9.

[240] S. S. Tufekci, C. Wang, G. L. Kinzel, and T. Altan, “Drawbead Design and Estimation of Drawbead Forces in Sheet. Metal Forming.” pp. 1–126, 1993.

[241] E. Üstünyagiz, “An Off-line Methodology to Determine Limits of Lubrication in Sheet Metal Forming,” 2018.

[242] S. J. Moon, “Experimental Drawbead Dies for Measuring Drawbead Forces,” *Trans. Mater. Process.*, vol. 17, no. 7, pp. 511–516, 2008.

[243] J. Filzek and P. Groche, “Assessment of the Tribological Function of Lubricants for Sheet Metal Forming,” in *Bench Testing of Industrial Fluid Lubrication and Wear Properties Used in Machinery Applications*, no. 1404, 2008, pp. 97-97–12.

[244] V. Rangarajan, D. K. Matlock, and G. Krauss, “The effects of coating properties on the frictional response of zinc-coated sheet steels,” in *Zinc-based Steel Coating Systems : Metallurgy and Performance*, 1990, pp. 263–280.

[245] V. Rangarajan, V. Jagannathan, and K. S. Raghavan, “Influence of Strain State on Powdering of Galvannealed Sheet Steel,” in *SAE Technical Paper Series*, 1996, vol. 105, pp. 68–75.

[246] V. Rangarajan, “Galvanneal Powdering in Drawbeads,” *SAE Tech. Pap. Ser.*, vol. 1259, 1997.

[247] “DIN 8588:2013-08 Fertigungsverfahren Zerteilen - Einordnung, Unterteilung, Begriffe.” .

[248] J. Mucha, “An experimental analysis of effects of various material tool’s wear on burr during generator sheets blanking,” *Int. J. Adv. Manuf. Technol.*, vol. 50, no. 5–8, pp. 495–507, Sep. 2010.

[249] C. M. Choy and R. Balendra, “Effect of Punch Wear on Blanking,” in *Tenth National Conference on Manufacturing Research*, 1994, pp. 582–586.

[250] A. I, “Tool Wear and Lubrication in Blanking Process,” *J. JAPAN Soc. Lubr. Eng.*, vol. 30, no. 9, pp. 633–638, 1985.

[251] F. Faura, J. López, and J. Sanes, “Criterion for tool wear limitation on blanking 18-8 stainless steel strips,” *Rev. Metal.*, vol. 33, no. 5, pp. 304–310, 2010.

[252] Z. Tekiner, M. Nalbant, and H. Gürün, “An experimental study for the effect of different clearances on burr, smooth-sheared and blanking force on aluminium sheet metal,” *Mater. Des.*, vol. 27, no. 10, pp. 1134–1138, 2006.

[253] J. J. Hernández, P. Franco, M. Estrems, and F. Faura, “Modelling and experimental analysis of the effects of tool wear on form errors in stainless steel blanking,” *J. Mater. Process. Technol.*, vol. 180, no. 1–3, pp. 143–150, 2006.

[254] R. Hambli, “Design of experiment based analysis for sheet metal blanking processes optimisation,” *Int. J. Adv. Manuf. Technol.*, vol. 19, no. 6, pp. 403–410, 2002.

[255] A. Millard and J. Gasnier, “Performance evaluation of lubricants during blanking,” 1995.

[256] K. O. Pfaff, “Über das Lochen austenitischer rostfreier Feinbleche,” 1972.

[257] L. Lind, P. Peetsalu, E. Adoberg, R. Veinthal, and P. Kulu, “Description of punch wear mechanism during fine blanking process,” *Proc. 7th Int. Conf. DAAAM Balt. Ind. Eng.*, no. April, pp. 504–509, 2010.

[258] D. D. Olsson, N. Bay, and J. L. Andreasen, “Lubricant test for punching and blanking,” *JSTP Journal, Spec. Issue*, vol. 44 no.: 50, 2003.

[259] D. D. Olsson, N. Bay, and J. L. Andreasen, “Analysis of Pick-Up Development in Punching,” *CIRP Ann.*, vol. 51, no. 1, pp. 185–190, 2002.

[260] D. D. Olsson, N. Bay, and J. L. Andreasen, “Studies of lubricants and punch design in punching of stainless steel,” *Proc. Int. Conf. Recent Adv. Manuf. Use Tools Dies Stamp. Steel Sheets*, 2005.

[261] R. A. Schmidt, F. Birzer, and M. Op de Hipt, “Tribologie beim Scherschneiden und Feinschneiden,” *Tribol. und Schmierungstechnik*, vol. 52, no. 4, pp. 42–54, 2005.

[262] F. Klocke, T. C. Maßmann, C. Zeppenfeld, R. A. Schmidt, J. Schulz, and F. Mumme, “Fineblanking with non-chlorinated lubricants,” *Tribol. und Schmierungstechnik*, vol. 55, no. 4, pp. 33–38, 2008.

[263] S. Hogmark, K. Bengtsson, and O. Vingsbo, “Wear of steel punches,” *Scand. J. Metall.*, vol. 10, no. 2, 1981.

[264] C. Won, H. Kim, Y. Song, G. Chung, S. Lee, and J. Yoon, “Abrasive Wear in Punching Pin with Cryogenic Treatment for GPa-Grade Steels,” *Int. J. Precis. Eng. Manuf.*, vol. 19, no. 8, pp. 1179–1186, 2018.

[265] M. Çöl, D. Kir, and E. Erişir, “Wear and blanking performance of AlCrN PVD-coated punches,” *Mater. Sci.*, vol. 48, no. 4, pp. 514–520, 2013.

[266] L. Lind, P. Peetsalu, and F. Sergejev, “Wear of different PVD coatings at industrial fine-blanking field tests,” *Mater. Sci.*, vol. 21, no. 3, pp. 343–348, 2015.

[267] F. Klocke and H.-W. Raedt, “Formulation and testing of optimised coating properties with regard to tribological performance in cold forging and fine blanking applications,” *Int. J. Refract. Met. Hard Mater.*, vol. 19, no. 4–6, pp. 495–505, 2001.

[268] G. Straffelini, G. Bizzotto, and V. Zanon, “Improving the wear resistance of tools for stamping,” *Wear*, vol. 269, no. 9–10, pp. 693–697, 2010.

[269] B. Podgornik, B. Zajec, N. Bay, and J. Vižintin, “Application of hard coatings for blanking and piercing tools,” *Wear*, vol. 270, no. 11–12, pp. 850–856, 2011.

[270] F. Klocke and H. W. Raedt, “Formulation and testing of optimised coating properties with regard to tribological performance in cold forging and fine blanking applications,” *Int. J. Refract. Met. Hard Mater.*, vol. 19, no. 4–6, pp. 495–505, 2001.

[271] K. Kitamura, T. Makino, M. Nawa, and S. Miyata, “Tribological effects of punch with micro-dimples in blanking under high hydrostatic pressure,” *CIRP Ann. - Manuf. Technol.*, vol. 65, no. 1, pp. 249–252, 2016.

[272] N. H. Jayadas, K. Prabhakaran Nair, and G. Ajithkumar, “Vegetable Oils as Base Oil for Industrial Lubricants: Evaluation Oxidative and Low Temperature Properties Using TGA, DTA and DSC,” in *Proceedings of the World Tribology Congress III*, 2005, pp. 539–540.

[273] B. O. Haglund and P. Enghag, “Characterization of lubricants used in the metalworking industry by thermoanalytical methods,” *Thermochim. Acta*, vol. 282–283, no. SPEC. ISS., pp. 493–499, Jul. 1996.

[274] R. M. Matveevsky and I. A. Buyanovsky, “Investigation of the transition temperatures of lubricants under friction of steels,” in *Eurotrib 81: 3rd International Tribology Congress. Volume Iii: Lubricants and Their Applications*, 1982, pp. 171–179.

[275] R. M. Matveevsky, “Chemical modification of friction surfaces in boundary lubrication,” *ASLE Trans.*, vol. 25, no. 4, pp. 483–488, 1982.

[276] R. M. Matveevsky, “Evaluation of temperature stability of a lubricant film on rubbing surfaces,” *Tribology*, vol. 1, no. 2, pp. 115–117, 1968.

[277] R. M. Matveevsky, “The temperature of tribochemical reaction between e.p. additives and metals,” *Tribology*, vol. 4, no. 2, pp. 97–98, 1971.

[278] R. M. Matveevsky, “Problems of boundary lubrication,” *Tribol. Int.*, vol. 28, no. 1, pp. 51–54, 1995.

[279] M. Kawamura and K. Fujita, “Organic sulphur and phosphorus compounds as extreme pressure additives,” *Wear*, vol. 72, no. 1, pp. 45–53, 1981.

[280] Y. Wan and Q. Xue, “Effect of phosphorus-containing additives on the wear of aluminum in the lubricated aluminum-on-steel contact,” *Tribol. Lett.*, vol. 2, no. 1, pp. 37–45, 1996.

[281] M. Kawamura, “The correlation of antiwear properties with the chemical reactivity of zinc dialkyldithiophosphates,” *Wear*, vol. 77, no. 3, pp. 287–294, Apr. 1982.

[282] “Uddeholm Vanadis ® 23 SuperClean datasheet.”

[283] B. R. Hölm, K. Miclwelis, H. Collenberg, and L. Schlenk, “Effect of temperature on the scuffing load capacity of EP gear lubricants,” *TriboTest*, vol. 7, no. 4, pp. 317–332, 2001.

[284] N. Shimotomai, H. Ihara, and H. Nanao, “A Study of Hot Rolling Oil with Calcium Carbonate for Stainless Steel Process,” *Tribol. Online*, vol. 5, no. 3, pp. 181–186, 2010.

[285] C. Tianhua, “Tribological properties of calcium carbonate powders modified with Tween 40 as lubricant additives,” *Funct. Mater.*, vol. 24, no. 4, pp. 572–576, 2017.

[286] B. Kinsey, N. Song, and J. Cao, “Analysis of Clamping Mechanism for Tailor Welded Blank Forming,” in *SAE Technical Paper Series*, 2010, vol. 1.

[287] D. D. Olsson, N. Bay, and J. L. Andreasen, “Analysis of Pick-Up Development in Punching,” *CIRP Ann. - Manuf. Technol.*, vol. 51, no. 1, pp. 185–190, 2002.

[288] G. I. Shore, “Mechanism of action and express-estimation of performance of lube oils with additives,” *ZNIITEneftechim*, pp. 1–66, 1996.

[289] T. N. Mills, “Boundary Lubricated Contacts at High Repetition Rates,” 1979.

[290] J. S. Tse, Y. Song, and Z. Liu, “Effects of temperature and pressure on ZDDP,” *Tribol. Lett.*, vol. 28, no. 1, pp. 45–49, 2007.

[291] K. Komvopoulos, S. A. Pernama, J. Ma, E. S. Yamaguchi, and P. R. Ryason, “Synergistic effects of boron-, sulfur-, and phosphorus-containing lubricants in boundary lubrication of steel surfaces,” *Tribol. Trans.*, vol. 48, no. 2, pp. 218–229, 2005.

[292] M. N. Najman, M. Kasrai, and G. M. Bancroft, “Investigating binary oil additive systems containing P and S using X-ray absorption near-edge structure spectroscopy,” *Wear*, vol. 257, no. 1–2, pp. 32–40, 2004.

[293] “ASTM G99—17 Standard Test Method for Wear Testing with a Pin-on-Disk Apparatus.” .

[294] J. Wang, Y. Liu, D. Duan, and S. Li, “Comparative Study on the Tribological Performances of Barium Perrhenate, Molybdenum Disulfide, and Calcium Carbonate as Lubricant Additives in a Wide Temperature Range,” *Tribol. Trans.*, vol. 59, no. 1, pp. 139–148, 2016.

[295] N. N. Gosvami, J. A. Bares, F. Mangolini, A. R. Konicek, D. G. Yablon, and R. W. Carpick, “Mechanisms of antiwear tribofilm growth revealed in situ by single-asperity sliding contacts,” *Science (80-.).*, vol. 348, no. 6230, pp. 102–106, 2015.

[296] P. Cann, G. J. Johnson, and H. A. Spikes, “The formation of thick films by phosphorus-based anti-wear additives,” in *I Mech E Conference Publications*, 1987, pp. 543–554.

[297] F. M. Piras, A. Rossi, and N. D. Spencer, “Combined in situ (ATR FT-IR) and ex situ (XPS) study of the ZnDTP-iron surface interaction,” *Tribol. Lett.*, vol. 15, no. 3, pp. 181–191, 2003.

Appendix A Developed wear scar in the four-ball test

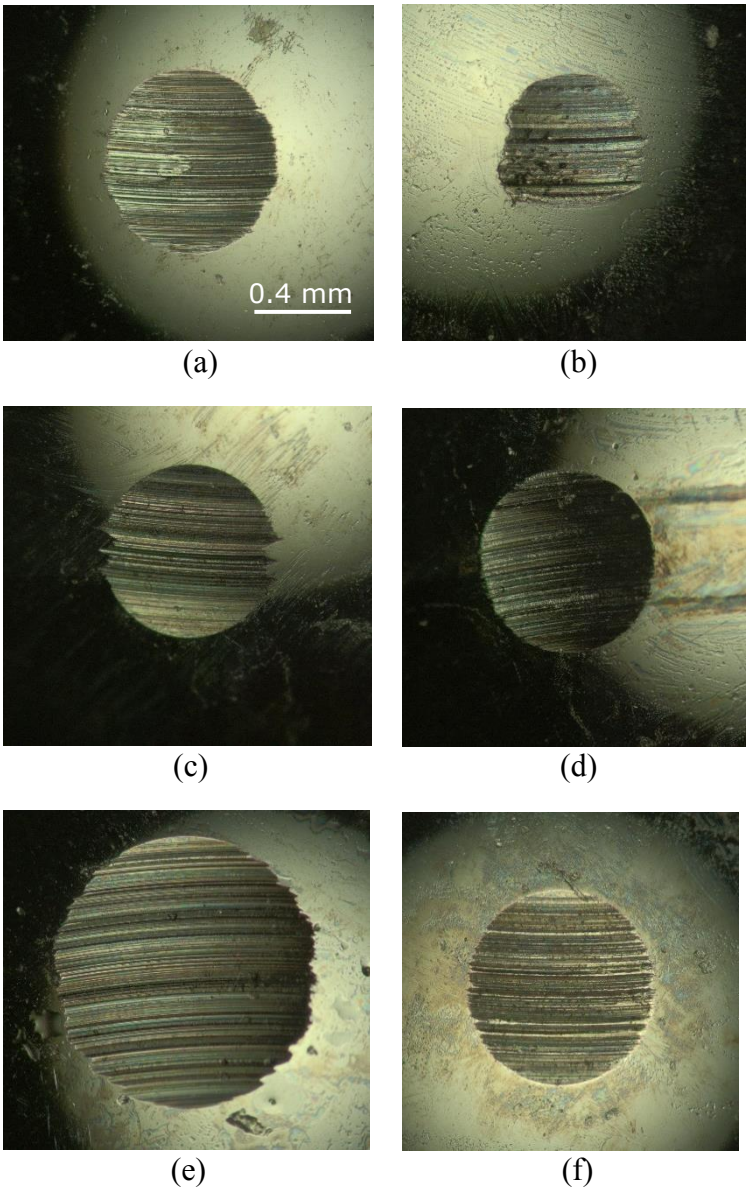

Figure 91: Wear scar developed in four-ball test with the tested lubricants: (a) DB 4265, (b) Drosera MS 5, (c) Paraffin oil, (d) Pn226, (e) SF125 and (f) TDN81.

Appendix B XPS analysis of tribofilms

The pin-on-disc test was conducted on a CSM tribometer with a Ø6mm AISI 316 grade 100 stainless steel ball with a hardness of 39 HRC and a disc of AISI M3:2, hardened to 64 HRC. The test was furthermore conducted with a rotational velocity of 55mm/s and normal force of 10N, resulting in a maximum Hertzian pressure of approximately 1400 MPa in the contact surface. A surface finish of R_a = 0.08µm was obtained by lapping of the disc as recommended in the ASTM G99-17 standard [293]. The test duration ranged from approximately 3500-4000s until at full stabilization of the COF was achieved, see Figure 92.

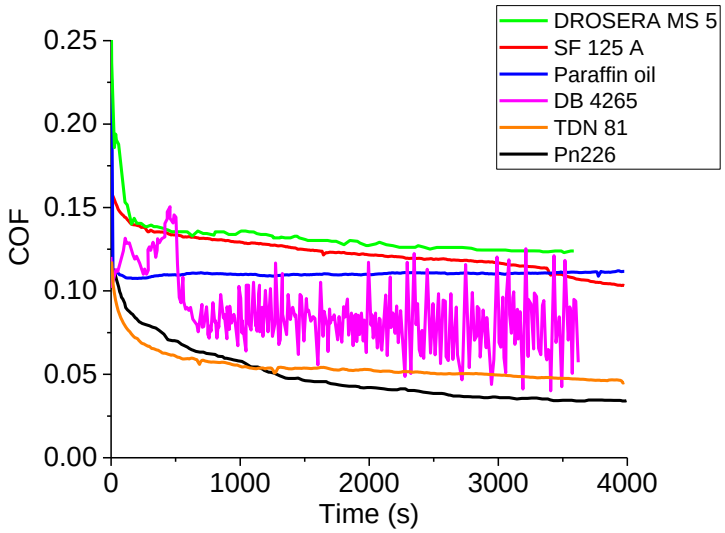

Figure 92 COF measured during the pin-on-disc test.

All the lubricants containing film-forming additives were found to have a development of the COF that was gradually reduced within the first 1000s of testing, whereafter the COF assumed stabilized values. The pure paraffin oil was however found to result in a stabilized COF immediately upon testing. The stabilization of the COF is commonly attributed to either a run-in behavior of the two surfaces in the contact or the formation of a stabilized surface film initiated by the frictional heating developed during testing. The DB 4265 lubricant is seen to have a highly fluctuating COF throughout the duration of the test. This behavior is attributed to the lubricant formulation that is based on a suspension of solid particles, which inhibit direct metal-to-metal contact between the base body and the counter body of the tribosystem [286]. A main lubrication mechanism based on the

suspension of solid particles combined with a high rate of dilution of the lubricant is found to result in an inability to form a stable COF in the present study.

The surface of the wear scar, developed in the pin-on-disc test, was analysed with XPS for evaluation of the composition and film thickness of the formed surface films during testing. The analysis of the surface structure was carried out with a Thermo Scientific^{TM} K-Alpha XPS spectrometer. Prior to inspection of the surface composition, the test samples were rinsed with ethanol and afterwards ultrasonically cleaned with heptane in order to remove lubricant residue from the surface. The XPS survey reveals a range of different elements in the developed wear scar with the tested lubricants, see Figure 93.

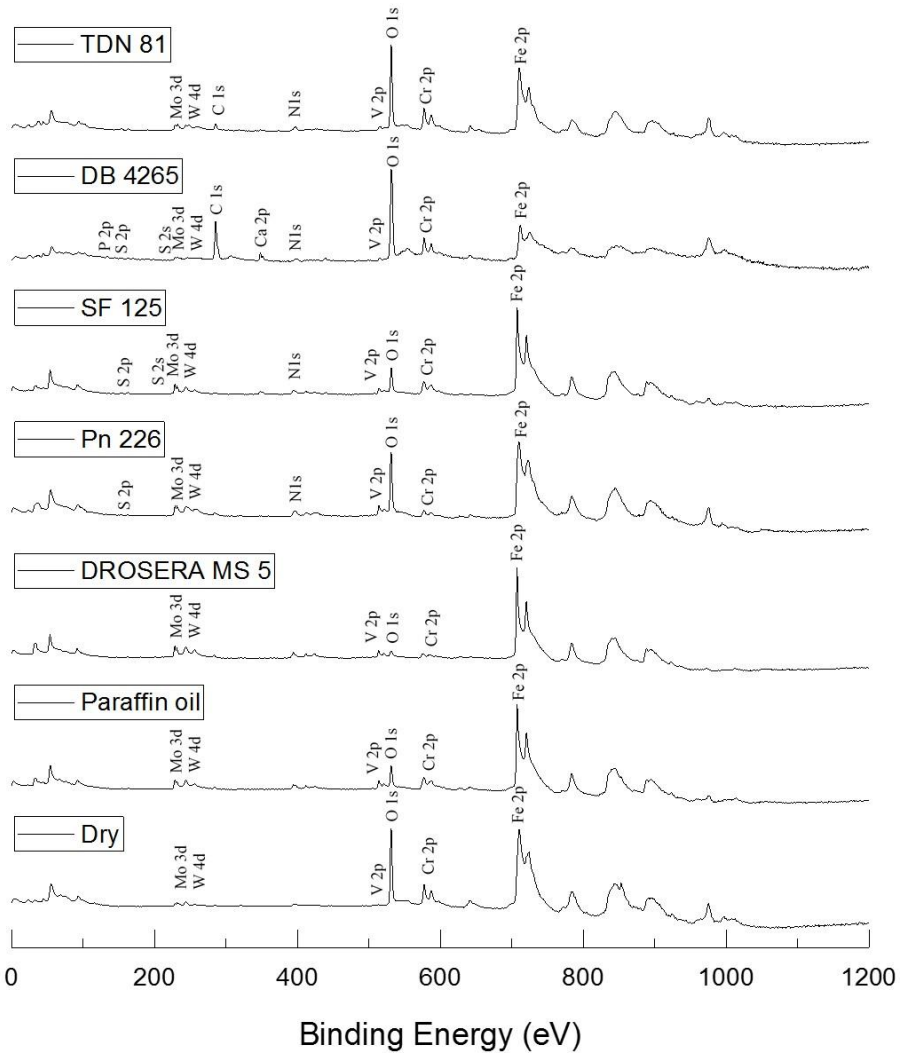

Figure 93: XPS spectra of the analyzed test specimens.

The test series conducted under dry conditions and with a pure paraffin oil encompass reference conditions without the influence of film-forming additives. Evaluation of the surface composition under these conditions, therefore, shows an overview of the main composition of the AISI M3:2 disc material and native oxides developed on the surface of the workpiece seen at a binding energy of 531.08 eV. Several test series are furthermore found to contain minor peaks of S2p at 164.04 eV, which is commonly attributed to the presence of sulfide. The DB 4265 lubricant exhibits minor peaks of P2p at 134.08 eV and Ca2p at 348 eV, respectively attributed to the presence of phosphates and calcium carbonate [290].

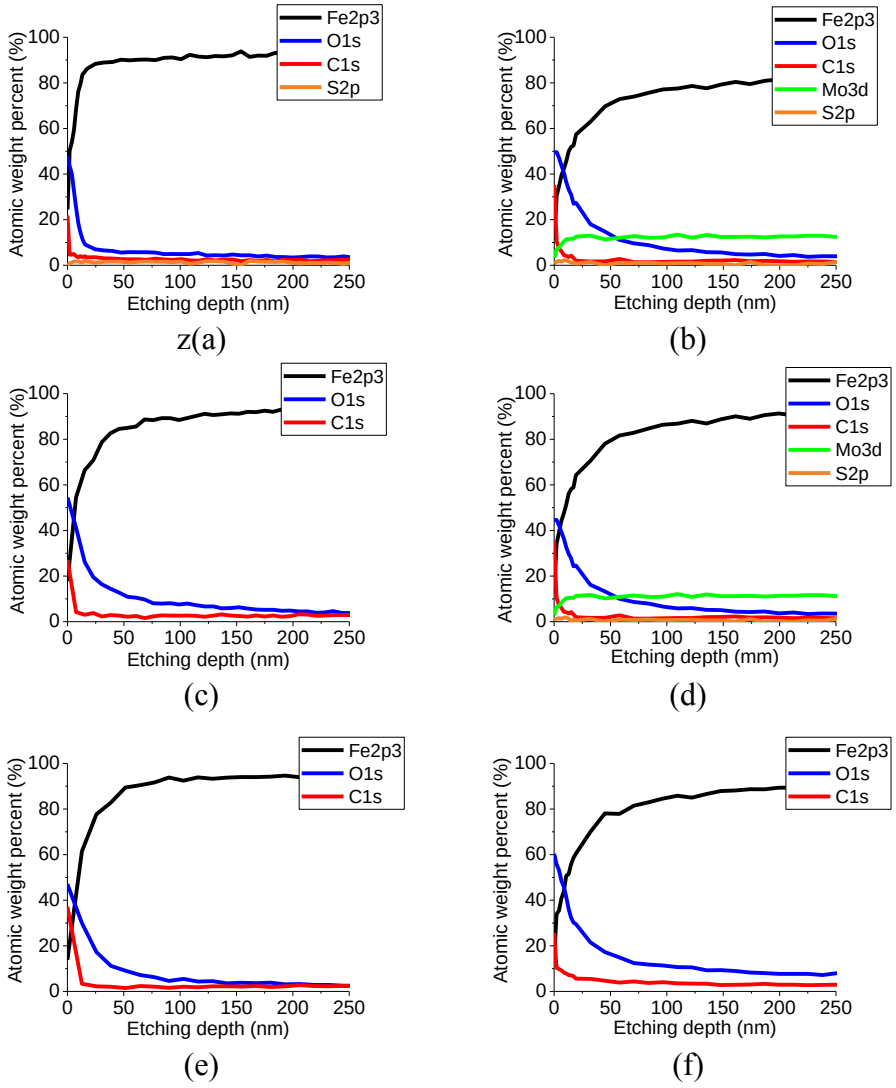

Figure 94: XPS depth profiles of disc surfaces tested with different lubricants: (a) Pn 226, (b) DB 4265, (c) Paraffin oil, (d) SF 125 A, (e) TDN 81 and (f) Drosera MS 5.

A survey of the thickness of the generated surface films is shown in Figure 94 with an XPS depth profile analysis. The depth profiles shows minor levels of S2p within an etching depth of 250 nm for the SF125 A, DB 4265 and the Pn 226 lubricants. No traces of Cl was found in the developed wear scar of the test specimens tested with the chlorinated lubricants. Ex situ spectroscopy methods like XPS require thorough cleaning of the specimens with aggressive solvents and exposure to vacuum for application of the analytical technique. This can, however, render the analyzed tribofilm as unrepresentative of the original surface during testing as weakly bonded tribofilm constituents are likely to be removed during preparation of the samples [295]–[297]. The test conditions of the pin-on-disc test could possibly also be unable to introduce a stable tribofilm with the Cl-based lubricants, contrary to the high-temperature pin-on-disc test conducted with an external heating source.

DTU Mechanical Engineering
Section of Manufacturing Engineering
Technical University of Denmark

Produktionstorvet, Bld. 425
DK-2800 Kgs. Lyngby
Denmark

Tlf.: +45 4525 4763
Fax: +45 4525 1961

www.mek.dtu.dk

April 2019

ISBN: 978-87-7475-571-5